MdfA as a Model for Structural and Functional Characterization of Putative Multidrug Transporters

A Thesis submitted to the College of
Graduate Studies and Research
in Partial Fulfillment of the Requirements
for the Degree of Master of Science
in the Department of Biochemistry
University of Saskatchewan
Saskatoon

By Tahereh Haji

Copyright Note

Abstract

Numerous members of the Major Facilitator Superfamily of membrane transporters are involved in multidrug resistance (MDR) of gram-positive bacteria, such as *Staphylococcus aureus* (*S. aureus*). Genome data indicate that MDR transporters (MDT) constitute up to 1.0% of total cell proteins, but the majority remain uncharacterized: substrates, transport rates, and structures remain unknown (Forrest *et al.*, 2011; Tsai and Ziegler, 2010; Ward *et al.*, 2001). The main goal of this project was to develop a technique for substrate profile analysis and transport kinetics measurement of putative MDT from *S. aureus*, and other bacteria, using a well-characterized transporter, the multidrug facilitator A (MdfA), from *Escherichia coli* (*E. coli*), as a model protein. To provide structural basis for drug transport and binding studies, we also conducted preliminary MdfA crystallization trials.

MdfA was expressed and purified using a procedure previously established in our lab (O'Grady, 2010). MdfA couples substrate transport across the cell membrane to the counterflow of protons. To test substrate transport by MdfA, we developed an assay based on monitoring proton transport in membrane vesicles using 9-amino-6-chloro-2-methoxy acridine (ACMA), a pH-sensitive fluorophore. We confirmed MdfA activity in membrane vesicles by this assay. In proteoliposomes containing co-reconstituted MdfA and F_oF_1 ATPase, addition of ATP generates a transmembrane pH gradient, which can be used as the driving force for MdfA-mediated substrate transport. Substrate binding to MdfA was investigated by nuclear magnetic resonance (NMR) experiments with ^{13}C-labeled chloramphenicol. We observed specific interactions between chloramphenicol, a known MdfA substrate, and MdfA with an estimated dissociation constant (K_d) on the order of 10 μM. Detergents that have been previously successfully used for structural studies of membrane proteins by NMR and X-ray crystallography were tested for structural studies of MdfA. We determined that MdfA is active; however, further work is required to optimize the substrate profile assay, confirm substrate-binding data, and obtain crystals suitable for structural studies.

Acknowledgements

First and foremost, I would like to thank Dr. Oleg Dmitriev for his support and guidance throughout my Master's project. To my committee members, Drs. Jeremy Lee, Yu Luo, Ramji Khandelwal and Bill Roesler, I must extend a strong word of gratitude for their support. I would also like to acknowledge the constant guidance, support, and encouragement of the members of the Dmitriev lab, Christopher O'Grady, Eva Uhlemann, Hannah Pierson, Sergiy Nokhrin, Nataliya Dolgova, and Corey Yu. I would like to thank Shazia Anjum from the Palmer lab for her assistance in the isolation and purification of acetyl chloramphenicol. Finally, I would like to thank my friends and family, especially my brother, Anis, for the loving support they have always provided me.

Dedication

To my dearest E.M., because you saw Orion.

Table of Contents

List of Tables

List of Figures

List of Abbreviations

ABC	ATP-binding cassette
AcCml	Acetyl chloramphenicol
^{13}C- AcCml	^{13}C-labeled acetyl chloramphenicol
ACMA	9-amino-6-chloro-2-methoxy acridine
K_d	Dissociation constant
$C_{12}E_8$	Dodecyloctaoxyethylene
CMC	Critical micelle concentration
Cml	Chloramphenicol
DCCD	N,N'-dicyclohexylcarbodiimide
DDM	N-dodecyl-β-D-maltopyranoside
DHPC	1,2-diheptanoyl-*sn*-glycero-3-phosphocholine
DSS	4,4-dimethyl-4-silapentane-1-sulfonic acid
DTT	Dithiothreitol
E. coli	*Escherichia coli*
EtBr	Ethidium bromide
FCCP	Carbonyl cyanide 4-(trifluoromethoxy)-phenylhydrazone
G3P	Glycerol 3-phosphate
HSQC	Heteronuclear single quantum coherence
P_i	Inorganic phosphate
IPTG	β-D-galactopyranosyl-1-thio-β-D-galactopyranoside
LB	Luria-Bertani
LDAO	N,N-dimethyldodecylamine
LMPG	1-myristoyl-2-hydroxy-*sn*-glycero-3-[phospho-*rac* -1-glycerol)]
MATE	Multidrug and toxic compound exporters
MdfA	Multidrug facilitator A
MDR	Multidrug resistance
MDT	Multidrug resistance transporters
MFS	Major Facilitator Superfamily
MOPS	3-(N-morpholino)propanesulfonic acid

MRSA	Methicillin-resistant *Staphylococcus aureus*
NAG	^{13}C-acetyl-^{15}N-glycine
Ni-NTA	Nickel nitrilotriacetic acid agarose
NBD	Nucleotide-binding domains
NMR	Nuclear magnetic resonance
C_8E_4	Octyltetraoxyethylene
OG	N-octyl-β-D-glucopyranoside
PDC	Protein-detergent complex
PEG	Polyethylene glycol
P. aeruginosa	*Pseudomonas aeruginosa*
P. modestum	*Propionigenium modestum*
PMSF	Phenylmethylsulfonyl fluoride
RND	Resistance-nodulation-division
S. aureus	*Staphylococcus aureus*
SDS-PAGE	Sodium dodecylsulfate polyacrylamide gel electrophoresis
SMR	Small multidrug resistance transporters
TMD	Transmembrane domains
TMH	Transmembrane helices
TPP^+	Tetraphenylphosphonium
WT	Wild type

1. Introduction

Membrane transport proteins are highly relevant to human physiology and disease. In fact, two of the most highly prescribed drugs in the world, fluoxetine (Prozac) and omeprazole (Prilosec), are targeted to transporters (Abramson *et al*., 2003). On the other hand, the simultaneous emergence of resistance in eukaryotic and prokaryotic cells to many chemically unrelated drugs, referred to as MDR, is also related to membrane transport proteins (Adler and Bibi, 2002).

MDR was first observed in the 1950s and 60s among bacteria such as *Shigella*, *Salmonella*, and *E. coli*, in the developing world (Levy and Marshall, 2004; Watanabe, 1963). At that time, MDR was not considered to be a problem for industrialized countries; however, since the 1970s, when drug resistance was observed in *Haemophilus influenzae* and *Neisseria gonorrhoeae*, healthcare providers and scientists have begun to acknowledge this area as one of growing concern (Levy and Marshall, 2004; Rice, 2010; Watanabe, 1963). Today, MDR pathogens are most commonly observed in healthcare settings, and include methicillin-resistant *S. aureus* (MRSA), vancomycin-resistant *Enterococcus* species, extended-spectrum β-lactamase producing *E. coli* and *Klebsiella* species, fluoroquinolone- or carbapenem-resistant *Enterobacteriaceae* and *Pseudomonas aeruginosa* (*P. aeruginosa*) and MDR *Mycobacterium tuberculosis* (Levy and Marshall, 2004; Rice, 2010; Watanabe, 1963). In Europe, half of all deaths from clinical infection are associated with MDR bacteria (Coates, 2011). In the United States and the United Kingdom, 40-60% of nosocomial *S. aureus* strains are MRSA and usually MDR. Treatment of MRSA involves the use of vancomycin, but in recent years, vancomycin-resistant strains of *S. aureus* have appeared, leading to treatment failure. It is estimated that, depending on the number of deaths, treatment of patients with MRSA alone costs up to $30 billion (USD) annually. This medical and financial burden is likely to grow as the frequency of drug resistance rises and extends beyond hospital walls: resistant pathogens are now increasingly being traced from the community to the hospital (Levy and Marshall, 2004).

Drug resistance emerges when two components come together in an environment or host: the antibiotic or antimicrobial, which inhibits susceptible organisms and selects those most resistant, and the genetic resistance determinant in pathogens selected for by the antimicrobial drug. The density of antibiotic usage enhances resistance selection and its effects

(Levy and Marshall, 2004). Bacteria can become resistant to drugs by acquiring the gene for a resistant trait via mobile genetic elements; acquiring sequential mutations in chromosomes leading to resistance genes; or an increase in the expression of membrane proteins that pump drugs out of the cell (Fig. 1.1) (Krulwich *et al.*, 2005; Levy and Marshall, 2004; Watanabe, 1963). These resistance mechanisms are reviewed in detail later. Curtailing widespread antibiotic use has been shown to reduce and sometimes reverse drug resistance levels. However, as agents and strategies were developed to overpower specific resistance to drugs, multidrug resistance caused by active efflux was increasingly observed (Fig. 1.1) (Coates, 2011; Cook *et al*., 1989; Gootz, 2010; Levy and Marshall, 2004; Nikaido, 1994; Rice, 2010). Some drug efflux transporters are substrate specific, while MDT can transport a variety of structurally unrelated compounds (Li and Nikaido, 2004).

In fact, active drug efflux by membrane transporters greatly enhances the intrinsic resistance of bacteria (Edgar and Bibi, 1999; Hancock, 1997; Markham and Neyfakh, 2001; Nikaido, 1994). This is especially critical for gram-positive bacteria and mycobacteria, which lack the poorly permeable outer membrane of their gram-negative counterparts, and as a result, rely on drug efflux for survival against toxic compounds (Almeida da Silva *et al*., 2011; Markham and Neyfakh, 2001). In other cases, the major advantage of these transporters is in maintaining subtherapeutic intracellular drug concentrations, allowing for the selection of other resistance mechanisms which are unrelated to active efflux (Doleans-Jordheim *et al*., 2008; German *et al*., 2008; Markham and Neyfakh, 1996).

Antibiotic efflux was first observed in 1980, when it was recognized as a mechanism for tetracycline resistance in enterobacteria (McMurry *et al*., 1980). Since then, efflux has been observed in virtually every living system, and efflux-based antibiotic resistance is increasing (Adler and Bibi, 2002; Fluman and Bibi, 2009; Forrest *et al.*, 2011; Li and Nikaido, 2004; Li and Nikaido, 2009). In particular, efflux of multiple drugs by a single transporter is of significant medical and biochemical interest. While advances in developing strategies against transporters implicated in MDR are being made, there is a need for methods that can demonstrate and characterize drug efflux pumps both in the lab and in the clinic (Viveiros *et al*., 2008). The goal of this project is to use MdfA, a model *E. coli* MDT of the Major Facilitator Superfamily (MFS), to develop universal methods for structural and functional characterization of putative MDT from MRSA.

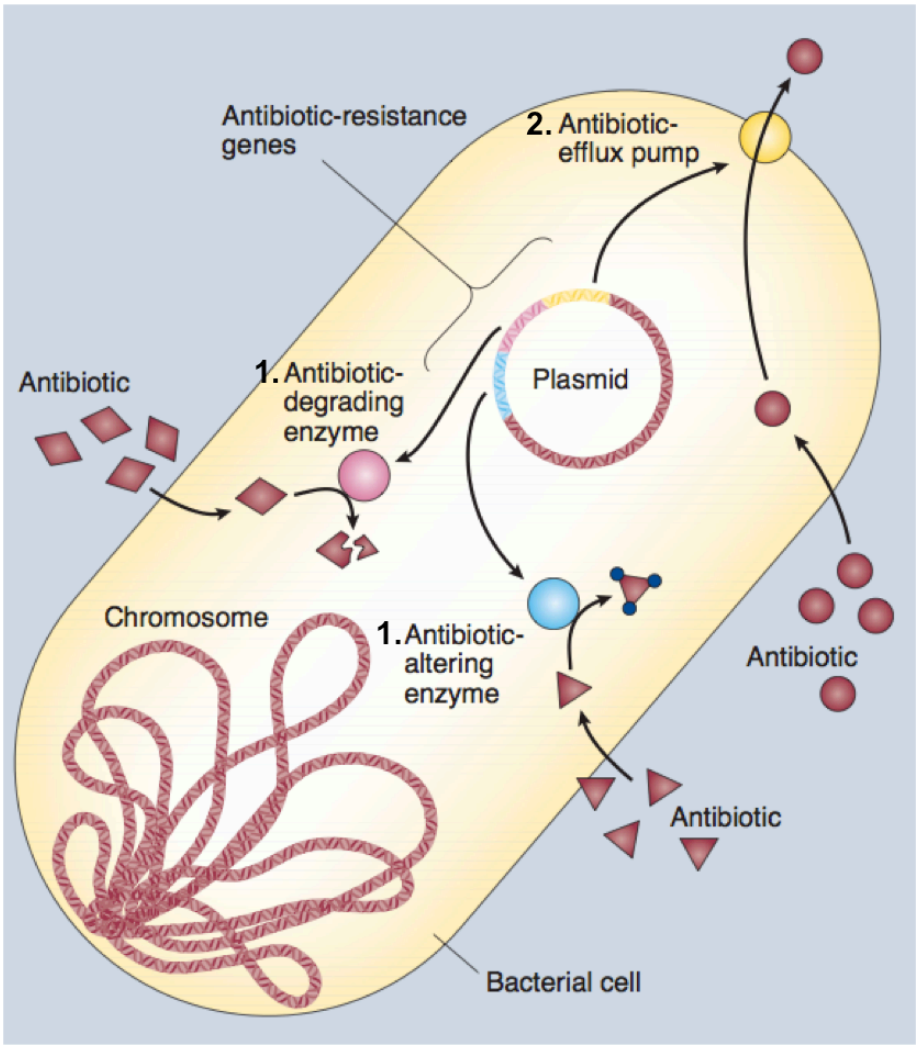

Figure 1.1. Mechanisms of bacterial antibiotic resistance. Antibiotic resistance can arise in a bacterial cell by one or more of the following mechanisms: 1. Inactivation of the antibiotic by chemical modification or breakdown; 2. Rapid efflux of the antibiotic, preventing an effective level of the compound from reaching its target; 3. Modification or replacement of the original target so that it is no longer sensitive to the antibiotic (not shown); or 4. Changes in the bacterial cell surface that reduce antibiotic uptake (not shown). Reproduced from Levy and Marshall (2004) with the permission of the publisher.

2. Background and state of the problem

2.1. Multidrug resistance in bacteria

2.1.1 Mechanisms of drug resistance in bacteria

When a drug is introduced to the external medium of a bacterial cell, it must first cross the cell wall, in gram-positive bacteria, or the outer membrane, in gram-negative bacteria, before it can permeate the cell membrane and exert its action. The mesh of the peptidoglycan cell wall of gram-positive bacteria is too coarse to offer much resistance to the diffusion of small molecules such as antibiotics. The outer membrane of gram-negative bacteria is much more impermeable, since it is composed of less fluid lipopolysaccharide, and as a result, drug penetration into the cell is hindered (Nikaido, 1994). Once a drug has passed the cell wall or outer membrane, it crosses the cell membrane. From the inner membrane leaflet, the drug can diffuse into the cytosol and find its target (Mazurkiewicz *et al*., 2005). It is clear that even the most effective permeability barrier cannot completely shut out the influx of small molecules (Hancock, 1997; Markham and Neyfakh, 2001; Nikaido, 1994). As the cell's first line of defense against an antibiotic fails, those cells with specific resistance mechanisms will be selected (Nikaido, 1994).

Antibiotic resistance can arise in a bacterial cell by one or more of the following mechanisms (Fig. 1.1) (Krulwich *et al*., 2005). First, changes in the bacterial cell surface can drastically affect antibiotic uptake. Antibiotics in gram-negative bacteria are often taken up using porins that are non-specific for small molecules (Nikaido, 1989). For example, in gram-negative bacteria such as *P. aeruginosa*, changes in the outer membrane porins affect drug uptake (Angus *et al*., 1982). Kropinski and coworkers were able to show that alterations in the lipopolysaccharide composition of the outer membrane of *P. aeruginosa* influenced the number of open functional pores, and could therefore enhance or decrease antibiotic susceptibility in this bacterium (Kropinski, 1982).

Second, the antibiotic may be deactivated by enzymatic modification, as is commonly the case for aminoglycosides (Fig. 1.1) (Shi *et al*., 2011). Aminoglycosides can be phosphorylated, adenylated, or acetylated, leading to reduced target binding to the ribosome, and increased survival of the bacterial cell (Alekshun and Levy, 2007; Shi *et al*., 2011).

Third, the antibiotic target may be modified so that it is no longer sensitive to the antibiotic itself, as seen in the case of erythromycin. Erythromycin binds to the 50S ribosomal

subunit and prevents peptide elongation (Sköld, 2011). Erythromycin resistance in *S. aureus* is caused by methylation of an adenine residue in the 23S rRNA subunit, which results in a conformational change that abolishes erythromycin binding (Lai, 1971; Sköld, 2011).

Finally, active efflux of the antibiotic from the cell, preventing a drug from reaching its target at an effective concentration, is a significant and ubiquitous form of antibiotic resistance (Fig. 1.1) (Krulwich *et al*., 2005). In *E. coli*, for example, AcrAB (discussed in more detail below), has been identified as a major pump responsible for resistance to such antibiotics as tetracycline, chloramphenicol, ampicillin and rifampin (Okusu *et al*., 1996).

2.1.2 Bacterial multidrug transporters

MDT, efflux pumps that transport a variety of cytotoxic compounds out of the cell, are found among all the major categories of bacterial membrane transporters that have been characterized on the basis of sequence homology (Lewinson *et al*., 2006; Saier and Paulsen, 2001). MDT from five transporter families have been identified: ATP-binding cassette (ABC) transporters; multidrug and toxic compound exporters (MATE); small MDR (SMR) transporters; resistance-nodulation-division (RND) transporters; and MFS transporters (Fig. 2.1) (Saier and Paulsen, 2001). The first four families listed here will be described in this section, while details regarding members of the MFS will be described in section 2.2.

Members of the ABC superfamily typically transport a diversity of substrates such as inorganic ions, amino acids, and polypeptides (Higgins, 2007). MDT from this family, however, can each transport a diversity of structurally diverse, lipophilic substrates: in human cancer patients, MDR1 (also known as P-glycoprotein), confers resistance to such chemotherapeutics as doxorubicin, Taxol and etoposide, and in other organisms ABC MDT have been shown to confer resistance to antibiotics, antifungals and herbicides (Higgins, 2007, 2004; Ramachandra *et al*., 1998). ABC transporters are composed of four domains: two

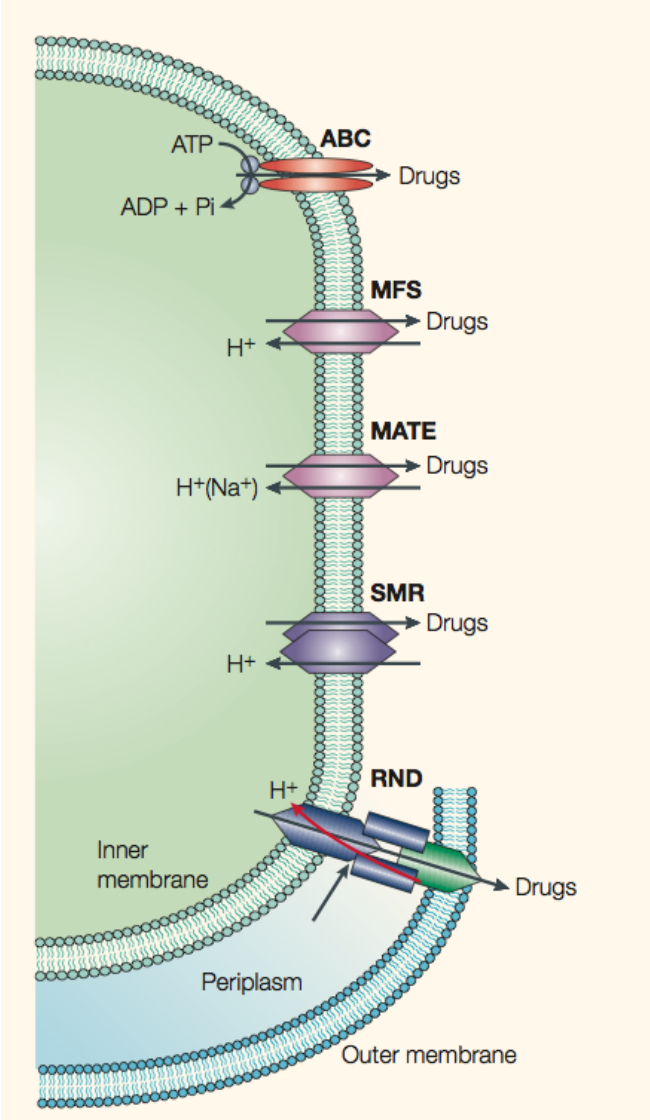

Figure 2.1. Bacterial drug and multidrug transporters. The ABC transporters use the energy from ATP hydrolysis to actively extrude drugs from the cell, while the members of the MFS, MATE, SMR and RND families use secondary energy sources in the form of a proton or sodium motive for active drug efflux. Reproduced from Krulwich *et al*. (2005), with the permission of the publisher.

transmembrane domains (TMD) and two nucleotide-binding domains (NBD) (Fig. 2.2). The recently solved structure of Sav1866, an ABC MDT from *S. aureus*, defined critical structural elements of these transporters. The ATP-binding site is located at the interface of the NBD (Fig. 2.2) (Dawson and Locher, 2006). Specialized "coupling helices" couple the conformational changes associated with ATP-binding, hydrolysis, and release to the export of drugs by drawing the TMD closer together, and shifting their conformation from inward-facing to outward-facing (Dawson and Locher, 2006; Locher, 2009; van Veen *et al*., 2000). The precise location of the substrate-binding site remains elusive, but is likely located at the interface of the TMD (Fig. 2.2) (Dawson and Locher, 2006; Higgins, 2004).

The SMR family is composed of over 250 members and is represented by EmrE of *E. coli* (Adam *et al.*, 2007; Li and Nikaido, 2009). EmrE is a proton/cation antiporter, shown to export such toxic substrates as ethidium, tetraphenylphosphonium (TPP^+), erythromycin, and methyl viologen (Fig. 2.3) (Paulsen *et al*., 1996; Rotem and Schuldiner, 2004). This small transporter functions as an antiparallel homodimer, each composed of four α-helices, which essentially form a pathway that is alternately accessible from either side of the plasma membrane (Fig. 2.3) (Butler *et al*., 2004; Chen *et al*., 2007; Higgins, 2007; Korkhov and Tate, 2009). The unusual dimer structure of SMR transporters has been a matter of considerable debate, but evidence now indicates that all SMR transporters, whether homo- or heterodimers, form in an antiparallel orientation (Fig. 2.3) (Chen *et al*., 2007). E14 is the only membrane embedded charged residue, and the E14s from each monomer face the substrate-binding pocket (Chen *et al*., 2007; Weinglass *et al*., 2005). E14 is essential for both substrate binding and proton translocation; the stoichiometry of transport is 2 H^+/substrate (Adam *et al*., 2007; Soskine *et al*., 2004). However, it is likely that EmrE binds substrates not only by charge interactions, but also by cation/π interactions between positively charged substrates and aromatic residues in the binding pocket (eg. W63) (Adam *et al*., 2007; Dougherty, 1996). This type of non-covalent interaction is able to compete with solvation; as a result, it creates binding sites that are at once both polar and hydrophobic (Dougherty, 1996). Though biochemical evidence suggests that this is the case, a high-resolution structure of the native substrate-bound EmrE is required before the exact mechanism of substrate binding can be understood.

The tripartite MDT from the RND family are extremely efficient at extruding drugs across both membranes of gram-negative bacteria (Fluman and Bibi, 2009). These transporters

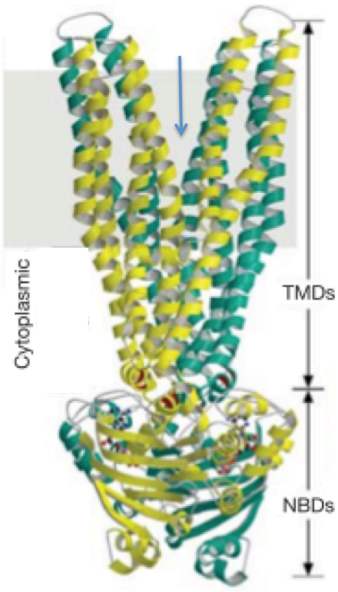

Figure 2.2. Ribbon diagram of Sav1866, an ABC multidrug transporter from *S. aureus*. The subunits of the homodimer are colored yellow and turquoise. Bound ATP is shown in ball-and-stick representation. The grey box indicates the probable location of the membrane bilayer. The substrate binding site is thought to be located at the interface of the two TMDs (indicated by an arrow). Reproduced from Dawson and Locher (2006), with the permission of the publisher.

Figure 2.3. Ribbon representation of EmrE-TPP^+ dimer. One monomer is in gradient and the other is in gray. Bound TPP^+ is colored red. The membrane bilayer is indicated in gray. Reproduced from Chen *et al*., (2007) with the permission of the publisher.

are expressed constitutively in the cell, contributing significantly to the intrinsic resistance of bacteria (Murakami *et al*., 2006; Nikaido, 1998). They have an extraordinarily broad substrate range, and are able to transport a variety of toxic compounds including drugs such as chloramphenicol, aminoglycosides, erythromycin and tetracycline, organic solvents,

isoflavenoids, fatty acids, bile salts, and steroids (Fig. 2.4) (Lomovskaya *et al*., 2007; Saier and Paulsen, 2001; Zgurskaya and Nikaido, 2000). One of the most well-studied RND systems is AcrAB-TolC from *E. coli* (Li and Nikaido, 2004). AcrB is a transmembrane protein with 12 TMH, the functional unit of which is a trimer (Fig. 2.4) (Higgins, 2007). It is a member of the RND family, and is the component responsible for substrate binding and specificity (Murakami *et al*., 2006). RND transporters in gram-negative bacteria function with a periplasmic protein from the membrane fusion family, in this case, AcrA, and an outer membrane channel from the outer membrane factor family, in this case, TolC, to pump substrates across two membranes (Lomovskaya *et al*., 2007). It is interesting to note that RND systems have also been shown to export drugs from the periplasm and show synergy with single component pumps in order to enhance their effectiveness (Li and Nikaido, 2004; Tal and Schuldiner, 2009). Transport by AcrAB-TolC occurs by a peristaltic movement. Each of the three AcrB monomers has a binding site that alternates between three states sequentially: access, binding and release. The large binding site is lined by hydrophobic and aromatic amino acids, and also has two polar residues, Q176 and N274, which neutralize the charge of cationic substrates, likely by hydrogen bonding. It is thought that the aromatic residues interact with substrates by hydrophobic or stacking interactions. The substrate-binding site allows multisite binding, evidenced by the binding of both minocycline and doxorubicin to the same cavity, in different, but overlapping locations. Binding and extrusion of substrates is based on steric considerations; substrates are essentially squeezed out of the binding site by conformational changes induced by the movement of protons down the electrochemical gradient (Murakami *et al.*, 2006). Essentially, energy is transduced mediated by conformational changes from one domain to a another domain that then mediates drug transport through changes in the affinity and orientation of the binding site (Higgins, 2007).

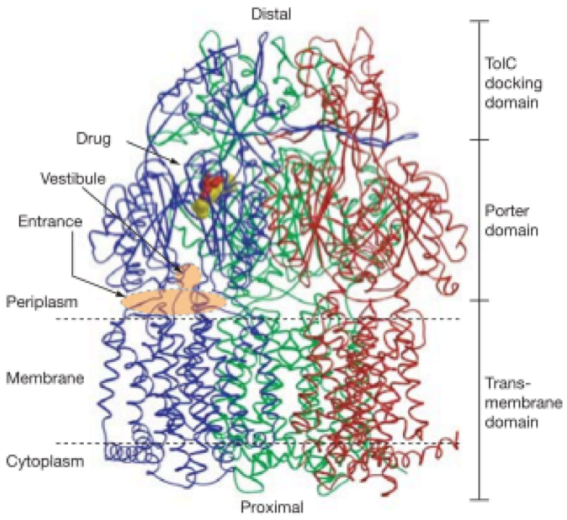

Figure. 2.4. Ribbon representation of the AcrB trimer. Bound substrate, minocycline, is indicated as "drug" in the figure. TolC and AcrA are not shown in this figure. Reproduced from Murakami *et al*. (2006), with the permission of the publisher.

Members of the MATE family are less well studied. They are represented by NorM of *Vibro parahaemolyticus* and confer resistance to multiple cationic agents, including fluoroquinolones, as proton and sodium antiporters (Kuroda and Tsuchiya, 2009). The use of a sodium gradient as an energy source is of biochemical interest (Kuroda and Tsuchiya, 2009).

All MDT substrate binding pockets, therefore, appear to have similar properties: a large, flexible binding cavity rich in polar and aromatic residues, which not only provides overlapping binding sites, but also allows for binding at different orientations and locations (Lewinson *et al*., 2006; Sennhauser *et al*., 2009). MDT are polyspecific: they interact with many dissimilar substrates with varying affinities, and do not interact with others at all (Lewinson and Bibi, 2001). Neyfakh explains multidrug binding elegantly. Briefly, proteins binding hydrophobic ligands do not have to compete with water molecules for substrate binding, as is the case with hydrophilic substrates. Comparable binding affinity can be achieved by simply creating a hydrophobic environment within the binding site, and this affinity can be enhanced by electrostatic attraction to charged residues within the site. In other words, for these proteins, ligand specificity is not an inherent property of the binding mechanism. Specificity would simply stem from the geometry of the binding site (Neyfakh, 2002). This agrees with other findings that for MDT, three factors affect binding: hydrophobicity, charge, and shape

(Zgurskaya and Nikaido, 2000). Indeed, most MDT substrates are hydrophobic and have at least one aromatic moiety (Fluman and Bibi, 2009). MDT from different families have overlapping substrate specificities and are inhibited by the same molecules; no family-specific resistance profile has been observed (Krulwich *et al*., 2005; Putman *et al.*, 2000). In fact, MDT mediated resistance is observed against all important classes of antibiotics (Putman *et al*., 2000).

The broad substrate specificity of MDT has raised questions about their effect on normal cellular metabolites. To date, evidence implicating MDT in the efflux of essential cellular metabolites has not been found, though this might simply be a result of the tight regulation of MDT and low endogenous expression levels (Fluman and Bibi, 2009; Li and Nikaido, 2004). It is important to note that most molecules normally present in the cytosol are too hydrophilic to bind with significant affinity to the hydrophobic binding site of an MDT (Fluman and Bibi, 2009). However, there is some evidence for the involvement of MDT in virulence, indicating that some MDT transporters do transport cellular products (Li and Nikaido, 2009). Furthermore, other MDT have been implicated in removal of excess toxic normal metabolites, and in alkalitolerance (Helling *et al.*, 2002; Krulwich *et al*., 2005; Lewinson *et al*., 2004). Thus it would seem that MDT have specific and beneficial effects in cellular processes in addition to their function in resistance.

The question of which effects of MDT represent true physiological functions, and which are simply opportunistic, has not yet been resolved. Studies of MDT at endogenous expression levels often show that they do not greatly alter the drug susceptibility profile of the bacterium (Fluman and Bibi, 2009). Since antibiotic resistance depends on genes that are either chromosomally encoded or encoded on mobile genetic elements, it has been proposed that these genes have been retained during evolution because MDT have primary functions that are unrelated to their drug extrusion capabilities (Krulwich *et al.,* 2005; Lewinson *et al.,* 2004; Lewinson *et al*., 2006; Neyfakh, 1997; Paulsen *et al.,* 2000). However, the fact that MDT are present in all kingdoms of life and are ancient suggests that organisms had to move lipophilic toxic chemicals all the time, and it is therefore possible that efflux of endogenous compounds is a trait that was acquired later in evolution (Li and Nikaido, 2004; Sköld, 2011). Many bacteria with large percentages of drug resistance pumps live in environments where natural biological warfare might be present, while others inhabit host species that produce chemicals toxic to

bacteria (Li and Nikaido, 2004; Li and Nikaido, 2009; Neyfakh, 1997; Paulsen *et al.*, 2000). While this debate is unlikely to be resolved in the near future, it is important to recognize that the clinical importance of MDT lies largely in providing a broad and effective resistance mechanism to bacterial pathogens (Markham and Neyfakh, 2001).

2.2. Structure and mechanism of MFS transporters

2.2.1 General features of MFS transporters

The MFS is a well-characterized, large and diverse superfamily that includes over 1000 members from all kingdoms (Saidijam *et al*., 2006). MFS proteins typically range in size from 400-600 amino acids, with 12-14 transmembrane helices (TMH) (Law *et al*., 2008). At the superfamily level, MFS members share low sequence similarity and are united only by a pair of conserved signature sequences, DRXXRR, at equivalent positions on the N- and C-terminal halves of the proteins (Law *et al*., 2008). The superfamily comprises 28 related families that catalyze substrate transport by uniport, symport, or antiport (Kaback *et al.*, 2001).

In bacteria, MFS proteins generally outnumber other membrane transporters (Saidijam *et al*., 2006). Transport is energized by a secondary energy source, either a proton, sodium, or other substrate gradient (Saidijam *et al*., 2006). Individual members of the MFS can show stringent specificity, yet as a group, the superfamily accepts an enormous diversity of substrate types including ions, sugars, nucleosides, drugs, amino acids, bile salts, and vitamins (Law *et al*., 2008; Saier, 2000). This phenomenon is readily explained by the observation that substitution of a few key amino acid residues in the substrate-binding site of several MFS proteins can change the specificity of the transporter while retaining the transport mechanism (Huang *et al.*, 2003).

Membrane proteins present a particular challenge to structural and functional studies due to their hydrophobicity, flexibility, and relative instability (Carpenter *et al*., 2008). However, diligent efforts have resulted in several well-characterized systems that help shed light on the general characteristics of the family. In fact, structural studies of MFS proteins show that even when sequence homology between individual transporters is low, the overall fold is conserved (Law *et al*., 2008; Sigal *et al*., 2005). Two model systems in the MFS are LacY and GlpT of *E. coli*. LacY is a 417 amino acid long symporter that catalyses the uptake of galactosides using the free energy released from the downhill translocation of protons

(Abramson *et al*., 2004). GlpT, a 452 amino acid long antiporter, exchanges glycerol 3-phosphate (G3P) for inorganic phosphate (P_i), using the P_i gradient as an energy source (Hayashi *et al*., 1964).

The first atomic resolution structures of MFS transporters, those of LacY and GlpT, were solved in 2003 (Fig. 2.5) (Abramson *et al*., 2003; Huang *et al.*, 2003). The structures revealed monomers with 12 TMH, with several α-helices protruding beyond the membrane surface on the cytoplasmic side (Fig. 2.5). Interestingly, both LacY and GlpT were solved in an inward facing conformation, revealing a large, hydrophilic internal cavity, open toward the cytoplasm, but completely closed from the periplasm (Fig. 2.5). The cavity is equidistant from both sides of the membrane, at the interface between two domains, one N-terminal and the other C-terminal (Abramson *et al.*, 2004; Abramson *et al*., 2003; Huang *et al.*, 2003). The N- and C-terminal domains consist of six-helix bundles, have the same topology, and are related by an approximate two-fold symmetry (Abramson *et al*., 2003; Huang *et al*., 2003).

Wild type LacY was mutated to trap this flexible protein into a single substrate-bound conformation. Thus the C154G mutant of LacY, which does not catalyze transport but binds substrate with high affinity, was solved in the presence of the lactose homolog, β-D-galactopyranosyl-1-thio-β-D-galactopyranoside (IPTG) (Fig. 2.5A). Its hydrophilic cavity is formed between helices I, II, IV, and V of the N-terminal domain, and helices VII, VIII, X, and XI of the C-terminal domain, while the remaining helices are embedded in the membrane. However, the sugar-binding site is only composed of helices I, IV, V, VII, and IX. Abramson and coworkers noted that a major portion of the substrate binding site involved in substrate specificity is on the N-terminal domain, while the residues involved in substrate binding affinity, but likely have little to do with specificity, are located in the C-terminal domain (Abramson *et al.*, 2003). R144 (helix V), E126 (helix IV), and E269 (helix VIII) all interact with various oxygen atoms on the galactopyranosyl ring (Fig. 2.6) (Abramson *et al.*, 2003; Nie *et al.*, 2006). W151 (helix V) is irreplaceable for sugar binding, and stacks hydrophobically

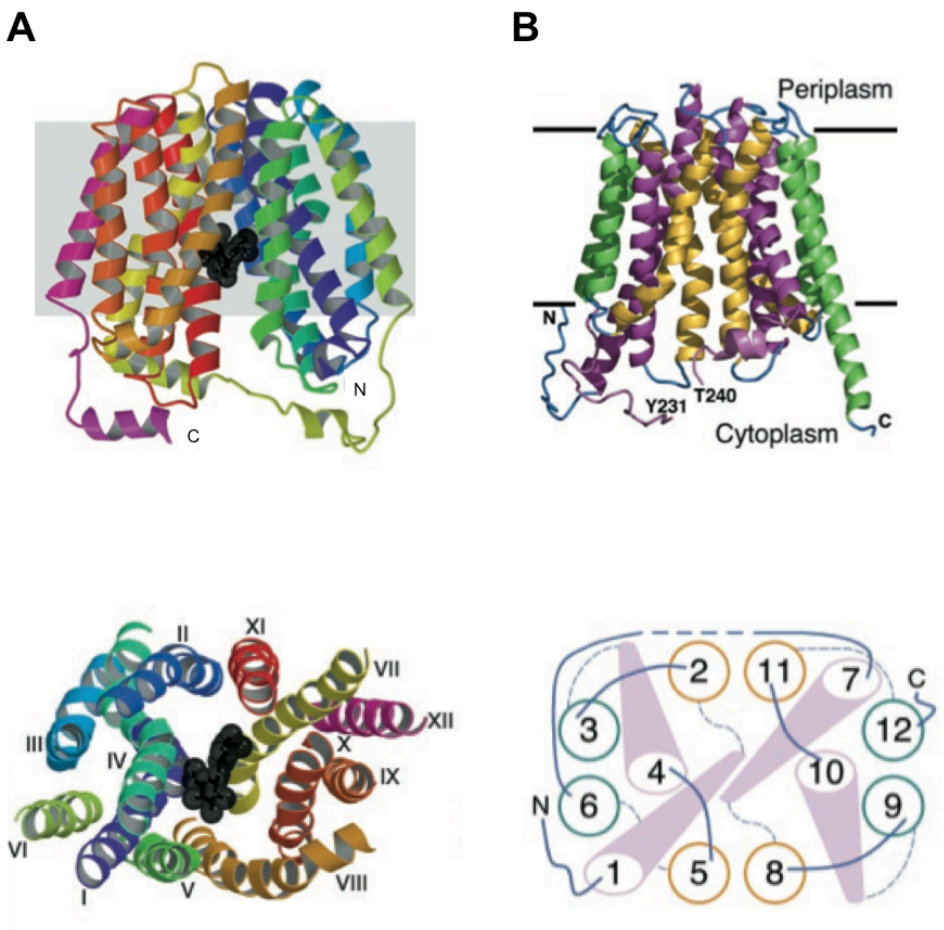

Figure 2.5. Ribbon representations of C154G mutant of LacY (A) and wild type GlpT (B). Both structures were solved in an inward-facing conformation. LacY was solved with IPTG, a lactose analog, bound (black). *Top,* both structures revealed N- and C-terminal α-helical bundles, with hydrophilic cavities located at the interface of the bundles. *Bottom,* helical organization of both proteins is the same, with the substrate binding sites formed by helices 1, 2, 4, and 5 (I, II, IV, and V) of the N-terminal bundle and 7, 8, 10 and 11 (VII, VIII, X and XI) of the C-terminal bundle. Substrate transport is proposed to occur by a rocker-switch mechanism that involves the rotation of these bundles to allow alternate access of the central cavity to either side of the cell membrane. Reproduced from Abramson *et al*. (2003) and Huang *et al*. (2003) with the permission of the publisher.

with the galactopyranosyl ring. Other important residues include H322 (helix X), E325 (helix X), R302 (helix IX), and W236; these are all thought to be involved directly in proton translocation. In fact, H322 may be the proton donor to E325, and R302 may interact with E325 to drive deprotonation (Fig. 2.6) (Nie *et al.*, 2006).

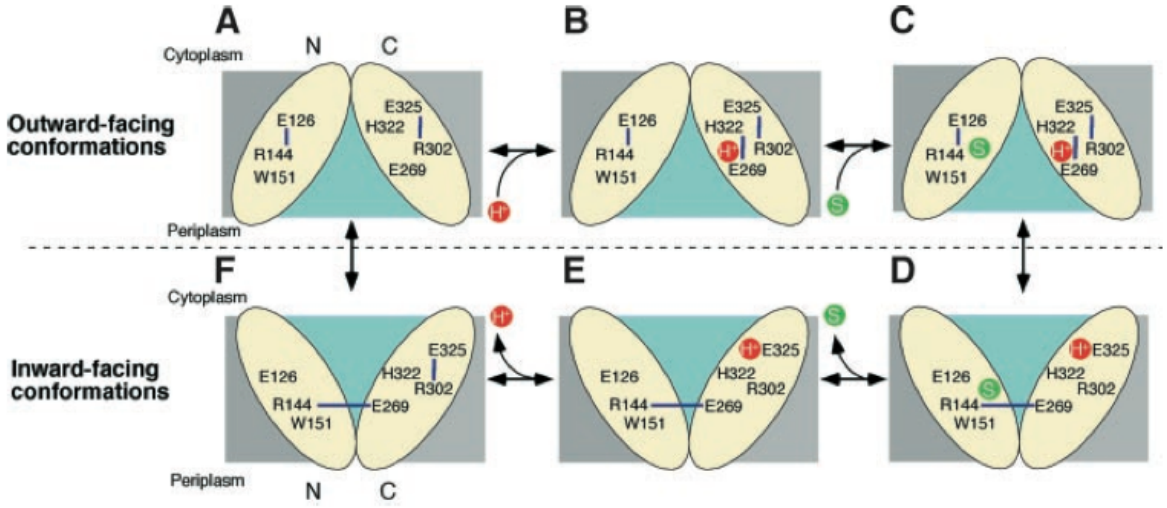

Figure 2.6. Putative mechanism of lactose transport by LacY. N- and C-terminal domains are shown as yellow ovals. Key residues are labeled; hydrogen bonds are shown as blue lines. The proton and the substrate are shown as red and green circles, respectively; the hydrophilic cavity is represented as a light blue area Reproduced from Abramson *et al.* (2003) with the permission of the publisher.

As in LacY, the hydrophilic cavity of GlpT is formed between helices I, II, IV, V, and helices VII, VIII, X and XI (Fig. 2.5B) (Huang *et al.*, 2003). However, since GlpT was not solved in its substrate-bound form, less is known about its binding site. Previous biochemical studies have indicated that substrate binding and transport are mediated by the phosphate moiety of G3P, suggesting a positive surface electrostatic potential in the GlpT substrate-binding site (Auer *et al.*, 2001; Huang *et al.*, 2003). Huang and coworkers therefore suggest that the substrate-binding site is located at the closed end of the central cavity in the middle of the membrane (Fig. 2.5B) (Huang *et al.*, 2003). Two positively charged residues, R45 and R269, are located at the proposed binding site, and docking experiments have confirmed that G3P is coordinated by these residues (Fig. 2.7) (Huang *et al.*, 2003; Lemieux *et al.*, 2004). While these residues are conserved in another bacterial sugar-phosphate/anion transporter, UhpT, these residues are generally not conserved in other MFS proteins, suggesting that they are specific to the sugar-phosphate/anion transporter subfamily (Auer *et al.*, 2001; Huang *et al.*, 2003).

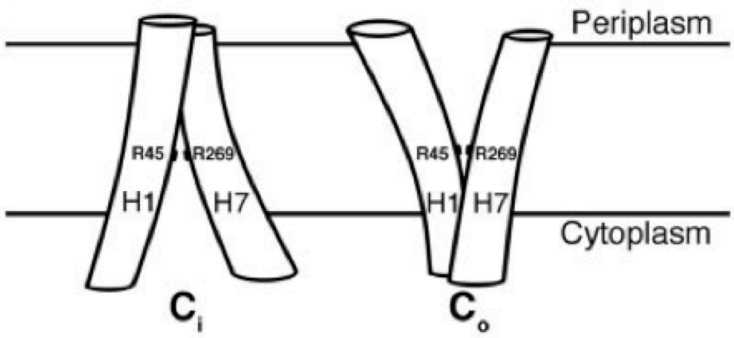

Figure 2.7. Schematic drawing of central helices H1 and H7 of GlpT in inward (C_i) and outward (C_o) conformations. Other helices are omitted for clarity. Rocker- switch–type movements of the helices that occur upon substrate binding allow the substrate-binding site, which comprises R45 and R269, to switch between the two sides of the membrane. Reproduced from Huang *et al.* (2003) with the permission of the publisher.

Since the hydrophilic cavity is located between the N- and C-terminal domains of both proteins, it is likely that the structural change between inward- and outward-facing conformations involves rotation between these domains around an axis parallel to the membrane. Biochemical data, in combination with the crystal structure, allowed for the production of a model of LacY in the outward-facing conformation. A ~60° rotation between the N- and C-terminal domains reveals conformations that allow for the substrate binding site to be alternatively accessible from both sides of the membrane. It is thought that tight closure of the binding site is obtained by flexibility in the helices lining the hydrophilic cavity (Abramson *et al*., 2003). Indeed, glycine and proline residues in these helices cause kinks and bends not found in helices that are not involved in substrate binding (Abramson *et al*., 2004; Abramson *et al.*, 2003). In contrast, the helices in GlpT are less distorted and do not have any kinks. However, superposition of the structures of LacY and GlpT show that some GlpT helices have bends in regions that overlap with the kinks in LacY. The bends in GlpT are also caused by a high glycine and proline content. It is thought that these irregular helices provide the structural flexibility required to catalyze transport by a rocker-switch mechanism (Abramson *et al.*, 2004).

The crystal structures of both LacY and GlpT suggest a rocker-switch mechanism of substrate transport (Fig. 2.5) (Abramson *et al*., 2003; Huang *et al*., 2003). In order to understand the transport mechanism, it is necessary to identify crucial side chains, delineate their function and relationship to one another, and acquire structural and dynamic information

at the level of helix packing in the context of ion binding and release, as well as interactions between ions and the substrate (Adam *et al*., 2007; Kaback *et al.*, 2001). A combination of molecular biological and structural techniques has provided some clues to the mechanism used by MFS transporters (Kaback *et al*., 2001; Law *et al.*, 2007). Substrate binding to both LacY and GlpT leads to widespread conformational changes that allow for transport (Law *et al.*, 2007; Nie *et al.*, 2006). Nevertheless, only a few residues appear to be involved in substrate binding and translocation (Kaback *et al.*, 2001; Nie *et al.*, 2006; Yerushalmi and Schuldiner, 2000).

Due to the reversibility of substrate transport by LacY, it has long been thought that the most likely trigger for turnover is substrate binding and dissociation on either side of the membrane (Fig. 2.8) (Kaback *et al*., 2001). Transport consists of six steps, as described in figure 2.8. The C154G LacY structure corresponds to step 4 in the transport cycle (Figs. 2.5A, 2.6D, 2.8). A comparison of the thermodynamics of substrate binding and transport catalysis by C154G and wild type (WT) LacY confirmed that the C154G mutant has tighter helix packing, providing an explanation for its increased thermostability, decreased tendency for aggregation, and inability to catalyze substrate transport. The N- and C-terminal domains in the C154G mutant cannot rotate against each other, thus preventing substrate transport. In fact, while both mutant and WT LacY have similar free energies of binding, the relative contributions of enthalpy and entropy vary greatly. C154G LacY has a large negative value of ΔH and a negative value of $T\Delta S$. A negative change in the entropic free energy component is related to H-bond formation, or a decrease in the number of isoenergetic conformations. In other words, a specific conformer of C154G LacY is selected from the ensemble of conformations upon substrate binding. This prevents the protein from overcoming the energy barrier to achieve the outward facing conformation. WT LacY, on the other hand, is a highly dynamic protein that experiences widespread conformational changes upon substrate binding. Given the increase in entropic free energy associated with substrate binding, it is likely that the number of conformers for ligand-bound WT LacY is greater than that of free protein. As a result, substrate-bound WT protein is able to catalyze transport by sampling different conformations. The critical interactions in this process are salt bridges alternatively formed between R144 and E126 and E269 (Fig. 2.6) (Nie *et al.*, 2006).

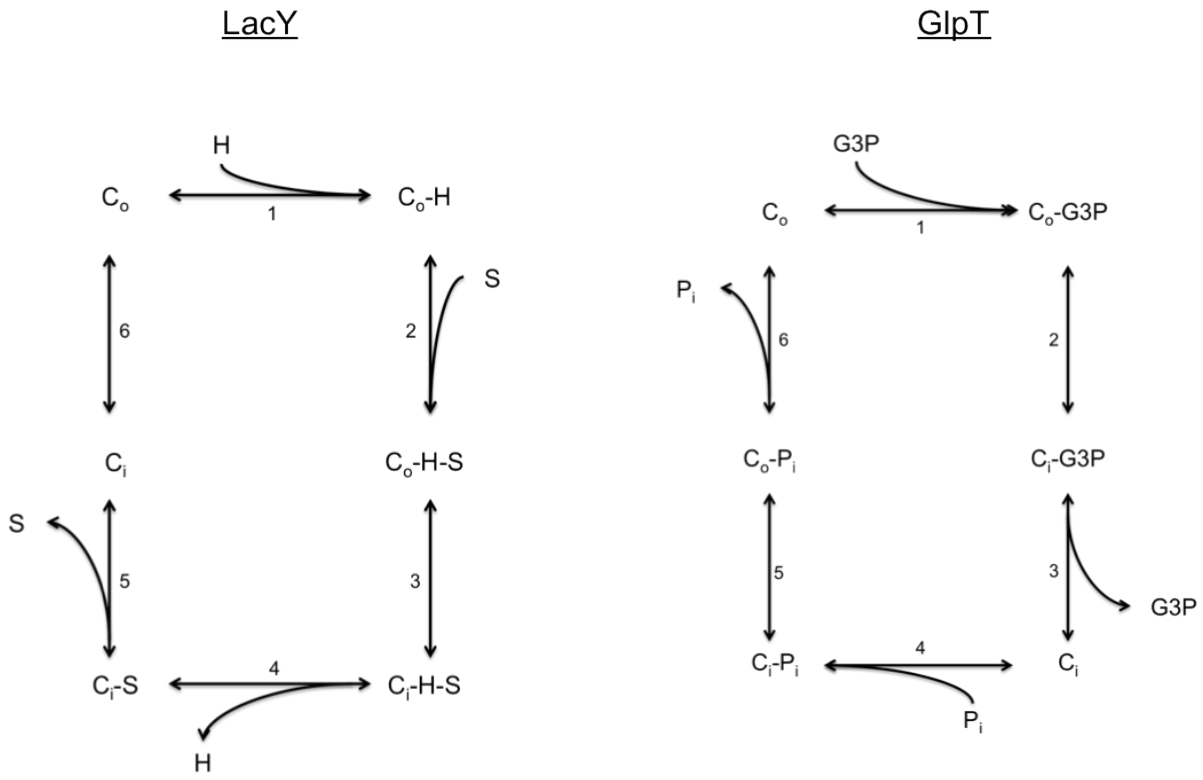

Figure 2.8. Substrate transport by LacY and GlpT. Both transporters are thought to transport substrates in six discrete steps, starting with the outward facing conformation (C_o). C_i refers to the inward, cytoplasm, facing conformation. LacY is a symporter that uses the proton gradient (H) to drive galactoside (S) transport into the cell in a 1:1 stoichiometric ratio. GlpT is an antiporter, and exchanges P_i for G3P.

Substrate transport by GlpT can also be broken down into six discrete steps (Fig. 2.8). The X-ray structure of GlpT corresponds to the inward, substrate-free conformation, step three in the transport cycle (Figs. 2.5B, 2.8). While structural data for the substrate-bound form is lacking, evidence from other studies provides insight into the antiport mechanism. Phosphate binding pulls R45 and R269 together, moving the N- and C-terminal domains closer and narrowing the cytoplasmic pore (Fig. 2.7) (Huang *et al*., 2003). Substrate binding further destabilizes the interface between the N- and C-terminal domains on the periplasmic side and allows tilting of the two domains to expose the substrate-binding site to the periplasm, yielding the outward-facing conformation (Lemieux *et al.*, 2004).

The GlpT and LacY structures and corresponding mechanisms have been proposed to be a paradigm for all MFS transporters. It is likely that all members of the MFS, be they

uniporters, sympoters, or antiporters, operate by lowering the energy barrier between inward- and outward-facing conformations by binding substrate. As a result, a substrate or ion gradient can drive transport for any of these processes (Lemieux *et al*., 2004).

2.2.2 Energetics of substrate transport by MFS transporters

Biological membranes have two complementary functions: first, to serve as a barrier for uncontrolled diffusion; and second, to provide channels and pumps for specific transport processes, such as ion and nutrient transport, toxin extrusion, and energy generation (Nelson, 2008). All living cells possess an energy-transducing membrane, composed of a phospholipid bilayer, and proteins, together with smaller amounts of associated carbohydrates (Nicholls, 1982; Stein, 1990). The essential feature of the lipid bilayer is that it has a hydrophilic exterior and a hydrophobic interior (Nelson, 2008). Energy-transducing membranes have an inherently high electrical resistance and can also withstand high electric fields (Nicholls, 1982). ATP synthase converts the energy of the electrochemical ion gradient into the chemical energy stored in the phosphoanhydride bond of the ATP molecule (Forrest *et al*., 2011; Nicholls, 1982). Proton or sodium pumps in the respiratory or photosynthetic electron transport chains replenish the ion gradients (Forrest *et al*., 2011; Nicholls, 1982). Maintaining the concentration of ATP in disequilibrium with its hydrolysis products, ADP and P_i, allows ATP to be used to do work in the cell (Nicholls, 1982).

The transport of most solutes across a membrane is catalyzed by membrane proteins (Abramson *et al*., 2003; Kaback *et al.*, 2001). Biochemical and phylogenetic analyses have revealed that up to 10% of total protein encoded in the bacterial and human genomes are transporters (Abramson *et al*., 2004). This is not surprising considering that biochemical pathways are dependent on a balance of transport reactions: the import of exogenous substrates and the export of metabolic end products (Paulsen *et al*., 2000). There are four main classes of transporters, classified on the basis of mode of transport and energy coupling source: channels, primary transporters, secondary transporters, and group translocators (Saier, 2000). Channels use facilitated diffusion through a transmembrane pore (Paulsen *et al*., 2000).

Primary and secondary active transporters use the energy of ATP or an ion electrochemical gradient, respectively, to catalyze the thermodynamically unfavorable transport

of a substrate against its electrochemical gradient (Abramson *et al*., 2004; Paulsen *et al.,* 2000; Saier, 2000). Primary carriers function for the pumping of a diverse range of substrates, including inorganic ions, vitamins, drugs, fatty acids and proteins (Saier, 2000). Secondary transporters are responsible for the transport of most organic solutes across biological membranes (Saier, 2000). Finally, group translocators phosphorylate substrates during transport (Paulsen *et al*., 2000).

Secondary transporters function by either symport, in which two or more molecular species are transported in the same direction across a membrane, or antiport, in which one or more molecular species are exchanged for one another across a membrane (Fig. 2.9) (Forrest *et al*., 2011; Saier, 2000). Surprisingly, all forms of secondary active transport can be understood in terms of the alternating access mechanism (Fig. 2.9) (Forrest and Rudnick, 2009). In this model, the substrate-binding site is alternately accessible to the cytoplasm and extracellular medium via an occluded state (Jardetzky, 1966; Padan *et al*., 2009). Jardetzky outlined three features of a transporter that operates via an alternating access mechanism: 1. The protein must contain a binding pocket in its interior, large enough to admit a small molecule; 2. The transporter must have the ability to assume two different conformations, such that the binding pocket is open to one side in one conformation and the opposite side in the other; and 3. The transporter must contain a binding site for the substrate in its binding pocket, the affinity of which is different in the two conformations (Fig. 2.9) (Jardetzky, 1966). The conformational change itself can be very minor, in some cases a change of only a few angstroms in helices relative to each other is sufficient to determine whether the binding site is open or closed (Forrest and Rudnick, 2009; Jardetzky, 1966).

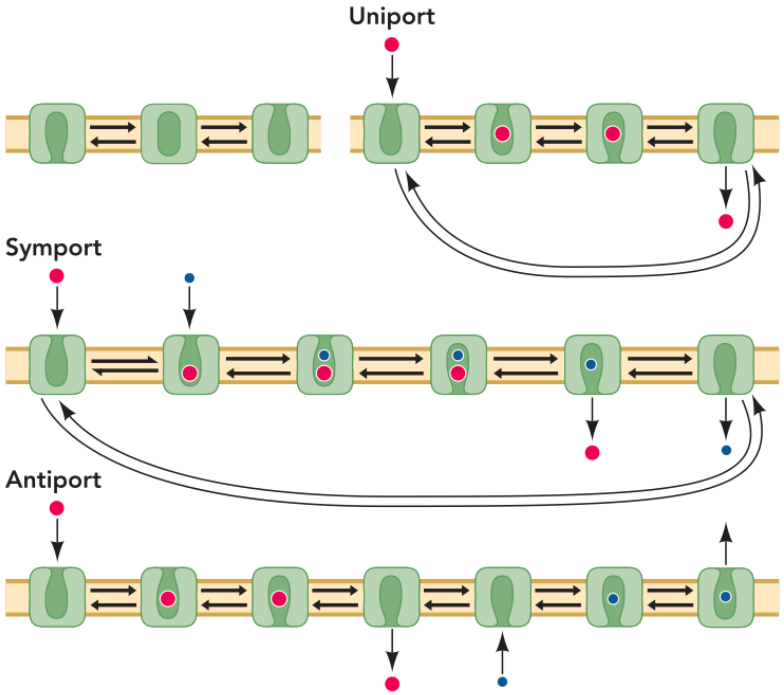

Figure 2.9. Alternating access mechanism of substrate transport. In each case, the substrate binding site is alternatively accessible to either side of the membrane via an occluded intermediate (top left). *Top right*. In uniport, a solute is transported from high to low solute concentration. *Middle and bottom, respectively*. In symport and antiport, the uphill transport of one solute is coupled to the downhill movement of another. Symporters catalyze the transport of solutes in the same direction, and cannot transition from alternately facing conformations with only one substrate bound. Antiporters catalyze the exchange of solutes from one side of the membrane to the other, and can only interconvert from one conformation to the other via a substrate bound form. Reproduced from Forrest and Rudnick (2009) with the permission of the publisher.

2.3. MdfA, a model for studies of MFS multidrug transporters

MdfA is a 410 amino acid *E. coli* multidrug transporter from the Major Facilitator Superfamily that is composed of 12 TMH (Fig. 2.10) (Edgar and Bibi, 1997). Cells overexpressing MdfA are resistant to a wide variety of structurally unrelated compounds including neutral, zwitterionic, and monovalent cations, such as chloramphenicol (Cml), ethidium bromide (EtBr), and TPP^+ (Edgar and Bibi, 1997; Lewinson *et al.*, 2006; Mazurkiewicz *et al.*, 2005). MdfA is restricted to a transport stoichiometry of one drug molecule per proton, and is essentially inactive toward divalent

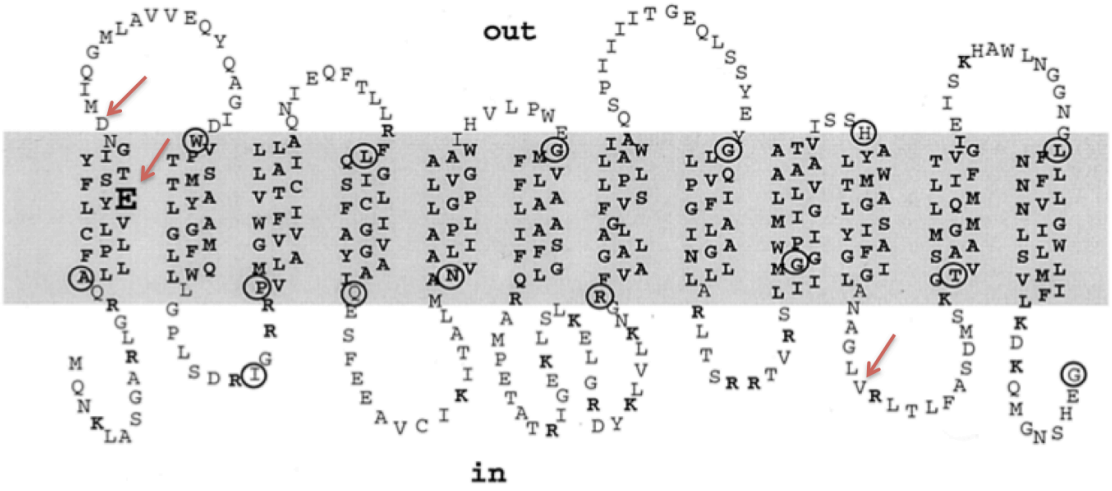

Figure 2.10. Secondary-structure model for MdfA based on the hydropathy profile and the distribution of positively charged residues (indicated in boldface type). E26, D34, and V335 are indicated by red arrows. Reproduced from Adler and Bibi (2002) with the permission of the publisher.

cations (Fluman and Bibi, 2009; Mazurkiewicz *et al*., 2005). MdfA also has a low affinity Na^+ (K^+)/H^+ antiport activity, and confers alkalitolerance up to pH 10, providing a potential answer to the debate over MdfA's physiological role in *E. coli* (Lewinson *et al*., 2004). Interestingly, MdfA is promiscuous not only in its substrate profile, but also in its use of components of the proton motive force, ΔpH and Δψ. In cases where the substrate transported is neutral, MdfA catalyzes an electrogenic reaction, while in cases where the substrate is charged, the reaction is electroneutral (Lewinson *et al.*, 2003). The exact mechanism of substrate transport remains to be elucidated, and the understanding thereof has been hindered by the lack of three-dimensional structural information (Sigal *et al*., 2005). However, the crystal structure of EmrD, a homolog of MdfA (26% identity and 39% similarity) was recently solved, and provides some insight into the binding pocket of MdfA (Yin *et al*., 2006).

EmrD is a 394 amino acid *E. coli* multidrug transporter from the Major Facilitator Superfamily. The EmrD structure was solved in the intermediate occluded state, in which the substrate-binding site is not accessible from either the cytoplasm or periplasm (Fig. 2.11). The outer helices of EmrD are organized similarly to LacY and GlpT (Fig. 2.11) (Yin *et al*., 2006). Toward the interior of EmrD, computer simulations have shown that proline and glycine residues contribute to helix flexibility, a characteristic reminiscent of LacY and GlpT

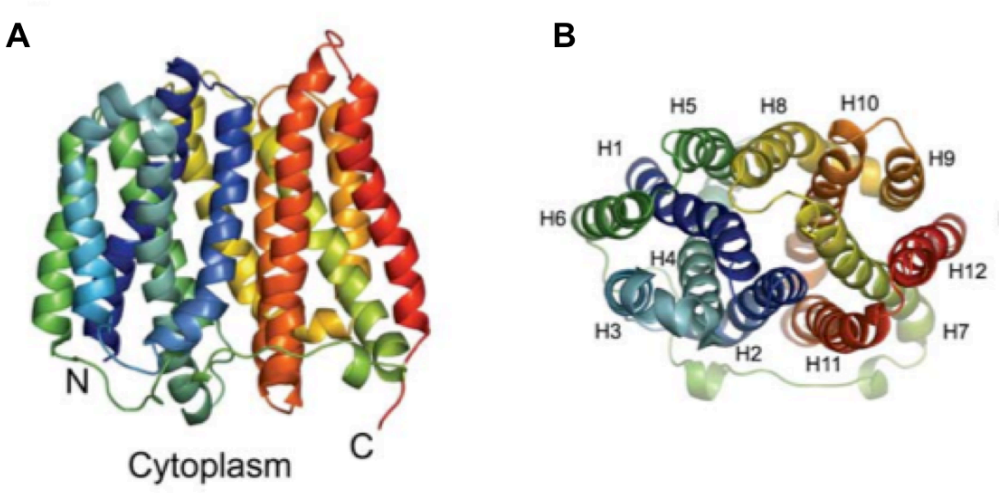

Figure 2.11. Ribbon representation of EmrD. A. Side view of EmrD, with N- and C-termini indicated. B. Helical organization of EmrD as viewed parallel to the membrane. Reproduced from Yin *et al.* (2006) with the permission of the publisher.

(Abramson *et al*., 2003; Baker *et al*., 2012; Huang *et al*., 2003). The interior cavity, which is the presumed substrate-binding site, is large, flexible, and hydrophobic (Baker *et al.*, 2012; Yin *et al*., 2006). It contains several bulky and aromatic residues, uncharged polar residues, and a single basic residue, R118. Yin and co-workers proposed that the hydrophobicity of the binding site may contribute to a general mechanism of substrate transport, and that steric and aromatic interactions are more directly related to drug specificity (Yin *et al.*, 2006). It is also thought that two pairs of stacked aromatic groups, Y52 and Y56, and W300 and F249, play key roles in multisubstrate binding. The biochemistry of EmrD has not been well studied; as a result, it is challenging to draw further conclusions regarding substrate recognition and binding (Baker *et al*., 2012; Yin *et al.,* 2006).

Nevertheless, this data supports other studies indicating that MdfA has a large binding pocket, which is capable of binding multiple substrates simultaneously (Mazurkiewicz *et al*., 2005; Sigal *et al*., 2005). Evidence also suggests that MdfA is capable of binding hydrophobic substrates from the inner leaflet of the cytoplasmic membrane (Adler and Bibi, 2004; Krulwich *et al.*, 2005). In both EmrD and MdfA, charged residues on the cytoplasmic end of TMH-4 are involved in substrate recognition from the inner leaflet of the membrane (Adler and Bibi, 2004; Baker *et al*., 2012; Yin *et al*., 2006). Transport of cationic drugs by MdfA appears to be dependent on E26, a membrane-embedded negatively charged residue in TMH-1 (Lewinson *et*

al., 2006). E26X mutants can have their cation-transport function restored by substituting a negatively-charged residue for V335 (Adler and Bibi, 2005). Site-directed mutagenesis experiments showed that residues S321, Y323, R336, F340, R112, and D132 are also involved in substrate recognition; however, their exact functions remain unclear (Adler and Bibi, 2002; Adler and Bibi, 2005; Sigal *et al*., 2005).

2.4. Characterization of membrane proteins

2.4.1 Purification and functional reconstitution of transport membrane proteins

Membrane protein structural and functional characterization is limited by the challenges associated with obtaining milligram quantities of pure, monodisperse membrane protein (Newby *et al.*, 2009; Ostermeier and Michel, 1997). The generalized approach to overexpression and purification of a target membrane protein is overexpression of the target protein, followed by cell membrane isolation, membrane solubilization, and, finally, protein purification (Newby *et al.*, 2009).

Generally, bacterial membrane proteins can be successfully expressed in *E. coli* (Carpenter *et al.*, 2008). Affinity tags are attached to the target protein by gene fusion, adding specific properties that can be used for protein purification via affinity chromatography (Arnold, 1991; Padan, 2003). A frequent problem with membrane protein overexpression is misfolding and protein aggregation in the form of inclusion bodies. Several tools exist to fight these challenges. Cell growth and protein expression can be performed under reduced temperatures, or molecular chaperones can be used to assist in protein folding (Baneyx, 1999). Fine-tuning expression levels using promoters such as the *ara* promoter allows for the optimization of expression while minimizing protein aggregation (Guzman, 1995).

Cells are harvested by centrifugation and lysed, generally, by mechanical disruption using a cell disrupter or sonicator. Cell membranes are isolated by ultracentrifugation of the cell lysate (Newby *et al.*, 2009). Membrane proteins are then extracted from the cell membrane by the addition of detergents, amphipathic molecules comprising a polar head group and a hydrocarbon tail, which allow solubilization by covering the hydrophobic surfaces of the protein (Fig. 2.12) (Carpenter *et al.*, 2008; Ward *et al.*, 2001). At the critical micelle concentration (CMC), detergent monomers aggregate, via hydrophobic effects, to form ordered structures into which membrane proteins can insert to create a protein-detergent complex

(PDC) (Ward *et al.*, 2001; Wiener, 2004). The CMC is characteristic of each detergent, but is also affected by the composition of the solvent (e.g. ionic strength) and temperature (Von Jagow *et al.*, 2003; Wiener, 2004). Detergents can be classified into three categories: ionic, which carry a net charge associated with their head group; non-ionic, which have uncharged hydrophilic head groups; and zwitterionic, which have both positive and negative charges but carry no net charge (Ward *et al*., 2001). As a rule of thumb, the head group of a detergent tends to have a strong effect on the interaction of the detergent with the protein, while the length of the alkyl chain affects the detergent CMC, and aggregation number. As a result, detergents with a larger head group and longer alkyl chain tend to be milder, and have lower CMCs. An additional consideration is the charge on the head group, with neutral head groups being gentler detergents, and less likely to denature the protein (Privé, 2007). Identifying the detergent most suitable for the purification of a particular protein target is an empirical process (Hunte, 2003; Newby *et al.*, 2009). One detergent may be optimal for solubilization and purification, whereas another may be best suited for structural studies (Hunte, 2003). The ideal detergent extracts all the target protein from the membrane, maintains its native fold, and forms a PDC that is stable throughout purification and characterization (Newby *et al*., 2009; Ward *et al.*, 2001). Cell membranes are incubated with the detergent, and then ultracentrifuged to recover the solubilized material (Ward *et al*., 2001).

This solution is then applied to an affinity chromatography column, and purified. These systems are designed to be highly specific and fast, allowing protein purifications with high-yield, and high-enrichment, often under mild-purification conditions. The ideal tag should not affect the activity or structure of the protein of interest, or interfere with targeting, folding, or membrane insertion (Padan, 2003). A variety of different affinity tags exist (eg. *His*-tag, *Strep*-tag, *Flag*-tag, etc), but by far the most widely applied tag is the His_6-tag (Padan, 2003; Ward *et al*., 2001). This tag is small and should not decrease expression levels or have a deleterious effect on protein folding or membrane insertion (Ward *et al*., 2001). Immobilized metal-affinity chromatography beads, loaded with transition metal ions such as Ni^{2+}, can be used to purify the tagged protein. The protein of interest binds to the resin by interaction of the histidine imidazole groups with the free ligand binding sites in the coordination sphere of the metal ions, unbound protein is washed off, and the target protein can be eluted by adding free imidazole to the elution buffer or by altering the pH. Nickel chromatography is also

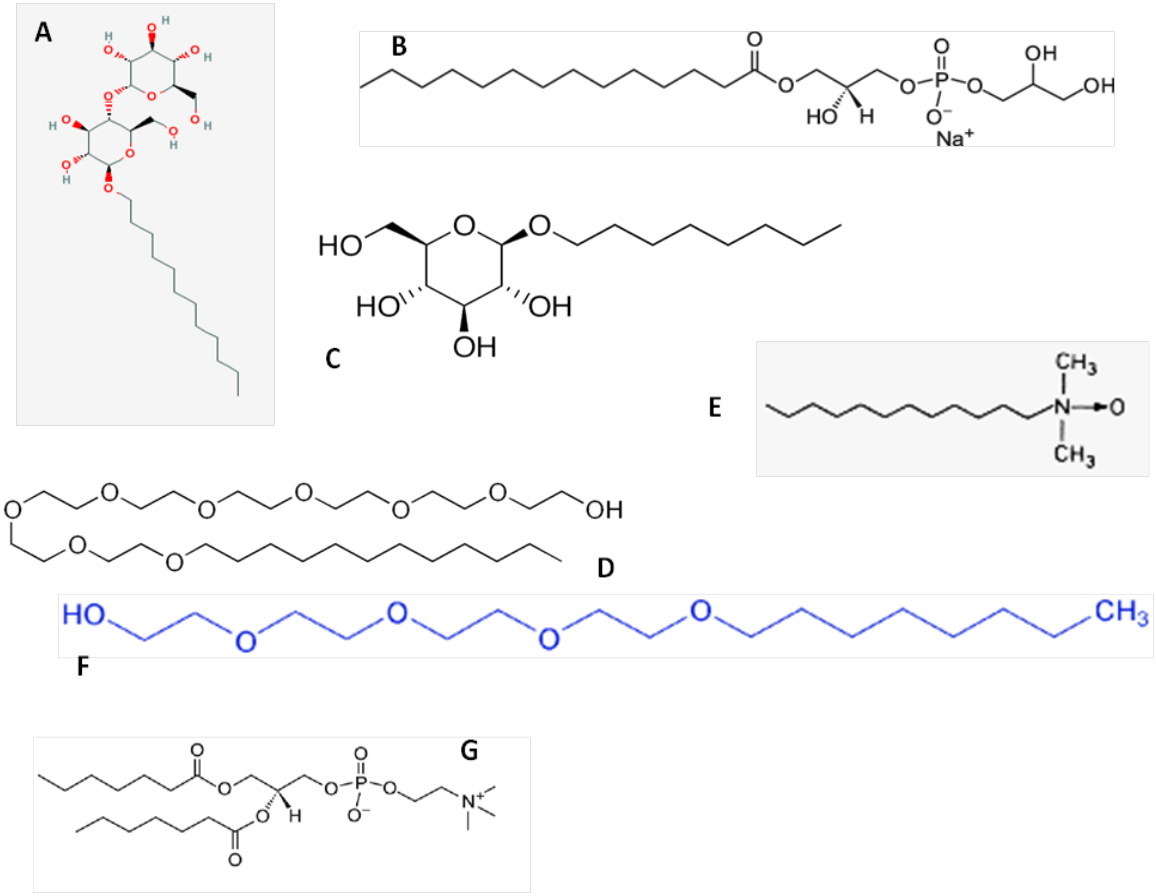

Figure 2.12. Structures of some detergents listed in Table 1 (Section 2.4.4), including 1-myristoyl-2-hydroxy-*sn*-glycero-3-[phospho-*rac* -1-glycerol)] (LMPG) and 1,2-diheptanoyl-*sn*-glycero-3-phosphocholine (DHPC). A. N-dodecyl-β-D-maltopyranoside (DDM). B. LMPG. C. N-octyl-β-D-glucopyranoside (OG). D. Dodecyloctaoxyethylene ($C_{12}E_8$). E. N,N-dimethyldodecylamine (LDAO). F. octyltetraoxyethylene (C_8E_4). G. DHPC.

successfully used for membrane protein purification (Newby *et al.*, 2009; Padan, 2003). This method allows 100-fold enrichments in a single purification step and up to 95% purity of the tagged protein. Furthermore, the matrices tolerate the presence of detergents (Padan, 2003). Optimization of the column purification can be achieved by adjusting the number of imidazole wash steps, and the concentration of imidazole used (Newby *et al*., 2009). In addition, since antibodies to the hexahistidine tag are commercially available, the purification steps can be easily monitored by Western blotting of the chromatography fractions and the resin to ensure that no protein is lost (Newby *et al*., 2009; Ward *et al.,* 2001). Additional purification using

size-exclusion chromatography and/or ion-exchange chromatography can be performed, but is not always necessary (Newby *et al*., 2009).

In order to determine if a membrane transporter has been purified in its native, active form, functional reconstitution into an artificial lipid membrane is required (Geertsma *et al*., 2008; Picard *et al*., 2012; Rigaud and Levy, 2003). Four general physical and chemical techniques for the insertion of membrane proteins into liposomes exist: mechanical means (e.g. sonication), freeze-thawing, organic solvents, and detergents (Rigaud and Levy, 2003). Of these, detergent-mediated protein reconstitution is the most successful and frequently used strategy, since most membrane proteins are isolated and purified using detergents. Reconstitution is achieved by first co-solubilizing the proteins and pre-formed liposomes in the appropriate detergent in order to form an isotropic solution of lipid-protein-detergent and lipid-detergent micelles. Detergent is then removed, resulting in the progressive formation of bilayer vesicles with incorporated protein. The detergent can be removed by dialysis, adsorption onto polystyrene beads, gel chromatography, or dilution (Rigaud *et al.,* 1995). The focus of this discussion will be on protein reconstitution using either dialysis or hydrophobic resin techniques, as these are the two methods used in this project.

Dialysis has been the most widely used method for detergent removal. Briefly, the lipid-protein-detergent micellar solution is placed in a cellulose membrane bag with a cutoff of 14 kDa, and dialyzed against a large volume of detergent-free buffer. Only detergent monomers diffuse through the dialysis membrane. Its main advantages are its simplicity, low cost, and the homogenous size dispersion of the resulting proteoliposomes. However, this technique can also have some disadvantages, namely poor reproducibility, an uncontrolled rate of dialysis, possible molecule retention on the dialysis membrane, and the duration of the experiments (Rigaud and Levy, 2003). Despite this, dialysis has been successful in the reconstitution of a variety of secondary transporters, including LacY and GlpT (Poolman and Konings, 1993).

Detergents that cannot be readily removed by dialysis can be removed by hydrophobic adsorption onto polystyrene resins such as Bio-Beads SM-2 (BioRad) and Amberlite XAD (Sigma-Aldrich) (Rigaud and Levy, 2003). In the batch procedure, Bio-Beads SM-2 are directly added to the protein-lipid-detergent mixtures, and replaced as needed (Rigaud and Levy, 2003; Venturi, 2003; Xie *et al.,* 2004). This method is predicted to be successful for the

removal of most detergents; however, its major limitation is the potential of lipid adsorption onto the beads (Rigaud and Levy, 2003).

Detergent-mediated protein reconstitution into liposomes can yield proteoliposomes of varied number of lipid layers, size, and protein distribution, depending on the nature of the detergent, the particular detergent-removal procedure, the nature of the protein, and the lipid composition. As a result, developing a reconstitution protocol is largely empirical (Rigaud and Levy, 2003). In addition to selecting an appropriate detergent-removal technique, several other criteria must also be considered for optimization of the proteoliposomes in membrane protein studies: the integrity and activity of the reconstituted protein, the morphology and size of the proteoliposomes, the homogeneity of their size and protein distribution, the number of protein units incorporated, the final orientation of the incorporated protein, and the permeability of the proteoliposomes (Rigaud *et al.*, 1995). Optimal protein distribution is achieved by varying the protein:lipid ratios used for reconstitution, and protein incorporation efficiency is tested by a sucrose density gradient (Rigaud and Levy, 2003; Rigaud *et al*., 1995). Unilamellar proteoliposomes of homogenous size are usually achieved by extrusion through a polycarbonate filter (Macdonald *et al.*, 1991).

2.4.2 Transport assays

Initial characterization of transport proteins can be performed in crude cell membrane vesicles to determine the general substrate profile of a transporter, but for a more detailed analysis, a defined system with pure protein is required in which parameters can be varied systematically (Geertsma *et al*., 2008). Transport of substrates or inhibition is studied *in vitro* using purified protein reconstituted into liposomes, as described in section 2.4.1 (Geertsma *et al*., 2008; Xie, 2008). Most bacterial transport systems show good transport activity when reconstituted in lipid mixtures of 3:1 *E. coli* total lipids and egg phosphatidylcholine; however, *E. coli* total lipids alone have also been used successfully (Chao and Fu, 2004; Poolman *et al*., 2005).

Transport assays require substrate or an energy source to initiate transport, as well as a means of detecting substrate translocation across the membrane (Picard *et al*., 2012; Xie, 2008). Traditionally, isotopically-labeled substrates are used to measure substrate uptake into liposomes (Xie, 2008). For example, to examine the kinetic mechanism of the lactose transport

system, LacS, of *Streptococcus thermophilus*, ^{14}C- and ^{3}H-labeled lactose and galactose were used as substrates. The system was driven using the proton motive force: ΔpH was generated by using internal and external buffers with different pH values, while Δψ was generated using valinomycin, a potassium-selective ionophore. The assay was started by the addition of the substrate, samples were withdrawn at selected time intervals, and then diluted and washed with buffer without substrate. The amount of transported substrate was determined by liquid scintillation counting of the collected samples (Foucaud and Poolman, 1992).

The basic assay described above can be modified as needed for a given transport system. Another study, which also used radiolabeled substrates, investigated the transport mechanism of the vesicular glutamate transporter, VGLUT2 (Fig. 2.13). Glutamate transport by VGLUT2 is driven by the membrane potential (positive inside). As a result, the researchers co-reconstituted VGLUT2 and the bacterial F_oF_1-ATPase into preformed liposomes, and generated Δψ by proton transport into the liposome lumen upon the addition of ATP (Juge *et al*., 2006).

On the other hand, radiolabeled substrates are not always readily available, and such experiments have distinct limitations. To this end, it is often useful to test the transport reaction by using a fluorescent indicator that can indirectly probe transport, or to couple the substrate transport to an enzymatic reaction that can be detected spectroscopically (Heuberger and Poolman, 2000; Lewinson *et al*., 2003). Heuberger and co-workers developed a coupled assay to test the putative xyloside-transporter, XylP, using a homologous, and well-characterized, transporter, LacS. LacS-reconstituted liposomes were pre-loaded with pyrroloquinoline quinone-dependent aldose dehydrogenase. Oxidation of sugars transported into the liposome by LacS would lead to the reduction of pyrroloquinoline quinone, followed by reoxidation by the artificial dye, 2,6-dicholorindophenol and phenazine methosulfate. The reduction of 2,6-dichlorindophenol can be followed spectrophotometrically at 600 nm with high sensitivity. The authors of this study point out an advantage: as opposed to experiments with radioactive substrates, here the reactions can be followed in real-time, data sampling is continuous, and that high external substrate concentrations can also be used (Heuberger and Poolman, 2000).

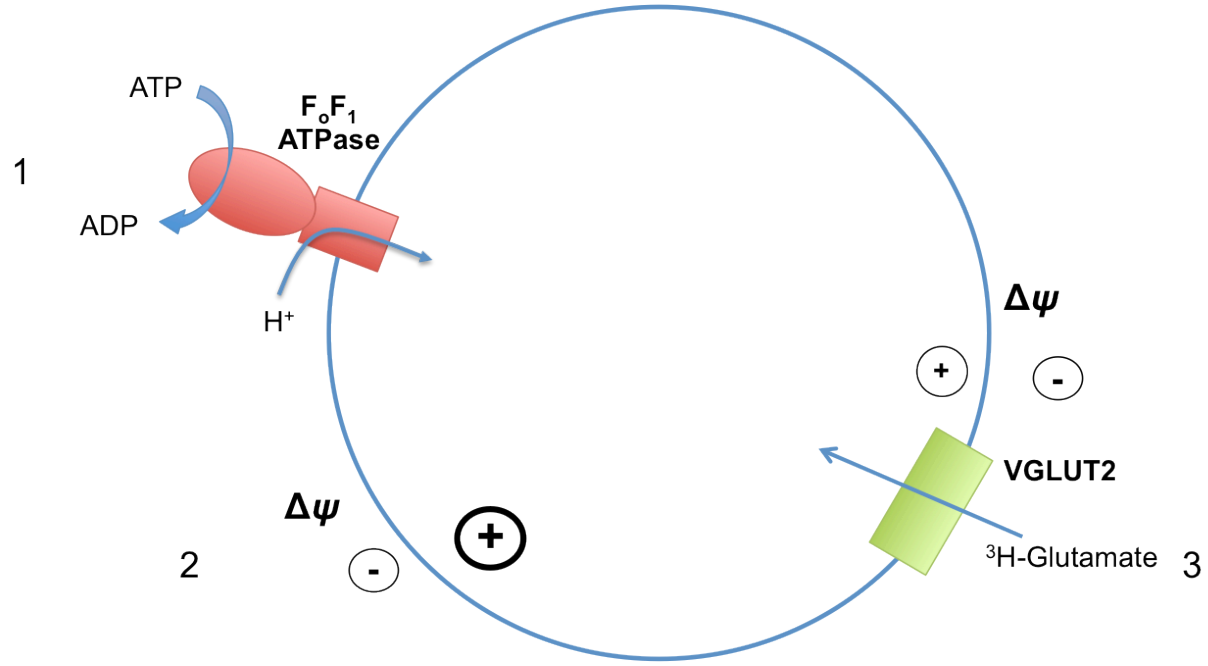

Figure 2.13. Illustration of VGLUT2 activity assay. VGLUT2 and F_oF_1 ATPase were co-reconstituted into liposomes. The addition of ATP (1) causes protons to be actively pumped into the liposome lumen by hydrolysis of ATP to ADP, creating a positive-inside membrane potential (2). ^{3}H-Glutamate is transported into the liposome, and partially relieves the membrane potential (3). At desired time points, the liposomes were separated from the assay mixture and the radioactivity of the buffer was measured in order to determine the amount of substrate transported (Juge *et al.*, 2006).

Indeed, for members of the MFS, changes in pH or Δψ can be used as indirect indicators of substrate transport across a membrane. Fluorescent probes such as 9-amino-6-chloro-2-methoxyacridine (ACMA) or oxonol V, which are sensitive to ΔpH or Δψ, respectively, are especially useful in this regard. As a proton gradient or electrical potential is generated, fluorescence is quenched. Transport is observed by an increase in fluorescence upon the exchange of substrate for protons (Lewinson *et al.*, 2003). Indirect assays are especially important if the substrate profile of the transporter is not well characterized.

2.4.3 Application of NMR spectroscopy to drug binding studies

NMR can be used to obtain physical, chemical, and structural information about molecules. The NMR spectra reflect the electronic environment of a nucleus, which produces a measureable change in nuclear resonance frequency characterized by the chemical shift (Nelson, 2003). As a result, NMR spectroscopy can be used to monitor and measure the

interaction between ligands and proteins (Meyer and Peters, 2003; Xie, 2008). Membrane proteins pose a variety of challenges for NMR-based ligand screening since they require a membrane-mimetic environment, such as detergent micelles, in order to maintain stability and function. Detergents add to the molecular weight of the protein, increase the viscosity of the solution, overlap with protein signals, modulate protein dynamics and conformational exchange, as well as compromise sensitivity by adding highly intense background signals (Yanamala *et al*., 2010). While minimizing the size of the detergent micelle can improve NMR spectra, this is not always the case, and does not ensure a functional protein (Warschawski *et al.*, 2011).

The reversible binding reaction, P + L = P*L, is characterized by the dissociation constant, K_d = [P][L]/[P*L], where P refers to free protein, L refers to free ligand, and P*L refers to the protein-ligand complex. K_d is a measure of binding affinity. Protein-ligand interactions can be observed by NMR by chemical shift and/or linewidth changes. Either the protein or the ligand can be observed, as long as it is labeled with NMR-active isotopes such as ^{13}C and/or ^{15}N (Meyer and Peters, 2003; Xie, 2008).

Changes in linewidth indicate the overall relaxation time of the molecule; that is, as the relaxation time decreases, the linewidth broadens. Relaxation times and the size of the molecule are directly related: larger molecules have shorter relaxation times (Doucleff, 2011). Therefore, free ligand has long relaxation times, and relatively narrow linewidth, while bound ligand has a shorter relaxation time, and broader linewidths.

Ligand binding to the protein can result in changes in chemical shifts and relaxation parameters, which can be observed by NMR. Chemical shift perturbations are either observed as the appearance of a separate peak corresponding to the protein-ligand complex (slow exchange), or a single peak that changes in chemical shift as more ligand or protein is titrated (fast exchange) (Zartler *et al.*, 2003). In other words, in slow exchange systems where the reporter group is on the ligand, separate peaks are observed for L and P*L. Slow exchange indicates tight binding, and K_d cannot be calculated in this case (Evans, 1995). However, for fast exchange, the observed chemical shift is the weighted average of the chemical shifts of the free and bound ligand states: both L and P*L are observed in one peak (Zartler *et al*., 2003). In this case, K_d can be determined from the chemical shift changes. For the reversible reaction P+L = P*L at equilibrium, the chemical shift of the reporter group in L is δ_L and the chemical

shift of the same reporter group in P*L is δ_{P*L}. The observed chemical shift, δ_{obs}, will be a weighted average of the chemical shifts of P and P*L: $\delta_{obs} = \delta_P \times [P]/([P]+[P*L]) + \delta_{P*L} \times [P*L]/([P]+[P*L])$. The ligand binding constant, K_d, can then be determined from the chemical shift titration curve given that $K_d = [P][L]/[P*L]$ and $[L]+[P*L]=L_{total}$, where L_{total} and δ_L are known (Evans, 1995). In contrast to chemical shift perturbations, changes in relaxation times cannot be observed directly; as a result, slow and fast exchange models have to be fitted to the measured linewidths, which can complicate the extraction of binding parameters (Meyer and Peters, 2003; Xie, 2008). In order to accurately distinguish between the affinity of ligand for protein, and binding site saturation, it is critical to use excess ligand for these studies (Zartler *et al.*, 2003). When observing ligand signals, it is important to distinguish whether signal changes are caused by ligand-detergent interactions or ligand-protein interactions; a reference spectrum is thus required (Yanamala *et al*., 2010).

Signal overlap in binding studies can be significantly reduced by using heteronuclear single quantum coherence (HSQC) experiments (Meyer and Peters, 2003; Yanamala *et al*., 2010). This is especially powerful for ligand screening and kinetic studies, where chemical shift perturbations of ^{15}N-labeled protein in ^{1}H,^{15}N-HSQC experiments can be more easily observed than one-dimensional proton spectra (Meyer and Peters, 2003; Shuker *et al.*, 1996). On the other hand, known ligands can also be labeled with NMR-active isotopes such as ^{15}N and ^{13}C and isotope-edited ^{1}H-NMR experiments can be used to detect ligand-protein interactions. The resulting spectra are one-dimensional proton spectra that correspond to the isotope used (Derrick *et al*., 1992). Chemical shift perturbations or linewidth broadening corresponding to protein binding of ligand is detected as with any other NMR experiment (Derrick *et al*., 1992; Zartler *et al*., 2003).

NMR can also be used for tertiary structure determination of proteins, but it has serious limitations that hinder its widespread application to the structural biology of membrane proteins. For multidimensional NMR experiments, samples must be labeled with NMR-sensitive isotopes, such as ^{13}C and ^{15}N. Labeling protein samples occurs during protein expression, and if the protein yield is low, as it generally is with membrane proteins, isotope labeling can be prohibitively expensive (Fernandez and Wuthrich, 2003). Cell-free synthesis of the protein of interest can lower costs, but is not a widely used technique (Basting *et al.*, 2006). As with any studies of membrane proteins, selection of a detergent, which simultaneously

maintains native structure and function and yields high quality NMR spectra, is largely a trial and error process. In addition, some proteins can bind up to twice their weight in detergent, adding to their size. Since large molecules tumble more slowly in solution, the resulting spectra are often poorly resolved and not amenable to structure determination studies (Sanders and Sonnichsen, 2006). For helical membrane proteins, three main challenges exist: 1. Low spectral dispersion that impedes resonance assignments; 2. A limited set of long-range distance constraints; and 3. Unstable tertiary folds that can enlarge linewidth (Lacapere *et al*., 2007; Sanders and Sonnichsen, 2006). Particular solution NMR techniques such as transverse relaxation-optimized spectroscopy can yield more useful spectra, and have applications to proteins ranging in size from 50-900 kDa (Fernandez and Wuthrich, 2003). Unfortunately, solid state NMR, particularly useful for beta-barrel membrane proteins, is presently limited to single or double spanning transmembrane proteins due to low spectral dispersion (Basting *et al.*, 2006; Lacapere *et al*., 2007). As a result, though it is extremely difficult to obtain high quality crystals of membrane proteins, X-ray crystallography remains the method of choice for high resolution structure determination of helical membrane proteins, and especially of MFS type transporters (Lacapere *et al*., 2007; Sanders and Sonnichsen, 2006).

2.4.4 Membrane protein crystallography

Tertiary structure of proteins can be visualized by X-ray crystallography. Briefly, protein crystallography entails growing high-quality crystals of purified protein, and measuring the directions and intensities of X-ray beams diffracted from the crystals (Lattman and Loll, 2008; Rhodes, 2000). The resulting diffraction pattern is collected, and a three-dimensional structure is calculated and refined using computer analysis (Lattman and Loll, 2008).

Finding optimal conditions for crystal growth largely involves trial and error. Protein crystals are grown by slow, controlled precipitation from aqueous solution. Crystal formation is affected by variables such as protein purity, concentrations of protein and precipitant, pH, and temperature. Moreover, the crystallized protein must retain its biological function in its crystallized form; an essential part of any structure determination project is an effort to show that the crystallized protein is not significantly altered. Membrane protein crystallography extends this challenge further by adding yet another dimension: hydrophobicity (Carpenter *et al.*, 2008). Hydrophobicity alone can account for the fact that while membrane proteins

represent a third of proteins encoded in most genomes, but only about 360 proteins of known structure to date (as compared to approximately 85,000 protein structures overall) (http://blanco.biomol.uci.edu/mpstruc/listAll/list, accessed 10 September 2012; http://www.pdb.org/pdb/home/home.do, accessed 10 September 2012; Carpenter *et al*., 2008; Loll, 2003).

Of course, most membrane proteins are crystallized in the presence of a solubilizing agent, such as a detergent, and detergent selection is a major limiting step in membrane protein crystallography (Lemieux *et al.*, 2003; Ostermeier and Michel, 1997). In general, the PDC is not very amenable to X-ray crystallography or NMR studies. Successfully obtaining a crystal is difficult because the flexible and dynamic nature of the detergent belt that surrounds the protein does not favor the formation of well-ordered lattices (Privé, 2007). Detergents are prone to partition out of aqueous solution at high precipitant concentrations, introducing a detergent-rich phase in the crystallization drop (Newby *et al.*, 2009). In addition, while attractive interactions between the detergent micelles may stabilize the crystal packing, detergent molecules require space in the crystal lattice, and these interactions do not lead to rigid crystal contacts (Hunte and Michel, 2002). The detergent micelle has to fit optimally into the crystal lattice (Ostermeier and Michel, 1997). Finding the optimal micelle size can be done by experimentation with longer or shorter homologs of the original detergent.

In practice, a variety of detergents should be tested for their ability to maintain the solubility and stability of the protein of interest (Iwata, 2003; Ostermeier and Michel, 1997). Typically, a detergent concentration of 2-3 times the CMC is used. Suitable detergents can then be used in protein crystal trials, and once crystals are obtained, further optimization of the detergent can be performed to get high-quality crystals (Iwata, 2003). A first set of alternative detergents to those used in protein purification can be selected on the basis of past success stories. Table 1 lists the most widely used detergents in X-ray crystallography studies of membrane proteins, based on statistics from the Membrane Protein Data Bank (http://www.lipidat.chemistry.ohio-state.edu/MPDB/index.asp, accessed May 2012).

Detergent-protein suspensions have to be screened to ensure that the protein is monodisperse, since proteins that aggregate in solution generally are not suitable for high resolution structure determination (Engel *et al.*, 2002; Lemieux *et al.*, 2003; Rhodes, 2000; Roth *et al*., 1989). Protein aggregation is also greatly influenced by pH: most proteins

crystallize over a pH range of 4-9 (Lemieux *et al.*, 2003). For those proteins that are unstable in detergent micelles, lipidic cubic phases have been found to be a possible alternative (Landau and Rosenbusch, 1996; Ostermeier and Michel, 1997). A lipid cubic phase is a quasisolid three-dimensional membrane array that is pervaded by an intercommunicating aqueous channel

Table 1. Detergents used in successful X-ray structural studies of membrane proteins, in order of number of reported structures (Raman *et al*., 2006).

Detergent	Number of reported structures	CMC (mM)
OG	79	20
DDM	52	0.16
C_8E_4	43	7
LDAO	22	1
CHAPSO	18	10
$C_{12}E_8$	18	0.08
Triton-X 100	16	0.24

system (Fig. 2.14). These matrices provide nucleation sites that can grow by lateral diffusion of membrane protein molecules (Fig. 2.14) (Landau and Rosenbusch, 1996).

In a sense, following the selection of an appropriate detergent, and the determination of the pH and salt concentration at which the protein remains monodisperse, crystallization and crystal analysis of membrane proteins is no different than that of soluble proteins (Ostermeier and Michel, 1997). However, the selection of precipitants that can be used is significantly less than those possible for soluble proteins. Organic solvents tend to disturb detergent micelles and, at high concentrations, can even denature proteins. Salts, on the other hand, reduce the solubility of detergent micelles and precipitate the membrane protein embedded in the detergent micelle before crystallization occurs. It is not surprising that, by one count, over 75% of membrane protein crystals have been grown using polyethylene glycols (PEG) or their monomethyl ether derivatives (Lemieux *et al.*, 2003). However, even after the careful selection of detergent, pH value, and precipitant, crystals suitable for detailed structural analysis may not form. Lemieux *et al*., in their attempts to crystallize GlpT, found that soaking crystals in heavy

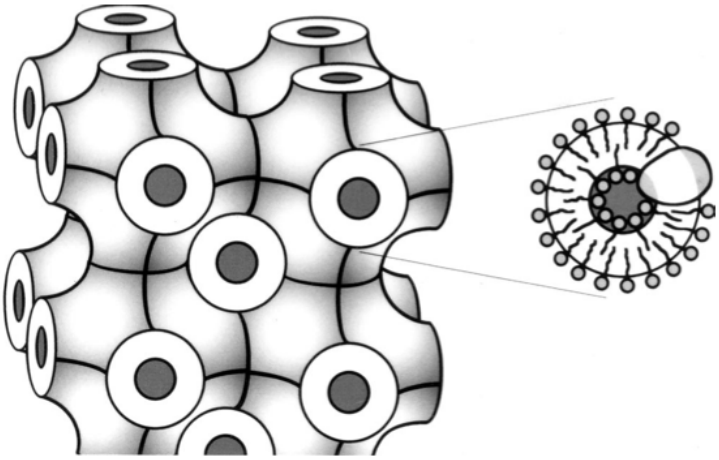

Figure 2.14. Schematic model of a bicontinuous cubic phase composed of monoolein, water, and a membrane protein. The matrix consists of two compartments, a membrane system with an infinite three- dimensional periodic minimal surface (Left), interpenetrated by a system of continuous aqueous channels (shown in black). The enlarged section (Right) shows the curved lipid bilayer (with an inserted membrane protein molecule) enveloping a water conduit. Lateral diffusion of membrane proteins through the lipid bilayer allows for crystal nucleation and growth to occur. Reproduced from Landau and Rosenbusch (1996), with the permission of the publisher.

metal salts such as $PbCl_2$ improved crystal order by a factor of 1.5-2.4, depending on the salt added (Lemieux *et al.*, 2003).

Secondary transporters, in particular, are a class of membrane proteins that are especially difficult to crystallize as their small extramembranous surface areas make them extremely hydrophobic, and they exhibit a high degree of internal flexibility (Carpenter *et al*., 2008; Engel *et al*., 2002). In order to extend the surface area of the soluble portion of the membrane protein and enhance crystal contacts, the protein of interest can be co-crystallized with the F_v fragment of a monoclonal antibody (Ostermeier *et al*., 1995; Ostermeier and Michel). Antibody fragments are well suited for use in co-crystallization with membrane proteins because they are readily available and have both high affinity and specificity. F_v fragments are optimal, as F_{ab} fragments show internal flexibility and may not enhance crystal contacts. In addition, the former can be efficiently produced in *E. coli*, purified by affinity chromatography, and often easily crystallized (Ostermeier *et al.*, 1995). An F_v fragment should be selected which extends out of the detergent micelle when bound, and which selectively binds the native protein (Hunte and Michel, 2002; Ostermeier *et al.*, 1995). This method has been

used successfully to solve the structures of membrane proteins such as cytochrome c oxidase from *Paracoccus denitrificans*, cytochrome bc_1 complex, and the potassium channel (Hunte and Michel, 2002; Knol *et al.*, 1996).

The solution structure of LacY demonstrated that the internal flexibility of a molecule must be considered, and if necessary, strategies to overcome it must be devised. Since LacY is known to be a very dynamic molecule, Abramson and coworkers tested a variety of LacY mutants for conformational flexibility, and selected C154G, a particularly stable, conformationally-arrested mutant, for crystal trials (Abramson *et al.*, 2003; Smirnova and Kaback, 2003). C154G LacY had the added benefit of being able to bind a substrate analog, which not only confirmed that the binding site of LacY was intact, but also allowed valuable insight into the binding site of MFS transporters (Abramson *et al*., 2003).

2.5 Implications for studies of putative bacterial multidrug transporters

MdfA is a model MDT from the MFS family. Since membrane proteins are extremely challenging to study, developing well-characterized models is a more efficient approach to tackling the question of active drug extrusion from the cell. MFS multidrug transporters are significant players in *S. aureus* multidrug resistance (Li and Nikaido, 2009). However, many of these transporters remain uncharacterized. Gaining a more detailed understanding of the structure, mechanism and substrate profile of known transporters such as MdfA will not only allow for the development of techniques by which to study putative drug transporters, but will also lead to the development of novel strategies to combat efflux mediated drug resistance in virulent pathogens such as MRSA.

The aim of this project was to develop techniques for the structural and functional characterization of putative MDT using MdfA as a model. MdfA can be used to develop substrate profile assays that are universally applicable to transporters energized by a proton gradient. Once the substrate profile of a transporter has been determined, the kinetics of substrate binding can be determined. We sought to develop a substrate profile assay by measuring ACMA fluorescence changes associated with substrate transport in MdfA-reconstituted proteoliposomes. Next, we tested whether NMR isotope-editing techniques can be used to determine the dissociation constant of substrate binding to pure MdfA in detergent

micelles. Finally, we sought to perform crystal trials of MdfA to identify conditions suitable for structural studies using X-ray crystallography.

3. Experimental Procedures[1]

3.1. MdfA expression and purification

3.1.1 Expression of MdfA in *E. coli*

MdfA was expressed as described previously (O'Grady, 2010). Briefly, *E. coli* strain LMG194/pCOG3 was plated onto a Luria-Bertani (LB) media (170 mM NaCl, 10 g/L tryptone, 5 g/L yeast extract) agar plate containing 100 µg/mL ampicillin and was incubated overnight at 37 °C. The starter culture was made by inoculating a single colony from the plate into 120 mL LB media with 100 µg/mL ampicillin. Large-scale growth was performed by inoculating either 6 or 12 L of LB media, containing 100 µg/mL ampicillin, with the starter culture (1:100 v/v), and growing the cells at 37 °C on a shaker platform at 200 r.p.m. to an optical density (OD_{600}) of 0.5. The cells were harvested and resuspended in casamino acid medium containing 2% casamino acids, 0.5% glycerol, 1 mM $MgCl_2$, 42 mM Na_2HPO_4, 22 mM KH_2PO_4, 9 mM NaCl, and 100 µg/mL ampicillin. MdfA expression was induced using 0.002% L-arabinose for 4 hours.

3.1.2 Preparation of *E. coli* cell membranes

Membranes were purified as described previously (O'Grady, 2010). Cells were harvested by centrifugation at 6000 x g, and then lysed using a Constant Systems Ltd (Daventry, Northants, U.K.) cell disruptor at 35,000 p.s.i. in TMDG buffer (50 mM Tris-HCl, pH 7.5, 5 mM $MgCl_2$, 10% (v/v) glycerol, 1 mM dithiothreitol (DTT), and 1 mM phenylmethylsulfonyl fluoride (PMSF)). Cell debris was removed by centrifugation (7,700 x g for 15 min at 4 °C), and the supernatant was centrifuged at 100,000 x g for 75 min at 4 °C to isolate the membranes. The membrane pellet was resuspended in TMDG buffer and centrifuged again under the same conditions. The pellet was then resuspended again in TMDG buffer, frozen in liquid nitrogen, and stored at -80 °C until use.

[1] Chemicals used in these experiments were purchased from Sigma-Aldrich (Oakville, Ontario), Fisher Scientific Company (Ottawa, Ontario), or Merck Canada Inc., (Kirkland, Quebec) unless otherwise stated.

3.1.3 MdfA purification by Ni^{2+}- affinity chromatography

A purification procedure for MdfA from *E. coli* cell membranes has been developed in our lab (O'Grady, 2010). MdfA was extracted by diluting the membranes to 10 mg protein/mL with TMDG buffer containing 2% (w/v) DHPC (Avanti Polar Lipids, Inc., Alabaster, Alabama) or DDM (Anatrace Detergents and Lipids, Maumee, Ohio). The sample was gently agitated for 30 min at 4 °C, and then centrifuged at 220,000 x g for 1 hour to separate soluble and insoluble protein. The supernatant was diluted 1:5 (v/v) in TMDG buffer, and centrifuged again under the same conditions. The supernatant was applied to a column containing nickel nitrilotriacetic acid agarose (Ni-NTA), pre-washed with TMDG buffer containing 0.2% (w/v) DHPC, at a ratio of 5:1 (v/v) membrane extract to Ni-NTA (Qiagen Inc., Toronto, Ontario). Purifications were performed with either TMDG or KP_i (50 mM KH_2PO_4, pH 7.5, 1 mM DTT) as buffer with additions as indicated below. Contaminating proteins were washed off with 20 column volumes of 0.4% (w/v) DHPC and 20 mM imidazole (Merck Canada Inc.). Detergent exchange was performed by washing the column with 10 column volumes of the detergent of interest at the desired concentration in the presence of 20 mM imidazole, followed by elution. MdfA was eluted from the column using 5 column volumes 250 mM imidazole and 0.2% (w/v) LMPG, 0.4% (w/v) DDM or 0.4% (w/v) DHPC. For crystallization trials, MdfA was exchanged into OG, DDM, $C_{12}E_8$, and LDAO by Ni-NTA chromatography. The final detergent concentrations used were 1.75% (w/v) OG, 0.4% (w/v) DDM, 0.013% (w/v) $C_{12}E_8$, and 0.07% (w/v) LDAO. Samples from each purification step were analyzed by sodium dodecylsulfate polyacrylamide gel electrophoresis (SDS-PAGE) (see section 3.7.4).

To improve the purity of the MdfA sample, an imidazole gradient elution from a nickel affinity column was used. A membrane sample was prepared and solubilized as described above using an ÄKTA FPLC system (GE Healthcare, Mississauga, Ontario) at a flow rate of 1 mL/min. The solubilized membrane sample was loaded onto a Qiagen Ni-NTA superflow column, and the column was washed with TMDG buffer containing 20 mM imidazole and 0.005 or 0.01% LMPG. A linear gradient of imidazole concentration 20-500 mM was applied, and the column was further washed with 500 mM imidazole and 0.005% or 0.01% LMPG. To further improve purity and to reduce nonspecific binding to the column, chromatography was performed as before, except that 0.5 M NaCl was added to the washes and elution buffers.

As a final step, buffer exchange was performed using a 10,000 molecular weight cutoff membrane concentrator by successive cycles of dilution and concentration of the protein in the desired buffers. Routinely, MdfA was concentrated to 5-11 mg/mL in 25 mM sodium phosphate, pH 6.0, 50 mM NaCl and 0.2% LMPG, or 0.4% DDM.

3.2. F_oF_1 ATPase expression and purification

3.2.1 Expression of F_oF_1 ATPase in *E. coli*

E. coli strain C43(DE3) containing pBWU13, a plasmid that encodes the *E. coli atp* operon with the atpB gene modified to include a hexahistidine tag at the N-terminus of subunit *a*, was used for F_oF_1 ATPase expression (Pierson *et al.*, 2011; Stalz *et al.*, 2003). Cell culture was plated onto an LB agar plate containing 100 µg/mL ampicillin and was incubated overnight at 37 °C. The starter culture was made by inoculating a single colony from the plate into 30 mL LB containing 100 µg/mL ampicillin. Large scale growth was performed by inoculating 6 L minimal media (15 mM NH_4Cl, 15 mM Na_2SO_4, 0.8 mM $MgSO_4$, 100 mM potassium phosphate, pH 7.0 (VWR International, Mississauga, Ontario) 0.05 µg/L $FeSO_4$, 0.3% glucose and 5 mg/L thiamine) containing 100 µg/mL ampicillin, with the starter culture (1:250 v/v), and growing the cells to an OD_{600} of 1.6 at 37 °C on a shaker platform at 200 r.p.m. The cells were harvested and membranes were prepared as described in section 3.1.2.

3.2.2 Detergent screening for F_oF_1 ATPase purification

The stability of F_oF_1 ATPase in different detergents was determined by testing ATPase activity using the malachite green assay (see section 3.7.1). *E. coli* cell membranes were prepared as described in section 3.1.2. An aliquot of *E. coli* membranes was pelleted by centrifugation at 220,000 x g for 20 min, and resuspended in 50 mM 3-(N-morpholino)propanesulfonic acid (MOPS)-KOH, pH 7.0. Membrane solubilization by Triton-X 100 was optimized by varying protein concentration (2.5, 5.0 or 10.0 mg/mL) and detergent concentration (0.5, 1.0, 1.5, 2.0, 2.5, or 3.0% (w/v)). Further screening was performed by preparing membrane extracts solubilized at 5.0 mg/mL protein concentration using 2.0% (w/v) Triton-X 100, or 2.0% (w/v) OG, or 1.0% or 0.2% (w/v) DHPC. The membrane-detergent suspension was agitated gently for 30 min, and centrifuged at 200,000 x g for another 30 min to

remove insoluble protein. The membrane extracts were tested for ATPase activity and N,N'-dicyclohexylcarbodiimide (DCCD) sensitivity as described in section 3.7.1.

3.2.3 Optimization of F_oF_1 ATPase purification by polyethylene glycol fractionation

F_oF_1 ATPase purification was based on *Propionigenium modestum* (*P. modestum*) F_oF_1 ATPase purification (Laubinger and Dimroth, 1988). All centrifugation steps were performed at 4 °C. An aliquot of *E. coli* membranes was pelleted by centrifugation at 220,000 x g for 20 min, and resuspended in 50 mM MOPS-KOH, pH 7.0. Membranes were solubilized at 5.0 mg/mL protein concentration using 2.0% (w/v) Triton-X 100. The membrane detergent suspension was agitated gently for 30 min, and centrifuged at 200,000 x g for another 30 min to remove insoluble protein. $MgCl_2$ was added to a final concentration of 50 mM, and the sample was divided in equal parts and treated with various concentrations of polyethylene glycol (PEG) 6000 (Alfa Aesar, Ward Hill, Massachusetts) while stirring. The final PEG 6000 concentrations tested were 0, 2, 4, 6, 8, 10, or 12%. These mixtures were centrifuged at 39,000 x g for 20 min. The pellet was resuspended in either buffer A (5 mM potassium phosphate, pH 7.0, containing 1 mM DTT, 1 mM PMSF and 0.05% Triton-X 100), or in buffer B (10 mM Tris-HCl, pH 8.0, containing 5 mM $MgCl_2$, 1 mM DTT, 1 mM PMSF, and 0.05% Triton-X 100). Insoluble material was removed by centrifugation at 39,000 x g for 15 min. The F_oF_1 ATPase was stored under liquid nitrogen until use.

Analysis of the purification steps was done by SDS-PAGE (see section 3.7.4). In some cases, Western blot analysis was also performed to test for the presence of the His-tagged subunit *a*, or for subunit *c* of the F_oF_1 ATPase complex (see section 3.7.4).

3.2.4 Ni^{2+}-affinity chromatography of F_oF_1 ATPase with imidazole gradient elution

The F_oF_1 ATPase was further purified by Ni-NTA column chromatography using the hexa-His tag attached to subunit *a*. The following steps were performed using an ÄKTA FPLC system (GE Healthcare), at a flow rate of 1 mL/min. The F_oF_1 ATPase sample was prepared by membrane solubilization using 2.0% (w/v) Triton-X 100, and PEG fractionation using 2.0% and 10.0% PEG 6000. This sample was then loaded onto a Ni-NTA superflow (Qiagen) column. The column was washed with buffer A, a linear gradient of imidazole

concentration 0-200 mM was applied, and the column was further washed with 200 mM imidazole. Fractions collected were analyzed by SDS-PAGE (see section 3.7.4).

3.3 Preparation of preformed liposomes and Bio-Beads

Preformed liposomes and Bio-Beads were prepared essentially as previously described (O'Grady, 2010). Lipid from an *E. coli* total lipid (Avanti Polar Lipids) extract in chloroform was dried under a gentle stream of argon, to remove the organic solvent, and resuspended in 25 mM potassium phosphate buffer, pH 7.0, 2 mM β-mercaptoethanol, and 1.5% OG to a final lipid concentration of 25 mg/mL. Liposomes were dialyzed against 25 mM potassium phosphate buffer, pH 7.0, and 2 mM β-mercaptoethanol using 12,000-14,000 MWCO Spectra/Por dialysis tubing to remove the detergent. Liposomes were stored under liquid nitrogen until use.

Bio-Beads SM-2 (BioRad Laboratories Ltd., Mississauga, Ontario) were prepared by addition to 100% methanol at a 1:7 ratio (w/v). The slurry was mixed for 15 min, then transferred to a column, and washed with 200 mL methanol, followed by 700 mL ddH_2O. The Bio-Beads were then degassed for three hours, washing with ddH_2O every hour. Bio-Beads were stored under water at 4 °C until use.

3.4. Reconstitution of MdfA and F_oF_1 ATPase in proteoliposomes

3.4.1 Reconstitution using Bio-Beads

MdfA was reconstituted into proteoliposomes by detergent disruption of preformed liposomes (see section 3.3), followed by detergent removal by Bio-Beads as described previously (O'Grady, 2010). Preformed liposomes were thawed and passed through a mini-extruder (Avanti Polar Lipids) using a Whatman 400-nm polycarbonate membrane filter (GE Healthcare) 20 times. Note that for all proteoliposomes reconstituted using Bio-Beads, MdfA in 0.005% LMPG was used. To each liposome sample, 30 µg MdfA was added, followed by either 2% (w/v) Triton-X 100 or 1% (w/w) DHPC. Samples were incubated at 30 °C for 15 min. Bio-Bead treatment was performed by sequentially adding 10, 10, 20, 20 and 60 mg of Bio-Beads to the 300 µL sample and incubating for 30 min at 30 °C after each addition. The Bio-Beads were then removed, and the proteoliposomes were stored on ice until use. Control liposomes were treated and prepared in the same way, without the addition of MdfA.

The F_oF_1 ATPase was reconstituted into proteoliposomes by detergent disruption of preformed liposomes, followed by detergent removal by Bio-Beads, similar to the procedure described above. Preformed liposomes were thawed, and 1% (w/w) DHPC was added to each liposome sample, followed by F_oF_1 ATPase at the desired protein:lipid ratio (w/w). Samples were then treated with Bio-Beads as described above. The Bio-Beads were removed, and samples were centrifuged at 220,000 x g for 20 min. The supernatant was discarded and the proteoliposomes were resuspended in quench buffer A (20 mM Tricine-NaOH, pH 8.0, 10 mM $MgCl_2$, and 300 mM KCl) in a volume equal to the starting liposome volume. The suspension was passed through a Whatman 400-nm polycarbonate membrane 20 times, and the proteoliposomes were stored on ice until use. Control liposomes were treated and prepared in the same way, without the addition of protein.

MdfA and F_oF_1 ATPase co-reconstitution was achieved in the same way, with the exception that in co-reconstitution experiments, the MdfA:lipid ratio was altered, while the F_oF_1 ATPase:lipid ratio was constant. Control liposomes were treated and prepared in the same way; however, MdfA was not added.

3.4.2 Reconstitution using dialysis and freeze/thaw cycles

For co-reconstitution of MdfA and F_oF_1 ATPase by dialysis, MdfA in 0.4% DHPC was concentrated to 5-11 mg/mL in KP_i buffer, and protein concentration was determined by densitometry (see section 3.7.4). MdfA and F_oF_1 ATPase co-reconstitution by dialysis was achieved by DHPC disruption of preformed liposomes, followed by detergent removal by dialysis. Initial experiments were performed with the F_oF_1 ATPase alone. Preformed liposomes were thawed, and 5 mM $MgCl_2$ and 1% (w/w) DHPC was added to each liposome sample, followed by F_oF_1 ATPase at the desired protein:lipid ratio (w/w). Samples were incubated at 30 °C and 400 r.p.m. for 30 min. The samples were then dialyzed against dialysis buffer B (20 mM Tricine-NaOH, pH 8.0, 5 mM $MgCl_2$, 200 mM KCl, 1 mM DTT), dialysis buffer C (5 mM Tricine-NaOH, pH 8.0, 5 mM $MgCl_2$, 200 mM KCl, 1 mM DTT), dialysis buffer D (1 mM Tricine-NaOH, pH 8.0, 5 mM $MgCl_2$, 200 mM KCl, 1 mM DTT), or dialysis buffer E (20 mM Bis-Tris propane-MES (EMD Inc., Mississauga, Ontario), pH 8.0, 5 mM $MgCl_2$, 1 mM DTT) twice over 20 hours using 12,000-14,000 MWCO Spectra/Por (VWR

International) dialysis tubing at 4 °C. Proteoliposomes were collected, incubated at 25 °C for 10 min and submitted to three freeze/thaw cycles in liquid nitrogen.

MdfA and F_oF_1 ATPase co-reconstitution was achieved in the same way, with the exception that in co-reconstitution experiments, the MdfA:lipid ratio was altered, while the F_oF_1 ATPase:lipid ratio was constant. Control liposomes were treated and prepared in the same way, without the addition of MdfA.

This procedure was optimized by first reconstituting each protein individually using the dialysis method described above. The F_oF_1 ATPase:lipid ratio used was 1:80, and the MdfA:lipid ratio was 1:40. Following dialysis, the mono-reconstituted liposomes were mixed at the desired ratio, incubated at 25 °C, and submitted to three freeze/thaw cycles in liquid nitrogen.

All liposomes suspensions were passed through a Whatman 400-nm polycarbonate membrane 20 times, and the proteoliposomes were stored on ice until use. Control liposomes were always treated and prepared in the same way, without the addition of MdfA.

3.4.3 Fractionation of proteoliposomes by ultracentrifugation in sucrose density gradient

Co-reconstitution of MdfA and F_oF_1 ATPase was confirmed by density fractionation. Sucrose solutions were prepared in quench buffer B (20 mM Tricine-KOH, pH 8.0, 5 mM $MgCl_2$, 300 mM KCl, 1 mM DTT). Proteoliposomes were layered over a 10-45% (w/w) sucrose density gradient and ultracentrifuged in a swing-out rotor at 150,000 x g for 16 hours at 4 °C. Fractions collected were analyzed by silver stained SDS-PAGE gels, Western blot (see section 3.7.4) and turbidity measurements at OD_{600}.

3.5. NMR experiments for measurement of substrate binding to MdfA

3.5.1 Synthesis of ^{13}C-labeled and natural isotopic abundance acetyl chloramphenicol

^{13}C-labeled and natural isotopic abundance acetyl chloramphenicol (^{13}C-AcCml and AcCml, respectively) were synthesized by acetylation of chloramphenicol with ^{13}C-acetyl chloride or natural isotopic abundance acetyl chloride as described previously (Derrick *et al*., 1991). Mono- and di-acetylated products were separated as follows. The crude reaction product was dissolved in dichloromethane, and loaded onto a silica column. A 0-30% (v/v) ethyl acetate:hexane gradient was used to separate mono- and di-acetylated Cml. Separation

was confirmed by thin layer chromatography with 50% (v/v) ethyl acetate:hexane as a mobile phase. Plates were viewed using shortwave ultraviolet light. Each product was dried in a rotor evaporator, and redissolved in deuterated acetonitrile (Cambridge Laboratories Isotopes, Inc., Andover, Massachusetts).

All $^{1}H,^{13}C$-HSQC experiments were performed on a 600 MHz Avance NMR spectrometer (Bruker) at 27 °C. NMR spectra were processed and analyzed using Felix-2000 (Accelrys).

3.5.2 Determination of [^{13}C]-acetyl chloramphenicol concentration by NMR

The concentration of ^{13}C- AcCml was determined using a ^{13}C-acetyl-^{15}N-glycine (NAG) (Cambridge Laboratories Isotopes, Inc.) standard. NAG and ^{13}AcCml solutions were made in NMR buffer (25 mM Na_2HPO_4, pH 6.0, 50 mM NaCl, 0.5 mM 4,4-dimethyl-4-silapentane-1-sulfonic acid (DSS), 5% D_2O (Cambridge Laboratories Isotopes, Inc.), and 0.005% (w/v) LMPG). One-dimensional $^{1}H,^{13}C$-HSQC spectra were recorded using 1024 scans. A standard curve was made by measuring signal intensity of the methyl group of NAG as a function of NAG concentration. The ^{13}C- AcCml concentration was determined by comparing the signal intensity of the methyl group of ^{13}C- AcCml to the standard curve.

3.5.3 Measurement of [^{13}C]-acetyl chloramphenicol binding to MdfA by one-dimensional $^{1}H,^{13}C$-heteronuclear single quantum coherence experiments

MdfA was titrated in NMR buffer containing 20 μM ^{13}C- AcCml to 4, 8, 12, 16, or 20 μM. A one-dimensional $^{1}H,^{13}C$-HSQC spectrum of each sample was recorded using 1024 scans. This same set of experiments was repeated in the presence of 1.5 mM Cml. To control for nonspecific binding of LMPG to ^{13}C- AcCml, the titration experiment was repeated by titrating 0.005% (w/v) LMPG to the substrate solution, in the absence of MdfA.

3.6 Development of crystallization conditions for structural studies of MdfA

Prior to this project in our lab, initial crystallization screens were performed (O'Grady, 2010). These studies were used to select crystallization conditions for further optimization (Table 2). Trials with the MemSys kit (Molecular Dimensions) were also performed as listed in

Table 2. Phosphate buffer was composed of 25 mM Na_2HPO_4, pH 6.0, 50 mM NaCl. All trials were checked at days 1 and 3 and weekly thereafter. A 5.2 mg/mL MdfA sample in phosphate buffer was also sent for high-throughput screening at the Hauptman-Woodward Institute.

Table 2. List of conditions selected for crystallization trials.

Conditions for crystal trials	Temp (°C)	Crystallization method	[MdfA] (mg/mL)	Buffer used for MdfA
0.39 M Zinc acetate, 0.1 M Sodium acetate, pH 5	18	Hanging drop	4.5	MES buffer with 0.01% LMPG
0.1 M Zinc acetate, 0.1 M Sodium acetate, pH 5, 40% (w/v) PEG 400				
0.1 M Calcium acetate, 0.1 M Sodium acetate, pH 5, 20% (w/v) PEG 400				
0.05 M CsCl, 0.1 MES monohydrate, pH 6.5, 30% (v/v) Jeffamine M-600				
0.2 M $CaCl_2$, 40% (v/v) MPD				
0.2 M CsCl, 40% (v/v) MPD				
MemSys Kit	4 and 18	Microbatch under oil	4.5	MES buffer with 0.01% LMPG
			6.4	Phosphate buffer with 0.01% LMPG
	4 and 18		2.8	MES buffer with 0.4% DDM

3.7. Analytical methods

3.7.1 Measurement of ATPase activity using Malachite Green assay

ATPase activity of membrane and pure protein samples was tested in buffer B, using 2 mM ATP (final concentration) over a time range of 15 min, at 37 °C. Membrane samples were tested using 0.25 µg membrane protein, while for pure F_oF_1 ATPase, 0.1 µg was tested. We measured the inorganic phosphate released upon ATP hydrolysis by F_oF_1 ATPase using the malachite green assay. Reaction of inorganic phosphate with molybdate results in a complex that can be visualized colorimetrically using the dye, malachite green. The protocol of Henkel

(Henkel *et al.*, 1988) was used with the following modifications. Malachite green reagent was made using 0.0406% (w/v) malachite green. To determine whether the F_oF_1 ATPase was intact, ATPase activity was measured in the presence of the F_o domain inhibitor, DCCD. Purified F_oF_1 ATPase was incubated with 0.1 mM DCCD for 10 min at room temperature prior to testing ATPase activity. A phosphate standard curve was prepared by measuring the malachite green and phosphomolybdate complex light absorption of 0, 10, 25, 50, 75, 100, 125 and 150 μM KH_2PO_4, in duplicate. Forty microliters of samples or standards were mixed with 160 μL malachite green reagent, and incubated for 5 min at room temperature prior to absorbance measurement at 630 and 490 nm.

3.7.2 Dye fluorescence assay for transmembrane H^+-transport

Since MdfA is a drug/H^+ antiporter, MdfA substrate transport can be indirectly measured by observing proton transport using the fluorophore ACMA. In theory, MdfA reconstituted into liposomes will transport substrates in the presence of a pH gradient. A pH-sensitive fluorophore, such as ACMA, can be used to monitor changes in pH, and thus indirectly monitor substrate transport by MdfA across a lipid bilayer.

A fluorescence assay was performed as described (O'Grady, 2010) with changes noted. ACMA fluorescence was detected using an excitation wavelength of 410 nm and emission wavelength of 490 nm, with slit widths of 5 nm and 10 nm, respectively. MdfA-reconstituted proteoliposomes were added to a buffer containing 10 mM Tricine-NaOH, pH 7.0, 5 mM $MgSO_4$, and 50 mM Na_2SO_4, with 1 μM ACMA. Valinomycin (EMD Inc.) and carbonyl cyanide 4-(trifluoromethoxy)-phenylhydrazone (FCCP) were added to final concentrations of 12.3 nM and 25 nM, respectively, to generate a pH gradient. Fluorescence restoration upon the addition of MdfA substrate, Cml, was measured.

For optimization of the assay, various concentrations of FCCP (3-100 nM) valinomycin (1.1-12.3 nM), and proteoliposome amounts (10-250 μg) were tested to increase sensitivity of the assay to proton transport. Following optimization, 15 μg of proteoliposomes by lipid content was used. Cml was added to a final concentration ranging from 0-12 μM.

F_oF_1 ATPase was also used as pH gradient generator, by co-reconstitution of F_oF_1 ATPase and MdfA into preformed liposomes. In this system, a pH gradient is created upon the addition of ATP. ACMA was once again used to monitor changes in pH resulting from

substrate transport. This assay was also used to confirm MdfA activity in *E. coli* cell membranes. ACMA fluorescence was detected as before with slit widths of 10 nm and 1 nm, respectively. ACMA was added to a final concentration of 2 μM and ATP, pH 7.5, was added to a final concentration of 2 mM.

Membranes or proteoliposomes were added to 2 mL quench buffer B, quench buffer C (5 mM Tricine-KOH, pH 8.0, 5 mM $MgCl_2$, 300 mM KCl, 1 mM DTT), quench buffer D (1 mM Tricine-KOH, pH 8.0, 5 mM $MgCl_2$, 300 mM KCl, 1 mM DTT), or quench buffer E (20 mM Bis-Tris propane-MES, pH 8.0, 5 mM $MgCl_2$, 1 mM DTT) in the presence of 100 nM valinomycin. Valinomycin was not used in the case of quench buffer E. The amount of proteoliposomes, and ATP and FCCP concentrations used varied as needed, and are indicated in chapter 4.

A major challenge with proteoliposome formation is passive ion permeability due to poor detergent removal. Standard experiments were performed in the presence of valinomycin in order for membrane potential to be discharged continuously throughout the assay. As a result, it can be assumed that in a well-formed F_oF_1-ATPase reconstituted liposome, the rate of ΔpH generation will be slower if the membrane potential is not discharged by means of an ionophore. If the liposome is not well-formed and is "leaky", that is, it allows the passive flow of ions in the direction of thermodynamic equilibrium, the presence or absence of an ionophore will not affect the rate of ΔpH generation. The membrane integrity of co-reconstituted proteoliposomes was tested by performing the assay in the absence of valinomycin. Substrates tested were Cml, TPP^+, NaCl, LiCl, IPTG (BioBasic Canada Inc.), benzalkonium, betaine (National Biochemical Corporation, Cleveland, Ohio), phenylalanine, tryptophan and phenylpropionate.

3.7.3 Assay for fluorescent substrate transport using Ethidium bromide

Fluorescent MdfA substrates such as EtBr are incompatible with the assay set up described in 3.7.3. To develop an assay system that exploits the inherent fluorescent properties of the substrates, we used EtBr. We used MdfA-reconstituted proteolioposomes; however, a method of distinguishing between substrate inside and outside the liposome lumen was required. EtBr fluorescence intensity is increased in the presence of double stranded DNA. As a result, we entrapped double-stranded oligonucleotides inside the liposomes. EtBr

accumulation inside liposomes would then result in an increase in fluorescence intensity proportional to the amount of EtBr transported into the liposomes.

We prepared MdfA and F_oF_1-ATPase co-reconstituted liposomes as described in section 3.4.2 with the following modifications: 10 μM oligonucleotides (5'-TAATGAAAATGAAAGAAGATGGCAGTCGCTG-3' and 5'-CAGCGACTGCCATCTTCTTTCATTTTCATTA-3') (Eurofins MWG Operon, Huntsville, Alabama) annealed to form double stranded DNA, and added to proteoliposomes following incubation of mixed liposomes at 25 °C and submitted to three freeze/thaw cycles as described earlier. Proteoliposomes were collected by ultracentrifugation at 200,000 x g for 20 min at 4 °C, resuspended in quench buffer B and extruded through a Whatman 400-nm polycarbonate membrane 20 times. A pH gradient was generated using 2 mM ATP, and EtBr (EMD Inc.) transport was tested by addition of 0-10 μM EtBr to 1.25 mg liposomes. EtBr fluorescence was detected using an excitation wavelength of 518 nm and emission wavelength of 605 nm, with both slit widths at 10 nm. The proton gradient was uncoupled at the end of the assay by the addition of 4 μM FCCP.

3.7.4 Other methods

Protein concentration in the absence of imidazole was determined by the method of Lowry (Lowry *et al.*, 1951) using bovine serum albumin (EMD Inc.) as a standard, with the following changes. Sodium dodecyl sulfate (Roche Canada, Laval, Quebec) was added to a final concentration of 1% to fully dissolve and denature the protein. Sodium citrate was used instead of sodium tartrate at the same concentration. Absorbance measurements were taken at 650 nm. When buffers contained imidazole, protein concentration was determined by densitometry on Coomassie-stained SDS-PAGE gels (see below) using BSA as a standard. Densitometry experiments were performed using Syngene Chemigenius^2, and GeneSnap version 6.03.

SDS-PAGE in 10% gels was performed according to Schägger and von Jagow (Schagger and Von Jagow, 1987). SDS-PAGE gels were stained either with Coomassie R250 or silver. Silver staining procedure was performed as follows. Gels were fixed first in 30% (v/v) ethanol, and 10% (v/v) acetic acid solution for 45 min, followed by incubation in 30% (v/v) ethanol and 6.8% (w/v) anhydrous sodium acetate for 30 min. The gels were washed

three times in double distilled water for 5 min each. They were then incubated in silver solution composed of 0.2% (w/v) $AgNO_3$ (VWR International), and 0.0075 (v/v) formaldehyde for 20 min. Bands were developed in a solution composed of 2.5% (w/v) $NaCO_3$ (VWR International), and 0.0037% formaldehyde and the reaction stopped by incubation for 30 min with 0.5% (w/v) glycine (EMD Inc).

Immunodetection of the histidine-tagged subunit *a* of F_oF_1 ATPase were performed according to manufacturer's instructions (Qiagen). Western blots of subunit c of F_oF_1 ATPase were performed using a polyclonal anti-subunit c antibody and an anti-rabbit antibody as a secondary antibody, according to Qiagen's instructions for detection by secondary antibodies. All F_oF_1 ATPase purification samples for analysis by SDS-PAGE and Western blotting were prepared by acetone precipitation. Protein samples wer added to acetone at a 1:4 (v/v) ratio, mixed well, and centrifuged at 12,000 x g for 10 min. The supernatant was discarded and the pellet was dried at 37 °C. The pellet was resuspended in sample buffer and incubated at 95 °C for 5 min prior to loading. MdfA samples were diluted in sample buffer prior to loading, but not heat-treated.

MdfA purified in 0.005% (w/v) LMPG and 0.4% (w/v) DDM was analyzed by DLS using the DynaPro/Micro Sampler with Dynamics Software package version 5.26.60.

4. Results

4.1 MdfA purification and characterization for structural studies

Our lab had developed a purification procedure for MdfA prior to the start of this project (O'Grady, 2010). In this protocol, MdfA was overexpressed in *E. coli*, and purified from the cell membranes by Ni^{2+}-affinity chromatography using LMPG, DHPC, and DDM for structural and functional characterization. Note that DHPC or DDM was used to disrupt cell membranes, and that the detergent was exchanged on the column during the purification into the desired final detergent (Fig. 4.1). SDS-PAGE analysis of MdfA purification in LMPG, DDM, and DHPC showed a band corresponding to MdfA at 31 kDa, as expected based on previous studies (Fig. 4.2). Average protein yield was 0.9 mg MdfA per liter cell culture, and protein purity of MdfA in LMPG was determined to be 80%. Since in all cases, except with initial DDM purification of MdfA, membrane solubilization was performed with DHPC, MdfA yields were similar regardless of final detergent used (Fig 4.2).

In order to minimize non-specific detergent-substrate interactions in kinetic studies and to enhance crystal contacts in structural studies, we sought to optimize the LMPG and DDM concentrations used for MdfA purification. LMPG concentrations ranging from 0.005%-0.2% (w/v) were tested in both TMDG and KP_i buffers by detergent exchange on a Ni-NTA column (Fig 4.3). A given detergent concentration was determined to solubilize MdfA if it could be used for both protein purification and concentration. In SDS-PAGE, MdfA migrates at 31 kDa. In these gels, a single band at 31 kDa in the lane corresponding to pure MdfA indicated pure, soluble protein (Figs. 4.2-5). For purification in TMDG buffer, MdfA was soluble in 0.005% LMPG (Fig. 4.3), while purifications using KP_i buffer required at least a concentration of 0.01% LMPG. DDM concentrations ranging from 0.02-0.4% (w/v) were tested in TMDG buffers. MdfA was soluble in a concentration of DDM as low as 0.02% (Fig 4.4).

To improve the yield and purity of MdfA, an imidazole gradient elution was performed using an ÄKTA FPLC. Imidazole gradients from 20-500 mM were used, in the presence and absence of 500 mM NaCl; however, neither modification improved MdfA purity or yield (data not shown).

Based on a search of the Membrane Protein Data Bank, OG, LDAO, and $C_{12}E_8$ were selected as potential detergents for MdfA solubilization (Table 1) (Raman *et al.*, 2006). Detergent exchange was performed by successive washes with the detergent of interest, prior to protein elution from the column (Fig. 4.2). OG, LDAO, and $C_{12}E_8$ were tested (Fig. 4.5). MdfA was found to be soluble in all three detergents. However, attempts to concentrate MdfA in OG or LDAO detergent micelles immediately resulted in precipitation, indicating that MdfA is not soluble in either OG or LDAO at the required protein concentration (Fig. 4.5B).

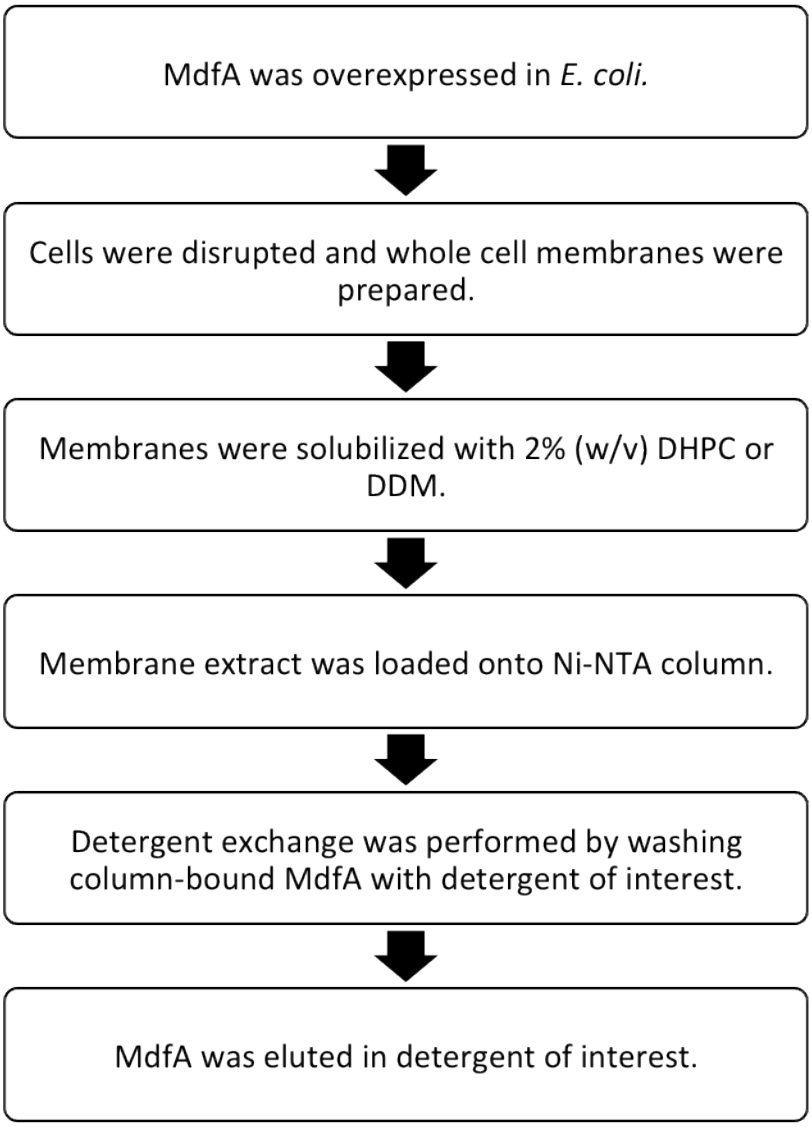

Figure 4.1. Standard protocol for MdfA expression in *E. coli* and purification from whole cell membranes.

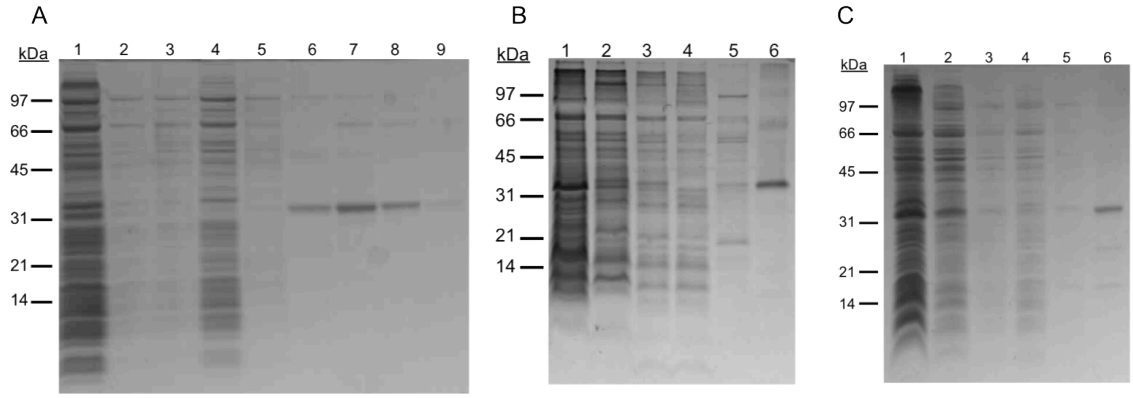

Figure 4.2. MdfA purification steps in different detergents analyzed by SDS-PAGE. Note that MdfA migrates at an apparent molecular weight of 31 kDa on an SDS-PAGE gel. Purifications were performed using a Ni-NTA column. All gels in this figure were stained with Coomassie R-250.

A. Purification of MdfA in 0.2% LMPG using TMDG buffer. Lane 1, 35 µg membrane protein solubilized in 2% DHPC; lane 2, detergent-soluble fraction; lane 3, column load sample; lane 4, column load flowthrough; lane 5, column wash using 0.4% DHPC; lane 6, column wash using 0.2% LMPG; and lanes 7-9, 2 mL column fractions of MdfA elution using 0.2% LMPG. For lanes 3-4, 3.5 µL was loaded, while for lanes 4-9, 7.5 µL of each column wash or fraction was loaded.

B. Purification of MdfA in 0.4% DHPC in KP_i buffer. Lane 1, 75 µg membrane protein solubilized in 2% DHPC; lane 2, detergent-soluble fraction; lane 3, column load sample; lane 4, column load flowthrough; lane 5, column wash using 0.4% DHPC; and lane 6, MdfA elution in 0.4% DHPC. For all lanes, 7.5 µL of each supernatant or column wash was loaded.

C. Purification of MdfA in 0.4% DDM using TMDG buffer. Lane 1, 50 µg membrane protein solubilized in 2% DDM; lane 2, detergent-soluble fraction; lane 3, column load sample; lane 4, column load flowthrough; lane 5, column wash using 0.4% DDM; and lane 6, MdfA elution in 0.4% DDM. For lanes 2-6, 5 µL of each supernatant or column wash was loaded.

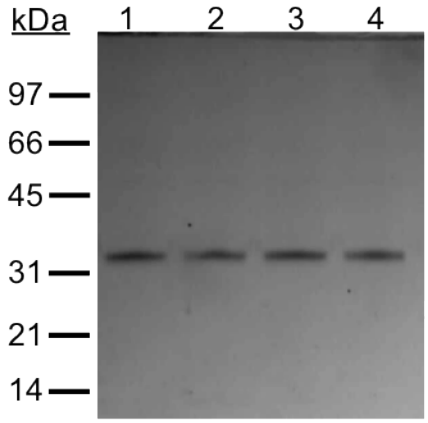

Figure 4.3. Effect of various concentrations of LMPG on MdfA solubility. Coomassie-stained SDS-PAGE gel of Ni-NTA column eluants in TMDG buffer. Lane 1, 0.005% LMPG; lane 2, 0.01% LMPG; lane 3, 0.02% LMPG; and lane 4, 0.2% LMPG. Samples were equalized by volume prior to loading.

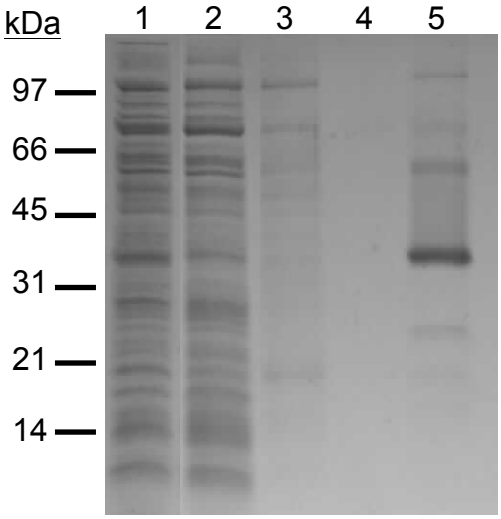

Figure 4.4. MdfA purification in 0.02% DDM. Coomassie-stained SDS-PAGE gel of Ni-NTA column fractions in TMDG buffer. Note that MdfA migrates at an apparent molecular weight of 31 kDa. Lane 1, column load sample; lane 2, column load flowthrough; lane 3, column wash using 0.4% DHPC; lane 4, column wash using 0.02% DDM and 20 mM imidazole; lane 5, MdfA elution in 0.02% DDM. For lane 1, 15 µg protein was loaded, while for lanes 2-5, 7.5 µL of each sample was loaded.

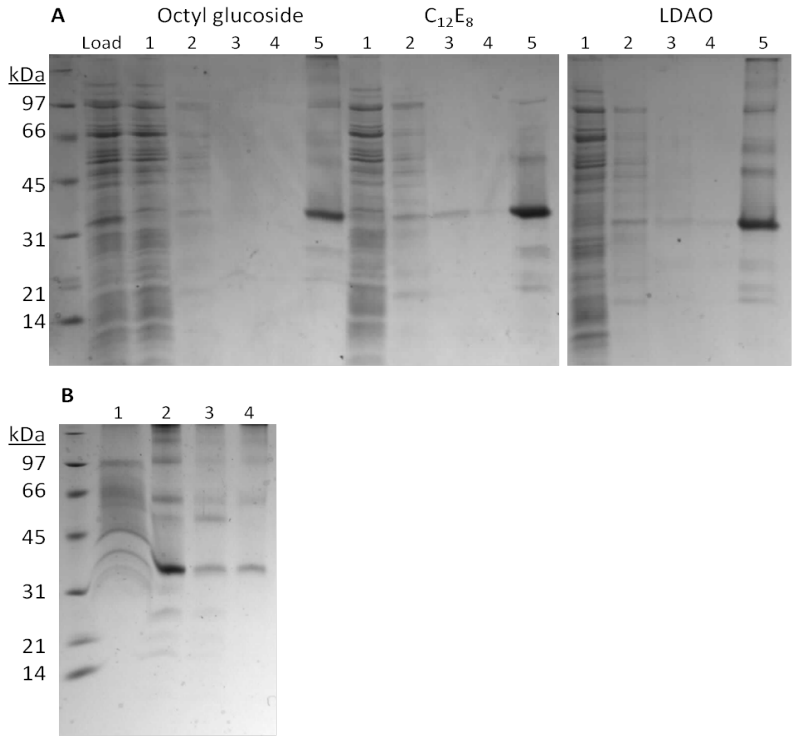

Figure 4.5. Coomassie-stained SDS-PAGE gels of MdfA purification using OG, $C_{12}E_8$, and LDAO. Note that MdfA migrates at an apparent molecular weight of 31 kDa. A. Load, 22 µg detergent-soluble membrane protein prior to detergent exchange. Lane 1, load flowthrough; lane 2, column wash with 0.4% DHPC; lane 3, wash with excess OG, $C_{12}E_8$ or LDAO; and lanes 4 and 5, wash and elution, respectively, with 1.75% OG, 0.013% $C_{12}E_8$ or 0.07% LDAO. Gels were loaded with 11.25 µL of each column wash and final eluant. B. OG and LDAO precipitates were resuspended in buffer volumes equal to the supernatant volume, and 11.25 µL of each supernatant and precipitate were loaded. Lanes 1 and 3, supernatants from MdfA in OG and LDAO, respectively. Lanes 2 and 4, resuspended precipitates from MdfA in OG and LDAO.

4.2 F_oF_1 ATPase purification

Since MdfA is a H^+/drug antiporter, a proton gradient is required to study its transport function across a membrane. In order to use the *E. coli* F_oF_1 ATPase to generate a proton gradient via hydrolysis of ATP to ADP in proteoliposomes with co-reconstituted F_oF_1 ATPase and MdfA, we purified F_oF_1 ATPase from *E. coli* by PEG fractionation. An F_oF_1 ATPase purification from *P. modestum* by PEG fractionation has been reported (Laubinger and Dimroth, 1988). To use this protocol in *E. coli*, three parameters were optimized: the protein:detergent ratio used for membrane solubilization, detergent type, and PEG concentration.

Wild type F_oF_1 ATPase was overexpressed in *E. coli*. *E. coli* membranes were prepared by ultracentrifugation (O'Grady, 2010). Membranes were then solubilized at ratios of 2.5, 5.0, or 10.0 mg protein/mL buffer, and Triton-X 100 concentrations of 0.5, 1.0, 1.5, 2.0, and 2.5% (w/v) (Fig. 4.6). Extracts prepared under these solubilization conditions were then analyzed by SDS-PAGE and Western Blot (Fig. 4.6). Solubilization was determined visually by the intensity of the bands corresponding to subunits α and β of the ATPase in the gel, and the disappearance of the subunit *a* band in lanes corresponding to insoluble fraction in the Western Blot. We selected 5.0 mg protein/mL buffer and 2.0% Triton-X 100 as optimal protein and detergent concentrations since this was the highest protein concentration at which the majority of protein was successfully solubilized (Fig. 4.6B).

This extract was submitted to PEG 6000 fractionation in the presence of 50 mM $MgCl_2$, at PEG concentrations ranging from 2.0-12.0% (w/v), and analyzed by SDS-PAGE and Western Blot. Fractionation was tracked by observation of the intensity of bands corresponding subunits α and β of the ATPase in the gel, and the subunit *a* band in the Western Blot. For PEG precipitation of contaminating proteins, 2.0% PEG was found to be the optimal concentration, since a majority of the F_oF_1 ATPase remained soluble, but much of the other membrane proteins were precipitated (Fig. 4.7). For F_oF_1 ATPase precipitation, 10.0% PEG was found to be ideal, since it was the lowest concentration of PEG at which a majority of the ATPase was precipitated (Fig. 4.7).

In this *E. coli* construct, subunit *a* of the F_oF_1 ATPase is His-tagged. We attempted further purification of the protein complex by imidazole gradient elution using a Qiagen Ni-NTA superflow column. Analysis by SDS-PAGE and Western Blot showed partial dissociation of the enzyme complex into individual subunits. These results indicated that Triton-X 100 is not a suitable detergent for purification of the *E. coli* F_oF_1 ATPase (data not shown).

To find conditions that would preserve the stability of the enzyme complex, we tested ATPase activity by measuring inorganic phosphate accumulation over time using the Malachite green assay. Protein samples from various steps of the purification protocol were tested in the presence and absence of the F_o inhibitor, DCCD. ATPase activity of the *E. coli* membranes was 1.7 U/mg with DCCD sensitivity of 93% (Fig. 4.8A). The purified F_oF_1 ATPase showed ATPase activity of 4.1 U/mg, corresponding to 96% recovery of activity, but it was not sensitive to inhibition by DCCD, indicating that the F_o and F_1 domains are uncoupled (Fig.

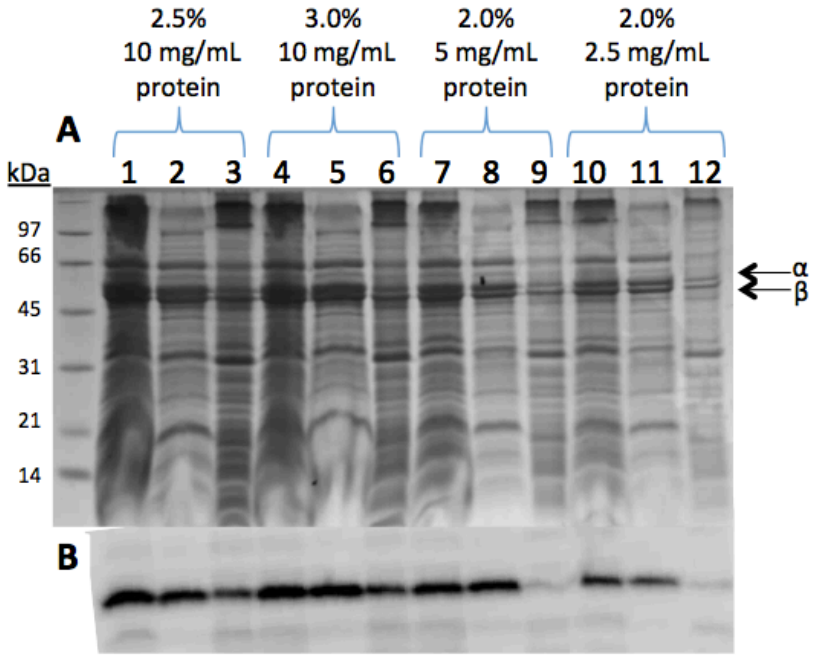

Figure 4.6. Analysis of Triton-X 100 solubilization of *E. coli* membranes for F_oF_1 ATPase purification at various detergent:protein ratios. A. Coomassie-stained SDS-PAGE gel. Subunits α (55.3 kDa) and β (50.3 kDa) were used to track F_oF_1 ATPase precipitation and are indicated by arrows. B. Subunit *a* detection by Western Blot. Low molecular weight markers are shown at left. Lanes 1, 4, 7, 10, membranes with detergent added; lanes 2, 5, 8, 11, detergent-soluble fraction; lanes 3, 6, 9, 12, insoluble protein. Sample volumes were normalized to account for the dilution factor, and 7.5 µL of each was loaded.

4.8B). These results suggested that our purification procedure has a destabilizing effect on the complex.

We next tested the effect of 2.0% Triton-X 100 (w/v), 2.0% OG (w/v), 1.0% DHPC (w/v) and 0.2% DHPC (w/v) on the F_oF_1 ATPase by preparing membrane extracts using these detergents. These extracts were then tested for ATPase activity and DCCD-sensitivity using the Malachite green assay. DCCD-sensitive ATPase activity was found only in 0.2% DHPC (Fig. 4.8A). This extract was applied directly to a nickel column and imidazole gradient elution was performed. However, analysis of the collected fractions by SDS-PAGE and Western Blot indicates that the protein complex was not stable on the column (data not shown).

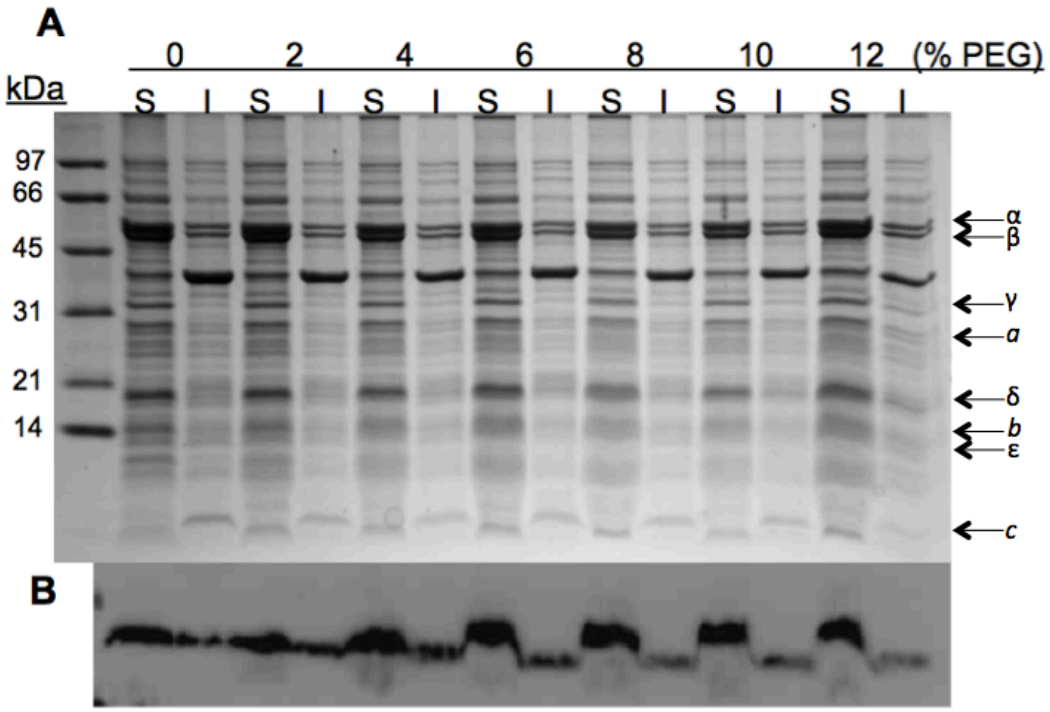

Figure 4.7. Analysis of PEG 6000 concentrations for selective fractionation of F_oF_1 ATPase. Subunits of the ATPase and their molecular weights are as follows: α (55.3 kDa), β (50.3 kDa), γ (31.6 kDa), *a* (30 kDa), δ (19.3 kDa), *b* (17 kDa), ε (14.9 kDa), and *c* (8.2 kDa). Membranes were diluted to 5.0 mg/mL and disrupted using 2.0% Triton-X 100. The detergent-soluble fraction was concentrated threefold, and fractionated using 0, 2, 4, 6, 8, 10, 12% PEG 6000 (final concentration) as indicated. "S" refers to soluble fraction, and "I" refers to insoluble fraction. Sample volumes were normalized to account for the dilution factor. (A) Coomassie-stained SDS-PAGE gel. Arrows indicate subunits of the F_oF_1 ATPase. (B) Subunit *a* detection by Western blot.

Fortunately, PEG precipitation of the 0.2% DHPC extract resulted in a stable F_oF_1 ATPase. The F_oF_1 ATPase in 0.2% DHPC was determined to have a specific activity of 3.8 U/mg, corresponding to 89% recovery of activity, relative to *E. coli* membranes, and was sensitive to inhibition by 0.1 mM DCCD (Fig. 4.9A). Protein purity was determined by densitometry. Comparison of bands corresponding to subunits of F_oF_1 ATPase, with the total density of bands appearing in the lane corresponding with pure protein in the SDS-PAGE gel

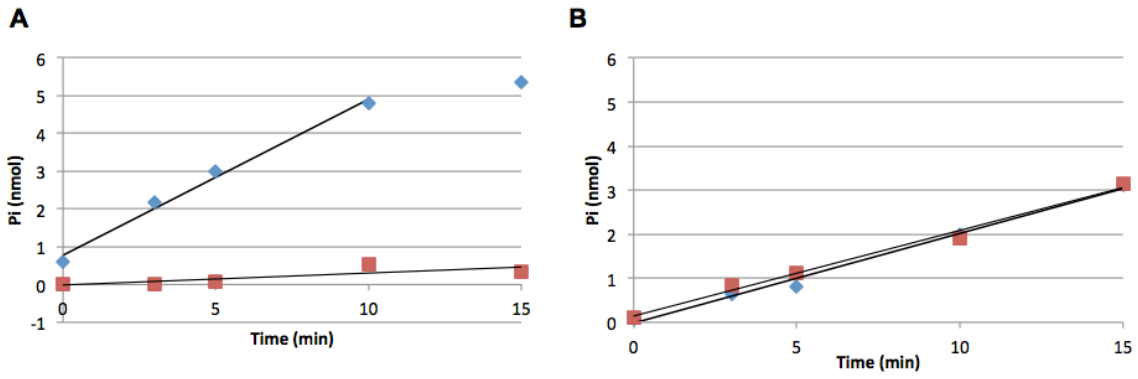

Figure 4.8. Characterization of F_oF_1 ATPase activity and DCCD-sensitivity in 0.05% Triton-X 100 in comparison to *E. coli* membranes. Inorganic phosphate accumulation over time in the presence (red) and absence (blue) of DCCD, an F_o inhibitor. ATP hydrolysis activity of F_oF_1 ATPase in *E. coli* cell membranes (A) and in 0.05% Triton-X 100 detergent micelles (B). Linear fit line was obtained by linear regression in MS Excel.

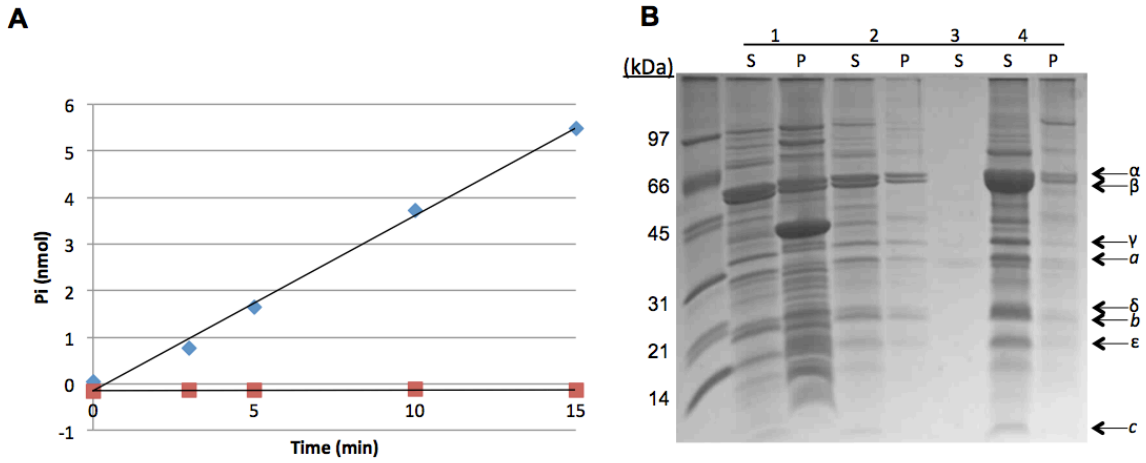

Figure 4.9. Analysis of F_oF_1 ATPase in 0.2% DHPC using the Malachite green assay and Coomassie-stained SDS-PAGE. The bands which correspond to subunits of the F_oF_1 ATPase are indicated by arrows, and are as follows: α – 55.3 kDa, β – 50.3 kDa, γ – 31.6 kDa, *a* – 30 kDa, δ – 19.3 kDa, *b* – 17 kDa, ε – 14.9 kDa, and *c* – 8.2 kDa. A. Inorganic phosphate accumulation over time in the presence (red) and absence (blue) of DCCD, an F_o inhibitor. Linear fit was obtained by linear regression in MS Excel. B. SDS-PAGE gel of F_oF_1 purification using 0.2% DHPC. Low molecular weight standards are shown at left. "S" indicates supernatant, while "P" indicates pellet. Lanes 1, membrane extract; 2, 2% PEG precipitation; 3, 10% PEG precipitation; 4, PEG pellet resuspended in buffer B. Lane 1S has ~40 µg protein loaded. Lanes 1P, 2, and 3 were equalized for volume with lane 1S, and 10 µL of each was loaded. Lane 4S was loaded with 26 µg protein, and lane 4P was equalized by volume with 4S. F_oF_1 purity in lane 4S is estimated to be 60%, by comparison with lane 1S.

showed that the final sample had a purity of 60% (Fig. 4.9B). The final protein yield was 0.5 mg F_oF_1 ATPase/L cell culture. These results indicated that this purification procedure was sufficient for use in co-reconstitution studies with MdfA.

4.3. Fluorescence based substrate transport assays

4.3.1 MdfA activity in *E. coli* whole cell membranes

We sought to develop a simple general assay to test the substrate profiles of putative MFS multidrug transporters. Prior to the start of this project, an assay that couples proton translocation to fluorescence was developed in our lab (O'Grady, 2010). Since MdfA is a H^+/drug antiporter, proton translocation is an indirect way of measuring drug transport. In this assay, MdfA-reconstituted proteoliposomes, pre-loaded with potassium at an internal pH of 7.0, are added to a potassium-free buffer, also at pH 7.0. In this state, the pH-sensitive fluorescent probe, ACMA, will freely diffuse across the liposome membrane. Upon the addition of valinomycin, the membrane becomes permeable to K^+ ions, and an electric potential difference is created. The addition of FCCP allows for protons to dissipate this electric potential difference, while creating a pH difference across the membrane. Protonated ACMA cannot cross the liposome membrane. The charged ACMA molecules are trapped in the liposome lumen, and ACMA fluorescence is quenched in a concentration dependent manner. When MdfA substrate is added to the buffer, MdfA will exchange substrate for protons in a 1:1 ratio, decreasing the transmembrane pH-gradient. ACMA molecules will then be able cross the liposome membrane, and fluorescence will be restored (Fig. 4.10).

Conditions such as buffer composition, liposome amount, the concentrations of FCCP and valinomycin for this assay were optimized (data not shown). Though MdfA-reconstituted proteoliposomes showed fluorescence restoration that correlated with Cml concentration, experiments with control liposomes showed similar effects (Fig. 4.11). In these experiments, ethanol was used as a solvent for Cml. Control experiments were performed to determine if ethanol affected liposome stability, and, as a result, was responsible for the observed fluorescence restoration. Liposomes that had not been treated with detergent were also tested. However, neither ethanol nor DHPC treatment showed results that corresponded to the effect of

Cml on fluorescence restoration (data not shown). We concluded from these experiments that a more robust assay system was required to test putative MDT. Such a system must be able to generate reproducible pH gradients, indicated by similar fluorescence quenching, and cannot be sensitive to substrates in the absence of transporter.

The method of generating the ΔpH is not important for this assay to function. However, it is critical that the assay be easily reproducible and amenable to fine-tuning of the gradient. ATP hydrolysis by F_oF_1 ATPase can be used to generate a pH gradient, and the pH- difference across the membrane is controlled by the amount of ATP in the system. As a result, we co-reconstituted F_oF_1 ATPase and MdfA into proteoliposomes to study MdfA activity. In this assay, reconstituted proteoliposomes are added to quench buffer. The proteoliposome lumen contains 25 mM potassium, and is at pH 7.0, while the buffer has 300 mM potassium, and a pH of 8.0. Valinomycin is added to discharge the electric potential difference that is generated upon the transport of protons by F_oF_1 ATPase into the liposome lumen. ACMA is added, and fluorescence is observed. As stated earlier, neutral ACMA freely crosses the membrane. Upon the addition of ATP, F_oF_1 ATPase hydrolyzes ATP and transports protons across the membrane, creating a pH gradient. Protonated ACMA is trapped in the liposome lumen, and ACMA fluorescence is quenched in a concentration-dependent manner. Fluorescence can then be restored by dissipating the proton gradient, either by the addition of MdfA substrate or the addition of FCCP (Fig. 4.12).

To validate the general assay design, we transport of a known MdfA substrate, Cml, in MdfA-induced and uninduced whole cell membranes. A proton gradient was generated using ATP hydrolysis by endogenous F_oF_1 ATPase, and the effect of Cml addition on fluorescence was observed. We expected that fluorescence would increase if Cml transport were occurring. Indeed, in MdfA-induced cell membranes, Cml transport was observed at concentrations ranging between 20-200 μM, while in uninduced cells, no Cml transport was observed (Fig. 4.13-14). Quench buffer was used as a solvent for Cml in these experiments; control experiments with buffer showed no effect on fluorescence (Fig 4.13-14).

Uninduced cell membranes showed a slightly decreased rate and extent of ATP-dependent fluorescence quenching than induced cell membranes (Fig. 4.13). The reasons for this are unknown. However, it is likely that this difference in the extent of pH gradient

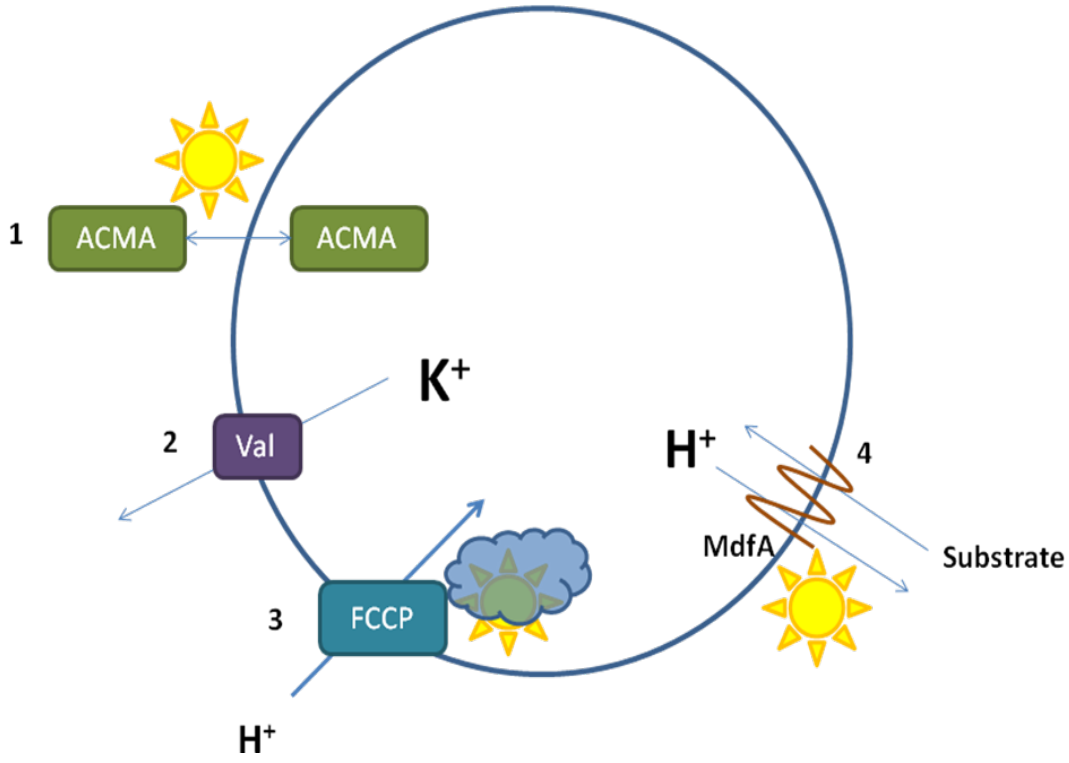

Figure 4.10. Principle of the proton-coupled fluorescence assay using MdfA-reconstituted proteoliposomes. 1. ACMA freely diffuses across the proteoliposome membrane in unprotonated (electroneutral) form. 2. Valinomycin allows K^+ to flow out down its concentration gradient, creating an electrical potential difference across the liposome membrane. 3. FCCP allows H^+ entry into the liposome driven by the electric potential difference. This creates a pH-difference across liposome membrane (acidic inside). ACMA is protonated in a low pH environment and is trapped in the proteoliposome lumen, causing a concentration-dependent fluorescence quenching. 4. The addition of an MdfA substrate to the system causes the coupled transport of a substrate molecule in and of a proton out. The previously trapped ACMA molecules are deprotonated and diffuse out of the proteoliposome resulting in a fluorescence increase.

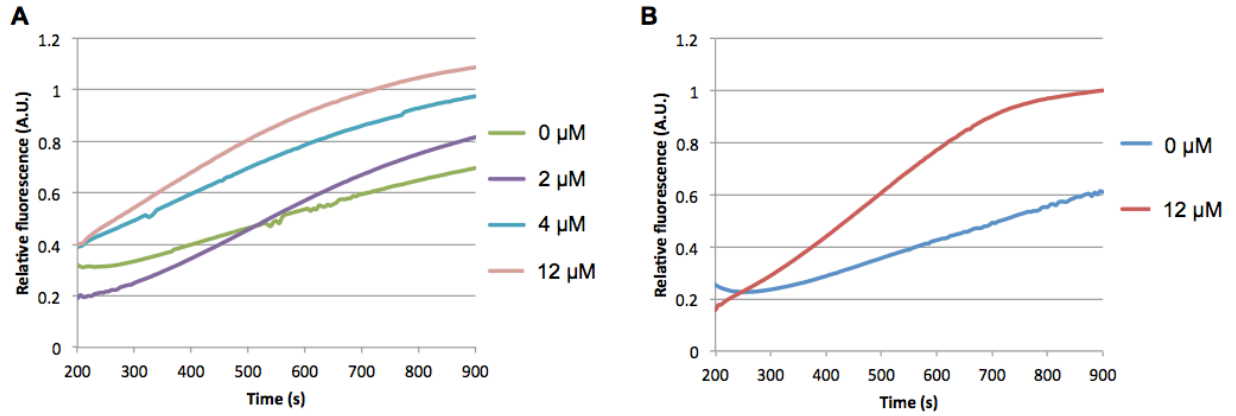

Figure 4.11. ACMA fluorescence restoration upon the addition of Cml to MdfA-reconstituted proteoliposomes (A) and liposomes without reconstituted protein (B). Energy for MdfA substrate transport was generated by conversion of a potassium gradient to a proton gradient using valinomycin and FCCP. The amount of Cml added is indicated in the legend. Cml was added to all samples at 200 s.

generation would not affect the observation of MdfA-independent Cml transport, and no Cml transport was observed (Fig. 4.13-14).

Interestingly, concentrations of Cml greater than 100 µM do not result in increased levels of fluorescence restoration (Fig. 4.14). It is possible that this occurs because high concentrations of Cml have an inhibitory effect on MdfA. Another less likely possibility is that at these concentrations, MdfA transports Cml out of, and protons into, the liposome lumen. Cml is hydrophobic and would readily intercalate into the liposome membrane. In that case, transport in the substrate-in/proton-out direction would still exist, but would be at a lower, and therefore less detectable, rate than the reverse reaction.

The objective of these experiments was to validate the assay system and to determine if MdfA was active in whole cell membranes. We conclude that the assay system designed is valid and can be used for the substrate profile determination of putative multidrug transporters. However, it must be noted that, especially for hydrophobic compounds, concentrations above 200 µM may give false negative results. These experiments also show that MdfA is active in whole cell membranes.

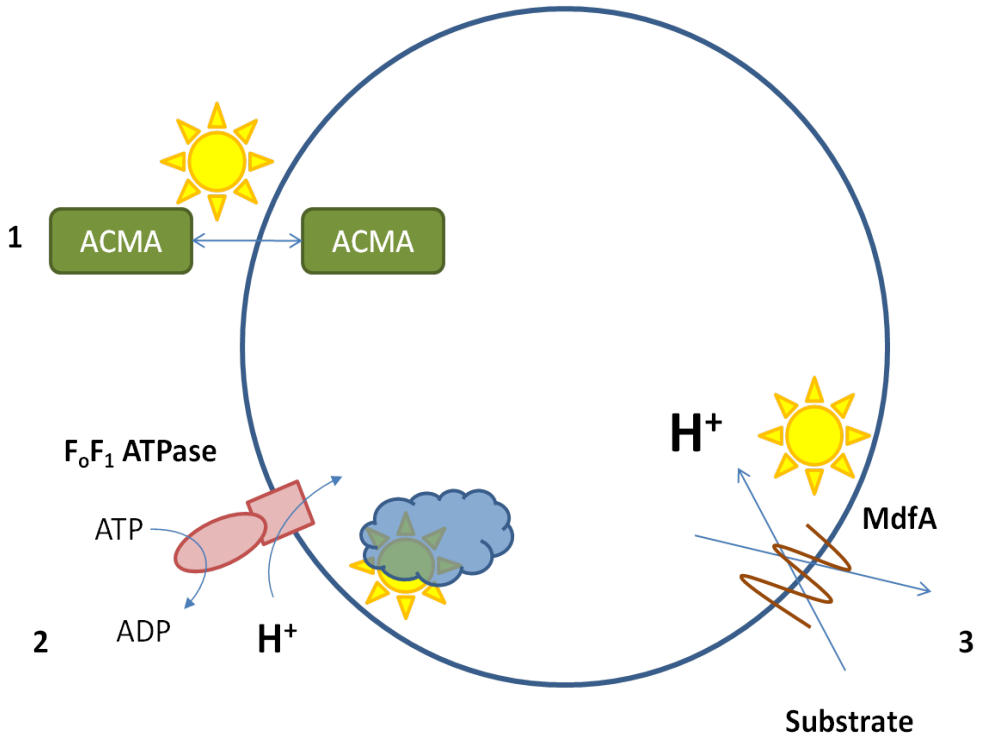

Figure 4.12. Illustration of proton-coupled fluorescence assay using MdfA and F_oF_1 ATPase co-reconstituted proteoliposomes. 1. ACMA freely diffuses across the proteoliposome membrane in unprotonated (electroneutral) form. 2. The addition of ATP causes protons to be actively pumped into the liposome lumen by hydrolysis of ATP to ADP creating a pH difference across the membrane (inside acidic). In this low pH environment, ACMA molecules are protonated and unable to cross the membrane; as a result, ACMA fluorescence is quenched in a concentration-dependent manner. 3. When an MdfA substrate is added to the system, MdfA will use the energy of the proton gradient to pump substrate into the liposome lumen in exchange for a proton. The pH gradient will decrease, causing ACMA molecules to become deprotonated, and able to cross the membrane, resulting in an increase in fluorescence.

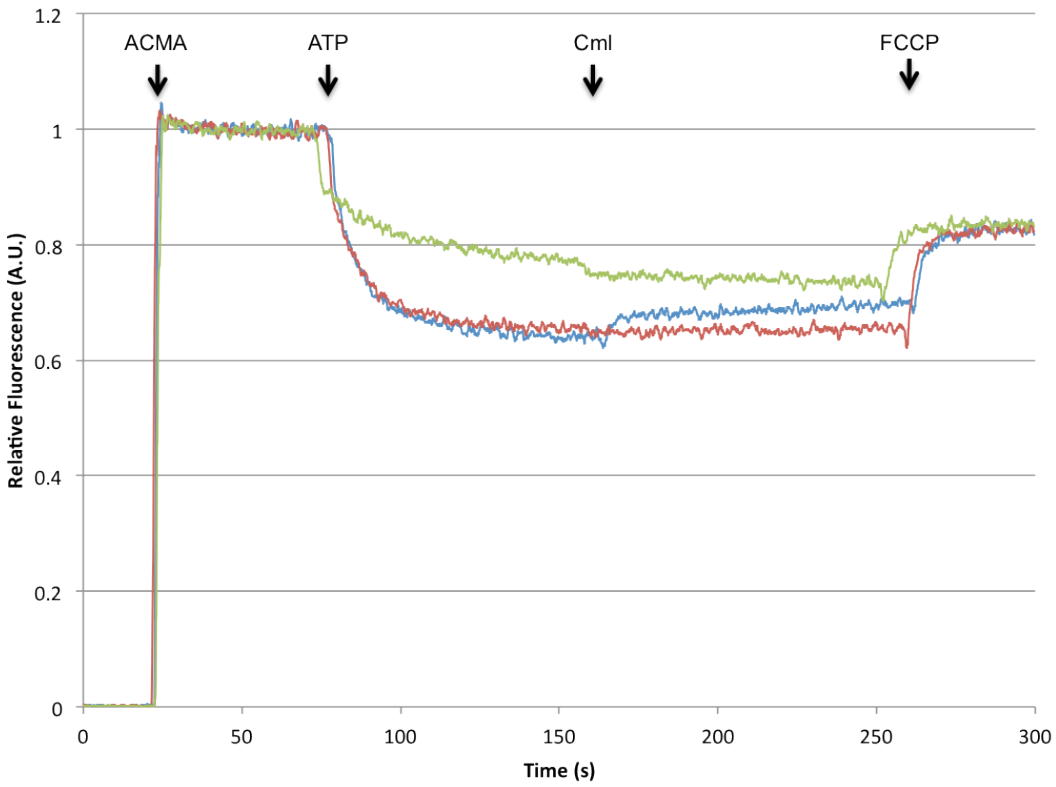

Figure 4.13. Transport of Cml by MdfA in *E. coli* whole cell membranes. A sample set of fluorescence traces showing ACMA fluorescence quenching upon the generation of a proton gradient by ATP hydrolysis, and restoration upon the addition of 100 μM Cml to 100 μg membranes. FCCP, a proton gradient uncoupler, was added as a control. All additions are indicated by arrows. Red, MdfA-induced membranes with buffer added; blue, MdfA-induced membranes with Cml added; green, MdfA-uninduced membranes with Cml added. All experiments were performed in duplicate. Note that the experiments shown here were performed using 0.75 mM ATP.

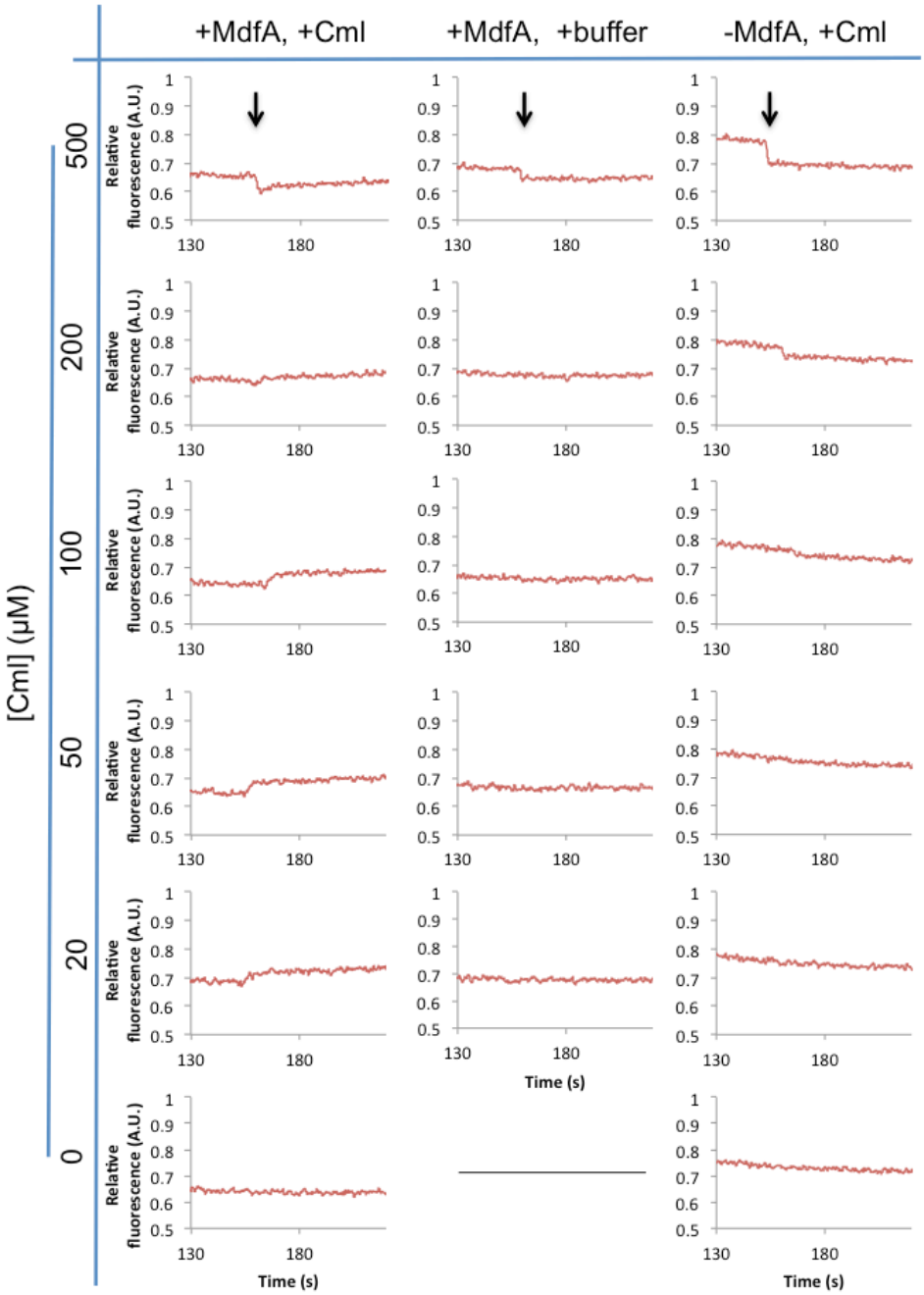

Figure 4.14. Detailed view of transport of 0-500 μM Cml catalyzed by MdfA in *E. coli* cell membranes. Cml transport by overexpressed MdfA in *E. coli* membranes was tested by measuring ACMA fluorescence restoration over time. Additions of Cml or buffer are indicated by black arrows. All experiments were performed in duplicate, though only one representative set is shown. Note that these experiments were performed using 0.75 mM ATP.

4.3.2 Functional co-reconstitution of F_oF_1 ATPase and MdfA for drug transport measurements

In order to develop an assay with greater MDT-specific sensitivity to substrates, we sought to generate a pH-gradient using F_oF_1 ATPase, as described in section 4.3.1 (Fig. 4.12). To test and optimize F_oF_1 ATPase-reconstitution into proteoliposomes, F_oF_1 ATPase was reconstituted into liposomes at 0, 1:40, 1:80, or 1:200 (w/w) protein:lipid ratios. Protein reconstitution was achieved by detergent disruption of preformed liposomes and incubation with protein followed by detergent removal by Bio-Beads. Amounts of liposomes added to quench buffer B were increased from 100 µg to 500 µg until complete fluorescence quenching was achieved. By observing the rate and extent of fluorescence quenching, the fraction of liposomes that have successfully reconstituted F_oF_1 ATPase can be estimated. At a protein:lipid ratio of 1:40, an adequate rate and extent of quench was observed at both 100 µg and 250 µg proteoliposomes (Fig. 4.15). Other protein:lipid ratios showed slower quench rates (data not shown). All future experiments, under these conditions, were performed with 125 µg liposomes at a 1:40 protein:lipid ratio.

Proteoliposome membrane integrity was tested by performing this assay in the absence of valinomycin. Upon the addition of ATP, F_oF_1 ATPase will pump protons into the liposome lumen, generating both ΔpH and $\Delta\psi$ across the membrane. The addition of valinomycin discharges $\Delta\psi$, allowing the F_oF_1 ATPase to generate a higher ΔpH at the same value of $\Delta\mu_H$, as determined by the ΔG of ATP hydrolysis. In the absence of valinomycin, F_oF_1 ATPase will still show some proton transport into the liposome lumen upon the addition of ATP to the system. However, this rate should be much slower than if the electrical potential difference is removed through the addition of valinomycin. Indeed, experimental results show that in the absence of valinomycin, both the rate of fluorescence quenching and uncoupling of the pH gradient by the addition of FCCP were significantly decreased (Fig. 4.16).

To determine the optimal MdfA:lipid ratio for these experiments, MdfA was reconstituted into F_oF_1 ATPase-reconstituted proteoliposomes (1:40 w/w) at a protein:lipid ratio of 0, 1:80, or 1:240 (w/w). Decreased fluorescence quenching was observed at a protein:lipid ratio of 1:80, possibly due to interfering effects of reconstituting a large amount of protein; however, reconstitution at 1:240 showed a fluorescence quenching rate comparable to MdfA-free liposomes (Fig. 4.17A). The addition of 100 µg/mL (310 µM) Cml shows a slight increase

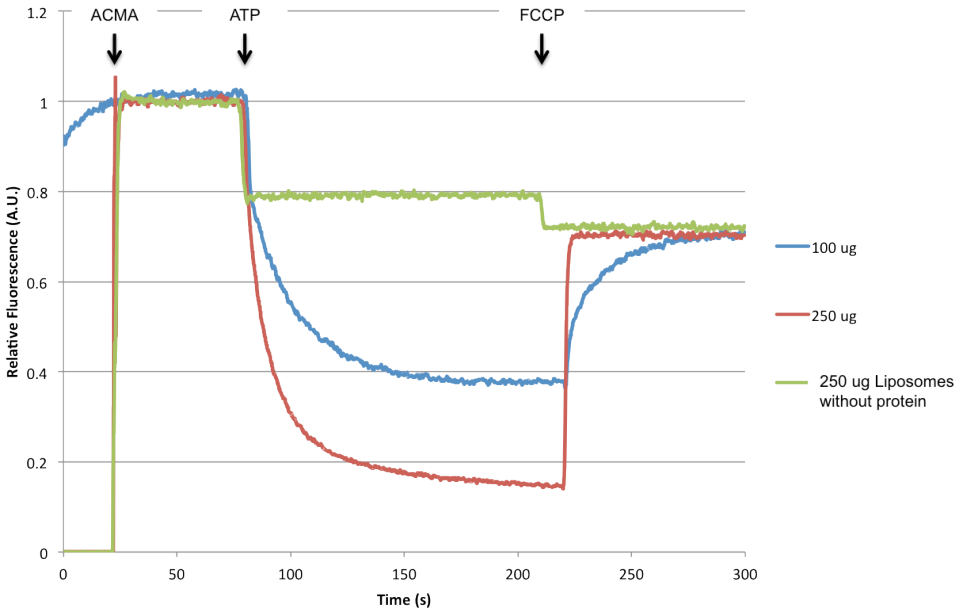

Figure 4.15. ACMA fluorescence quenching in F_oF_1 ATPase-reconstituted proteoliposomes (1:40 w/w protein:lipid). Additions of ACMA, ATP and FCCP are indicated by arrows. Green – 250 µg empty proteoliposomes; red – 250 µg proteoliposomes; and blue – 100 µg proteoliposomes. Note that the experiments shown here were performed using 2 mM ATP.

in fluorescence in MdfA-reconstituted proteoliposomes, indicating successful MdfA reconstitution (Fig. 4.17B). Decreasing the concentration of ATP slowed the rate of fluorescence quenching, but did not affect fluorescence restoration upon the addition of Cml (data not shown).

To improve sensitivity of the assay to substrate transport, and reproducibility between experiments, we sought a different strategy for protein reconstitution. Detergent-mediated reconstitution by dialysis has previously been successful with MFS type transporters such as LacY and GlpT (Poolman and Konings, 1993). Both strategies of detergent removal (Bio-Beads and dialysis) involve incubation of protein with detergent destabilized preformed liposomes, but it is possible that the hydrophobic Bio-Beads bind MdfA and therefore interfere with reproducibility. We developed a dialysis protocol for the co-reconstitution of MdfA and F_oF_1 ATPase. Following dialysis, we performed three cycles of freezing in liquid nitrogen and

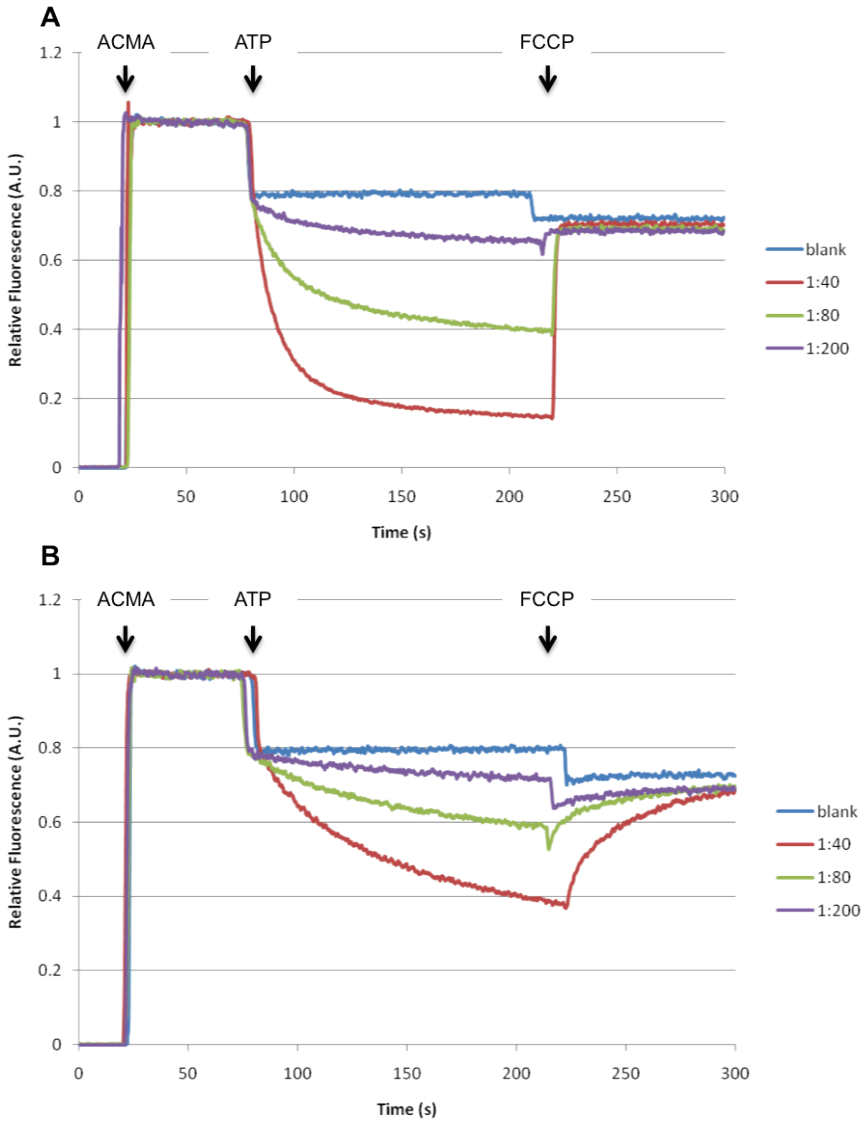

Figure 4.16. Increasing protein:lipid ratio in F_oF_1 ATPase-reconstituted proteoliposomes enhanced rate of ATP-dependent fluorescence quenching. A. ATP-dependent fluorescence quenching in the presence of valinomycin. B. ATP-dependent fluorescence quenching in the absence of valinomycin. Blue – liposomes without protein; red – F_oF_1 ATPase liposomes reconstituted at a 1:40 (w/w) protein:lipid ratio; green – liposomes reconstituted at a 1:80 (w/w) protein:lipid ratio; and purple – liposomes reconstituted at a 1:200 (w/w) protein:lipid ratio. Note that the experiments shown here were performed using 2 mM ATP.

thawing at 25 °C, in order to improve protein and distribution among liposomes. Freeze/thaw cycles cause the fusion and fission of liposomes, and, ideally, will decrease heterogeneity among proteoliposomes. The optimal protein:lipid ratios for F_oF_1 ATPase and MdfA reconstitution were determined as described above. We sought protein:lipid ratios at which the proton gradient, as detected by ACMA fluorescence quenching, was most sensitive, so that any substrate/proton exchange by MdfA would be detected. The optimal F_oF_1 ATPase: lipid ratio was 1:80 (w/w), while the optimal MdfA:lipid ratio was 1:40 (w/w) (data not shown).

Furthermore, we performed sucrose density fractionation of the co-reconstituted proteoliposomes to determine the efficiency of the dialysis-mediated reconstitution protocol. For all fractions, we performed SDS-PAGE and Western blotting to detect protein, and turbidity measurements to detect liposomes (Fig. 4.18). We expected that in a system in which protein reconstitution is occurring, protein and liposomes would be found in the same fractions. Analysis of reconstituted liposomes with and without MdfA demonstrated that while reconstitution of F_oF_1 ATPase was optimal, MdfA co-reconstitution was not ideal (Fig. 4.18). From these experiments, it was not clear whether F_oF_1 ATPase is better able to be reconstituted into liposomes during dialysis or if steric effects from F_oF_1 ATPase prevented co-reconstitution with MdfA. However, it was clear that co-reconstitution needed optimization.

We optimized the reconstitution protocol by first reconstituting each protein into liposomes individually, and then mixing them at specific ratios (w/w lipid) by freeze/thaw cycles to achieve co-reconstitution. The ideal conditions, as shown by fluorescence assays of various ratios, were at 4:1 MdfA-reconstituted proteoliposomes and F_oF_1 ATPase-reconstituted proteoliposomes (Fig. 4.19). In these experiments, 0.1 mM ATP was found to be non-saturating; that is, if a lower concentration of ATP were used, F_oF_1 ATPase would not maintain the fluorescence quench. In theory, a non-saturating concentration of ATP would allow for greater sensitivity to the detection of substrate/proton exchange by MdfA.

We did not observe Cml transport under these conditions (Table 3). However, in theory, the conditions in this setup are ideal. Since it was possible that MdfA transport activity is higher with a different substrate, we tested a variety of known MdfA substrates, and known MFS transporter substrates by MdfA under these conditions (Table 3). Transport was not observed for any substrate tested.

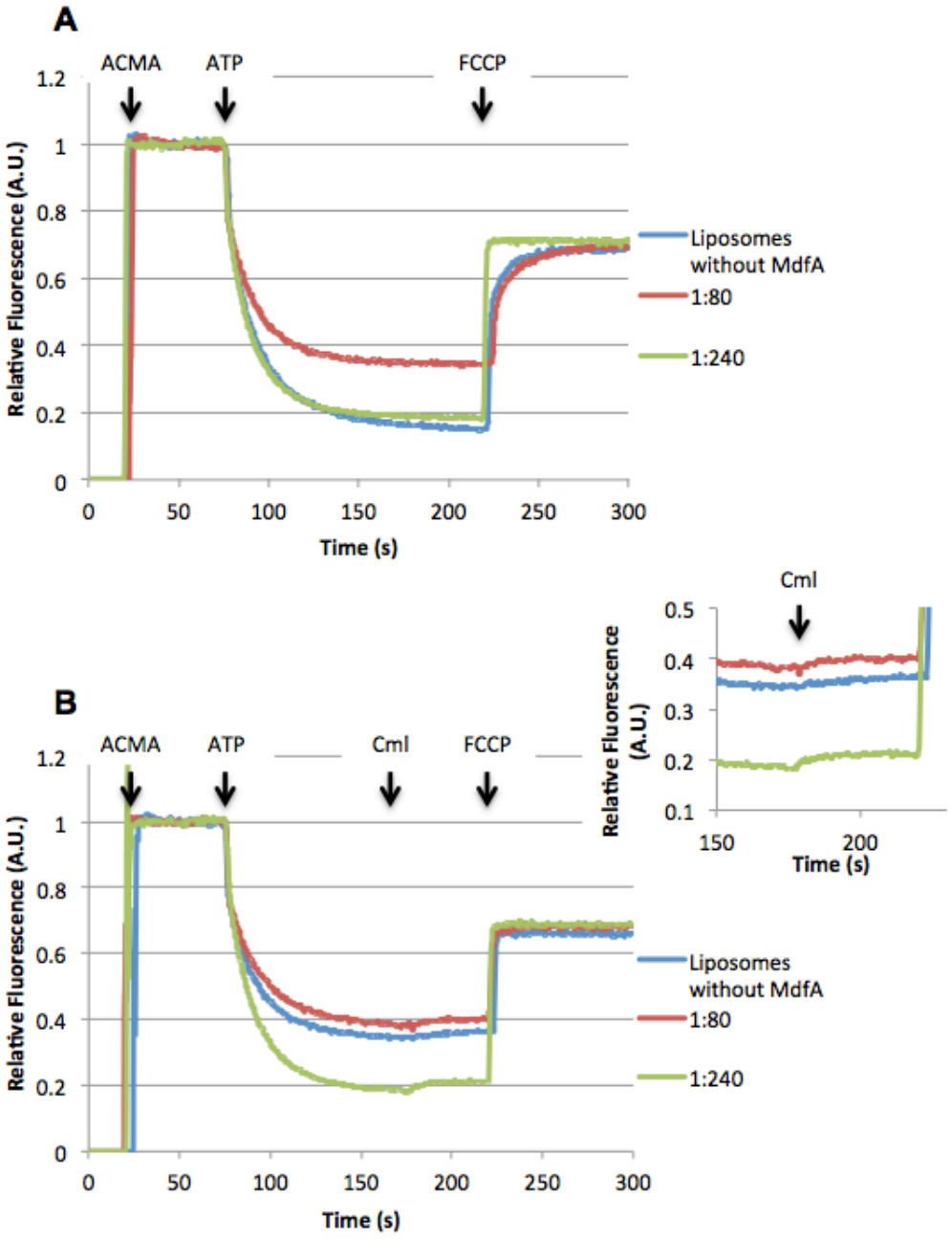

Figure 4.17. Fluorescence assays of co-reconstituted proteoliposomes at various MdfA:lipid ratios. A. Effect of increasing the MdfA:lipid ratio on the rate and extent of fluorescence quenching. B. Upon the addition of 100 µg/mL Cml (at 160 s), fluorescence is slightly restored. *Inset*, fluorescence restoration upon the addition of Cml. Addition of ACMA, ATP, Cml, and FCCP are indicated by arrows. Blue – liposomes without MdfA; red – MdfA and F_oF_1 ATPase-reconstituted proteoliposomes, MdfA:lipid = 1:80 (w/w); and green - MdfA and F_oF_1 ATPase-reconstituted proteoliposomes, MdfA:lipid = 1:240 (w/w).

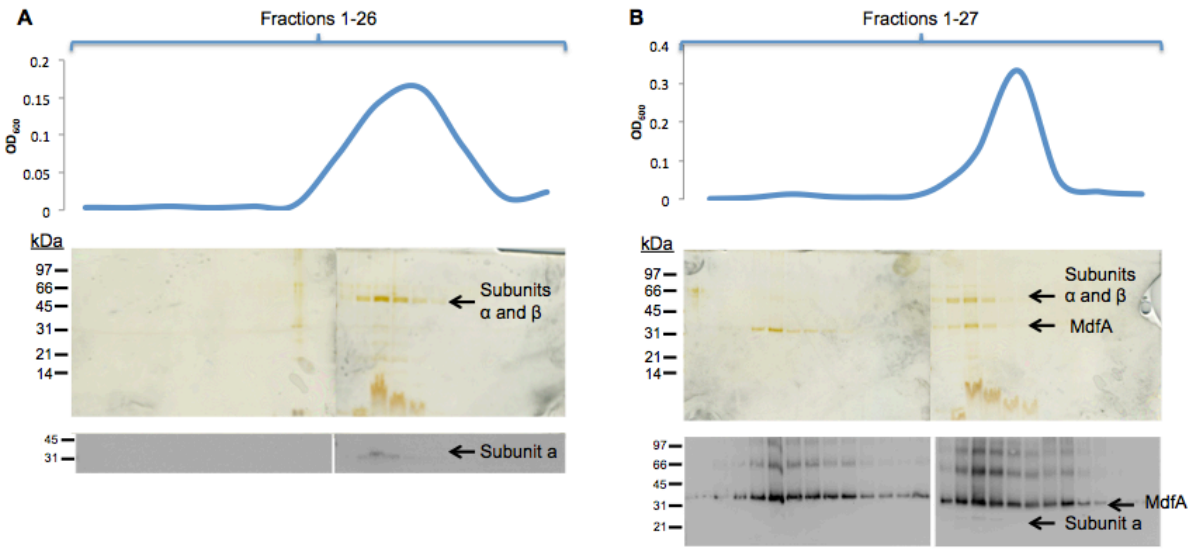

Figure 4.18. Sucrose density fractionation of F_oF_1 ATPase (A) and F_oF_1 ATPase and MdfA co-reconstituted (B) proteoliposomes. Reconstituted proteoliposomes were fractionated on a 45-10% (w/w) sucrose gradient. Top: Turbidity measurements at OD_{600} of all fractions. Middle: Silver-stained SDS-PAGE gels of all fractions. Bottom: Anti-His blot of subunit a from F_oF_1 ATPase and MdfA of all fractions.

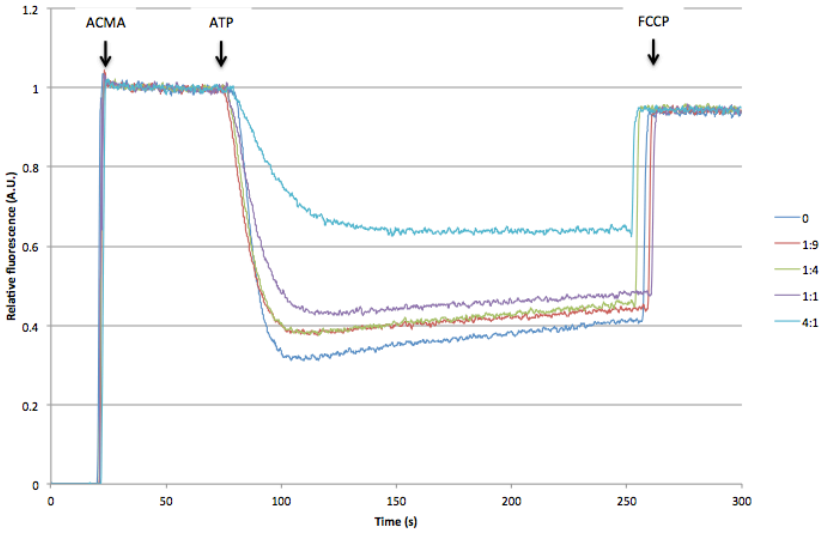

Figure 4.19. Optimization of MdfA and F_oF_1 ATPase co-reconstitution by mixing proteoliposomes at various ratios (w/w). Each sample contained a total of 125 µg liposomes. Ratios of MdfA-containing proteoliposomes to F_oF_1 ATPase-containing proteoliposomes are indicated in the legend. Additions of ACMA, ATP and FCCP are indicated by arrows. Assays shown here were performed using 0.1 mM ATP.

Further attempts at optimization did not yield improved results. The standard buffer used was composed of 20 mM Tricine-KOH, pH 8.0, 5 mM $MgCl_2$, and 300 mM KCl. We tested buffers with decreased pH-buffering capacity, (5 mM Tricine-KOH, pH 8.0 and 1 mM Tricine-KOH, pH 8.0). MdfA is also known to have some K^+/H^+ transport function. As a result, we also tested a potassium-free buffer composed of 20 mM Bis-Tris propane-MES, pH 8.0. However, these buffer compositions prevented the generation of a fluorescence quench, and it was not possible to test substrate transport by MdfA under these conditions (data not shown).

Table 3. Substrates tested for transport by MdfA in F_oF_1 ATPase and MdfA co-reconstituted proteoliposomes.

Substrate *indicates a known MdfA substrate	**Structure**	**Transport? (Y/N)**
Chloramphenicol*	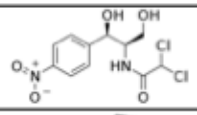	N
Tetraphenylphosphonium*	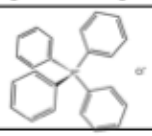	N
NaCl*		N
IPTG*	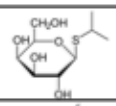	N
Benzalkonium*	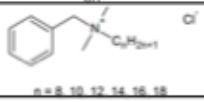	N/A
LiCl		N
Betaine	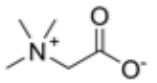	N
Tryptophan	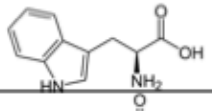	N
Phenylalanine	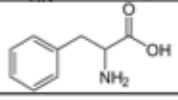	N
Phenylpropionate	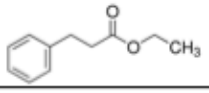	N

4.3.3 Ethidium bromide transport experiments in F_oF_1 ATPase and MdfA co-reconstituted proteoliposomes

The fluorescence assay described above is compatible with a wide variety of potential substrates; however, it has limited applications when the substrates themselves are fluorescent. For example, EtBr is a known MdfA substrate with absorption maxima at 518 nm (DNA-bound) or 480 nm (free EtBr in water). ACMA, on the other hand, is excited at 410 nm and emits photons at 490 nm. Thus, if EtBr was added to the assay system described above, the emission of photons from ACMA would simply excite the molecules of EtBr, and a true reading would not be obtained. This is known as the inner filter effect (Lakowicz, 2006).

As a result, an EtBr-specific assay was required. We designed an assay that exploits the fluorescence intensity increase when EtBr binds DNA. In theory, double-stranded oligonucleotides can be encapsulated into the proteoliposomes with co-reconstituted MdfA and F_oF_1 ATPase. In the assay, following the generation of a proton gradient by the addition of ATP, EtBr is added at the desired amount. EtBr outside the liposome would fluoresce at a lower intensity than any EtBr that would be transported into the liposome by MdfA since EtBr inside would readily bind DNA. It would then be possible to monitor EtBr transport by observing changes in fluorescence intensity. However, we did not observe any difference in fluorescence between liposomes with and without reconstituted MdfA (Fig. 4.20).

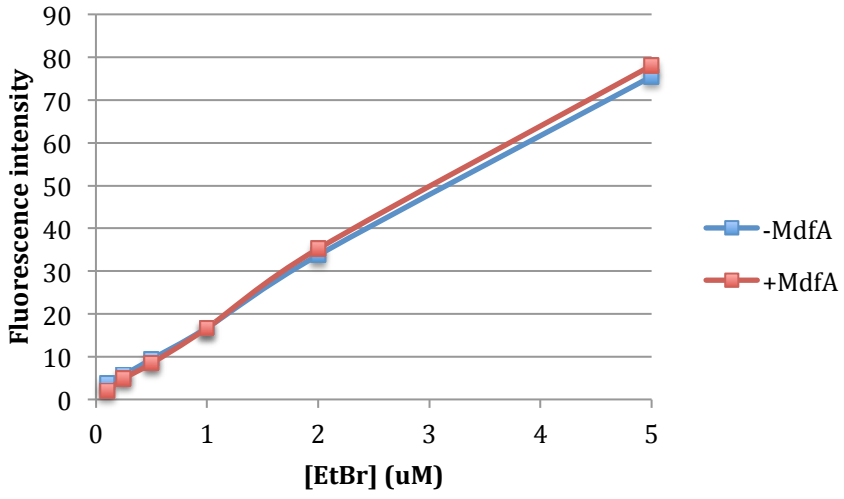

Figure 4.20. DNA-bound EtBr fluorescence intensity in proteoliposomes with and without MdfA.

4.4. NMR experiments for measurement of substrate binding to MdfA

4.4.1 Acetyl chloramphenicol synthesis and characterization

MdfA is a 45 kDa protein, and is too large to obtain useable NMR spectra. However, small molecules such as drugs can be labeled with NMR-active isotopes such as ^{13}C or ^{15}N, and their interactions with MdfA can be detected by monitoring chemical shift perturbations or linewidth broadening of the reporter group. We labeled Cml with a ^{13}C isotope for use in NMR studies. ^{13}C-labeled chloramphenicol was synthesized by acetylation of chloramphenicol with ^{13}C-acetyl chloride as described by Derrick *et al.* (Derrick *et al*., 1991). Both mono- and di-acetylated chloramphenicol were synthesized, and separated by thin layer chromatography. AcCml synthesis was confirmed by proton NMR (Fig. 4.21). The spectrum revealed several extraneous peaks (7.412, 5.159, 4,424, and 2.703 ppm), which are likely to be impurities (Fig. 4.21). As expected, one of the CH_3 peaks, at 2.22 ppm, was not observed, since mono-acetyl Cml was analyzed (Fig. 4.21). However, the $CHCl_2$ peak was shifted from 6.25 ppm to 6.145 ppm (Fig. 4.21). We suspect that this shift is due to the use of acetonitrile as the solvent. Derrick and coworkers used phosphate buffer (pH 7.5) as a solvent for their experiments. We were unable to do the same due to the extreme hydrophobicity of the product.

To confirm the concentration of ^{13}C-AcCml, a calibration curve was produced using NMR by measuring the ^{13}C-acetyl-^{15}N-glycine (NAG) peak intensities as a function of NAG concentration. NAG has two sites that are detectable using $^{1}H,^{13}C$-HSQC experiments, the methyl group and the alpha-proton. As a result, two calibration curves were produced. The NAG methyl group calibration curve was used, since the ^{13}C-AcCml signal is also from a methyl group. This calibration curve was also used to confirm ^{13}C-AcCml concentrations in subsequent experiments (Fig. 4.22).

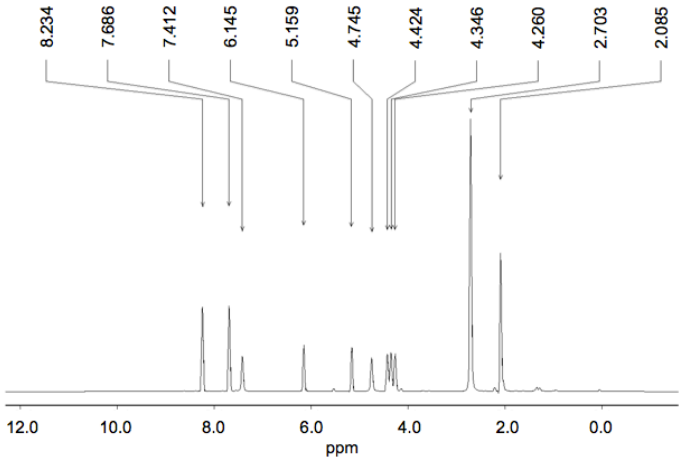

Proton detected	Peak position in Derrick *et al.* (1992) (referenced to dioxane)	Peak positions corrected for DSS as reference
d, meta to NO_2	4.51	8.26
d, ortho to NO_2	3.90	7.65
s, $CHCl_2$	2.50	6.25
d, C-1 H	2.34	6.09
q, C-2 H	0.90	4.65
C-3 H	0.57	4.32
C-3 H	0.48	4.23
d, C1 CH_3	1.53	2.22
d, C3 CH_3	-1.66	2.09

Figure 4.21. Proton NMR spectrum of mono-acetyl chloramphenicol in CD_3CN. DSS was used as a reference. *Left*, spectrum of AcCml with chemical shifts indicated. *Right*, table of expected AcCml proton peaks as described by Derrick and coworkers (Derrick *et al.,* 1992).

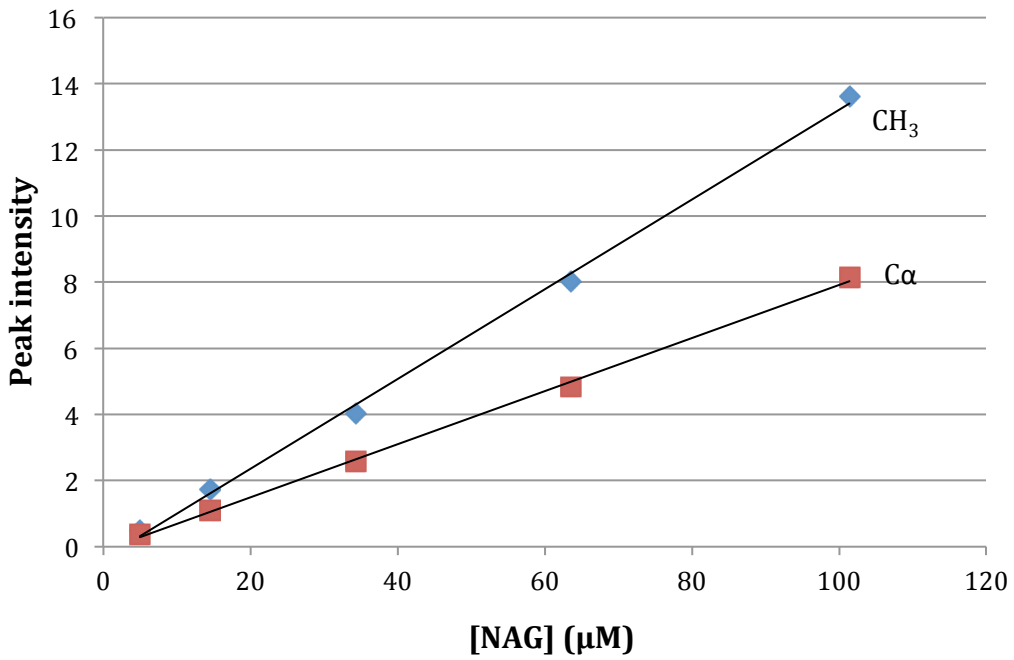

Figure 4.22. Calibration curve using $^{1}H,^{13}C$-HSQC peak intensities of methyl (CH_3) and alpha (C_α) carbons from NAG as a function of NAG concentration. Linear fit line was obtained by linear regression in MS Excel.

4.4.2 Analysis of chloramphenicol binding by NMR

To determine the dissociation constant (K_d) for the binding of Cml to MdfA, we titrated increasing concentrations of MdfA against a constant concentration of ^{13}C-AcCml and performed HSQC experiments at each titration point. We expected to see chemical shift perturbations in the peak corresponding to the methyl group of ^{13}C-AcCml, at 2.085 ppm, as ^{13}C-AcCml was bound by MdfA (Fig. 4.21). Instead, we observed loss of signal intensity corresponding to the increase in concentration of MdfA (Fig. 4.23). To determine whether the observed effects were the result of specific interactions between ^{13}C-AcCml and MdfA, we performed these experiments in the presence of excess unlabeled Cml. Loss of signal intensity was much less in competition experiments with unlabeled Cml, and was not seen at all in control experiments with detergent (Fig. 4.24).

Signal intensity loss may be caused by binding of ^{13}C-AcCml to MdfA under conditions of slow exchange, or line broadening resulting from fast exchange. From these data, it is not possible to distinguish the two possibilities. In the case of slow exchange, we would expect two peaks, at the chemical shifts corresponding to free ligand, L, and bound ligand, P*L, where L refers to ligand and P to protein. If the signal from P*L is unobservable due to fast relaxation (ie. large linewidth), then only the signal from L will be observed, with diminishing intensity as protein concentration increases. On the other hand, if we are actually observing fast exchange, L and P*L will have the same chemical shift. In this case, the only effect that will be observed is loss of signal intensity due to linewidth broadening. The signal-to-noise ratio is insufficient to perform accurate line fitting to distinguish between these two possibilities (Fig. 4.23). As a result, we estimated K_d with the assumption that the peak intensity is proportional to the fraction of free ^{13}C-AcCml (slow-exchange). In this case, K_d=[P]*[L]/[P*L]=[P_{total} (L_{total}-L)]*[L]/(L_{total}-L). Using this model, K_d of ^{13}C-AcCml was determined to be 10 μM. More data points are required in order to accurately fit the data to a model. We conclude that affinity constants for MDT can be determined by isotope labeling of substrates, but that care must be taken to ensure the collection of sufficient data, and to ensure that non-specific interactions to detergent are minimized.

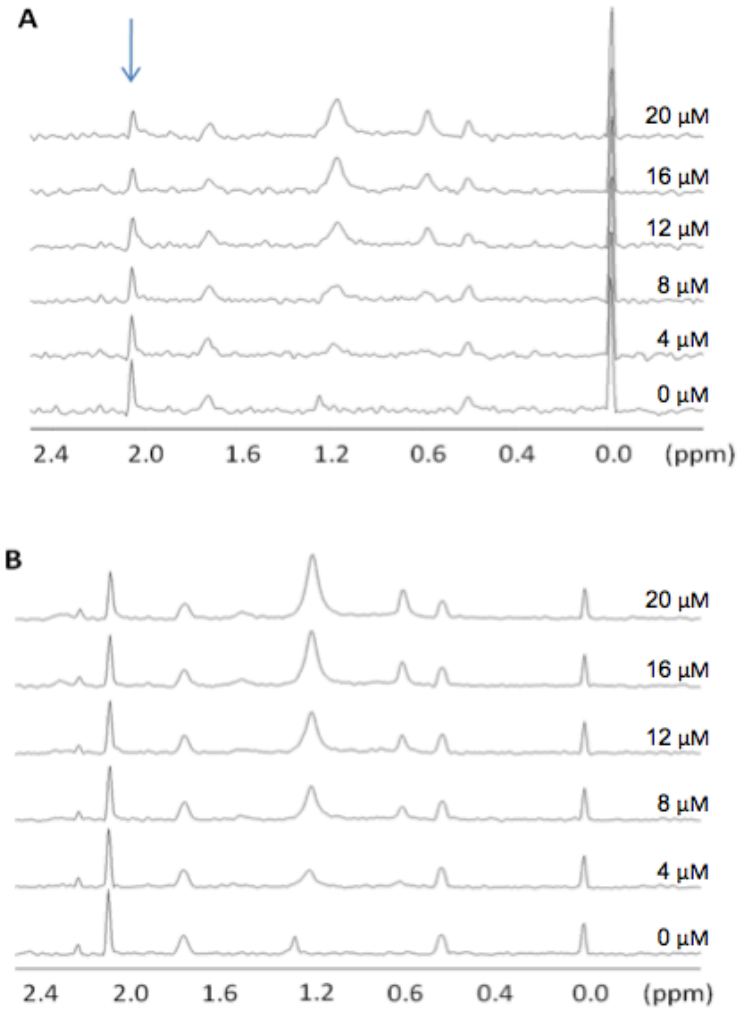

Figure 4.23. Effect of increasing MdfA concentration on methyl signal from ^{13}C-AcCml in the presence and absence of competitor. A. Addition of MdfA to ^{13}C-AcCml in the absence of competitor. B. Addition of MdfA to ^{13}C-AcCml in the presence of competitor (1.5 mM Cml). Methyl signal is indicated by an arrow. Concentration of total MdfA in each spectrum is indicated on right.

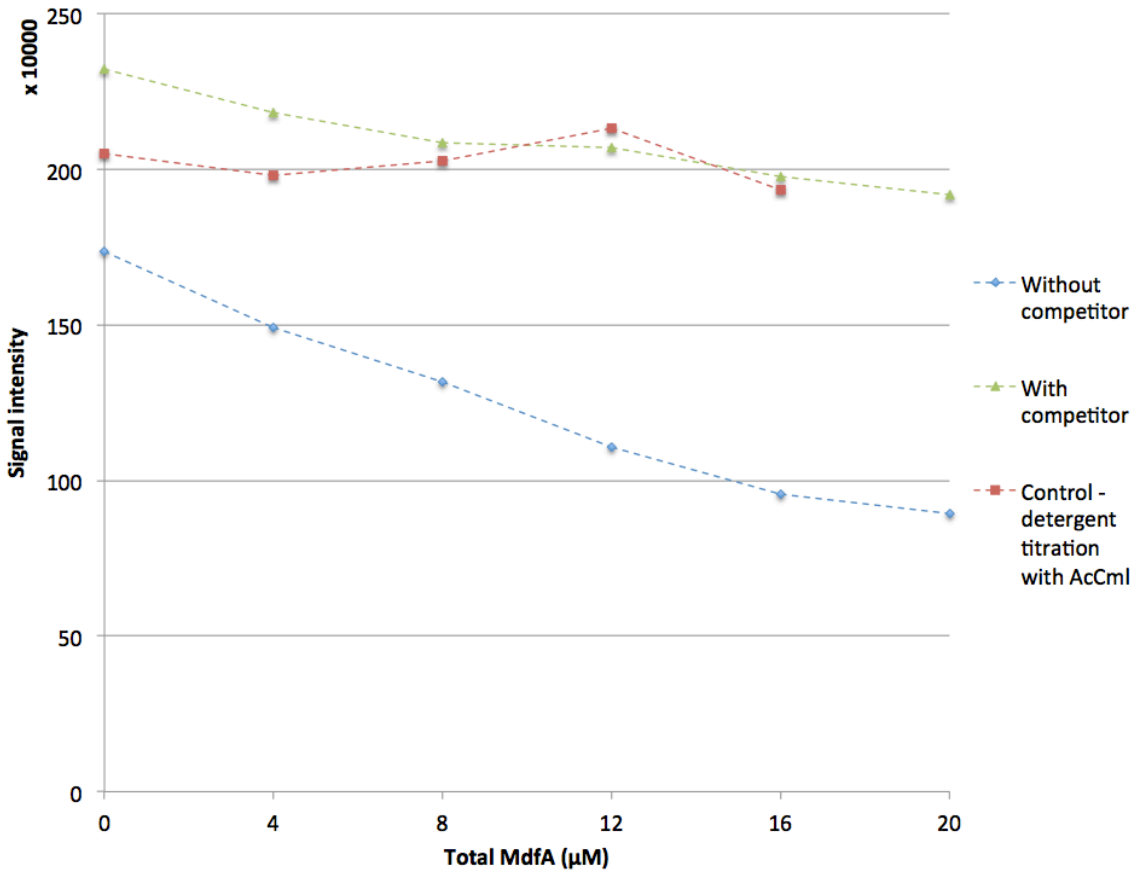

Figure 4.24. ^{13}C-AcCml binding by MdfA. Blue, MdfA titration in the absence of competitor; Green, MdfA titration in the presence of 1.5 mM Cml; and red, detergent control. Note that MdfA titration experiments with ^{13}C-AcCml were performed in duplicate and the average is shown here.

4.5 Initial MdfA crystallization trials

Following optimization of LMPG and DDM concentrations, we tested the aggregation state of MdfA to determine if it was monodisperse, since polydisperse protein samples are not suitable for crystallography. Dynamic Light Scattering (DLS) experiments were performed on MdfA samples in 0.005% LMPG and 0.02% DDM. DLS experiments show strong light scattering at 3 - 4 nm in an 8 mg/mL sample of MdfA in 0.005% LMPG and in a 6.7 mg/mL sample of MdfA in 0.02% DDM, typical of a protein molecule of 50 kDa, showing that MdfA is monodisperse in these conditions (Fig. 4.25). These experiments show that MdfA in LMPG and DDM at these concentrations can be used for crystal trials.

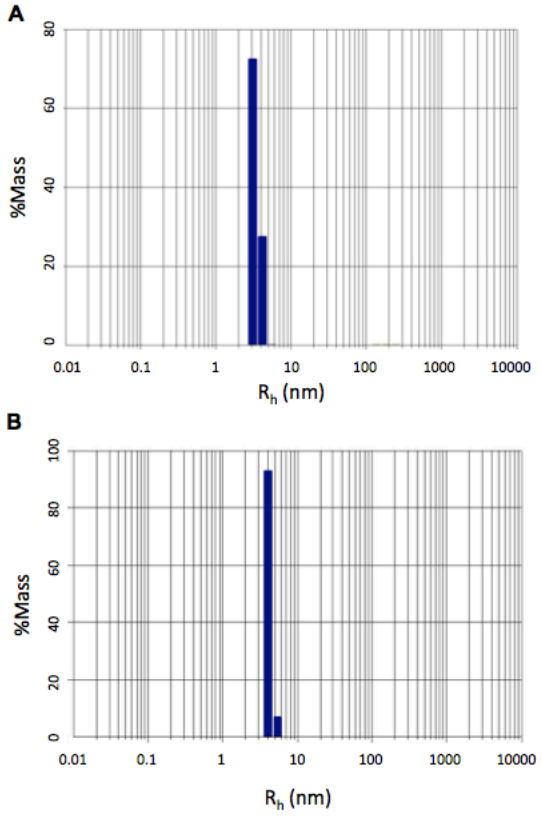

Figure 4.25. DLS experiment of MdfA in 0.005% LMPG and 0.02% DDM. A. DLS experiment of 8.0 mg/mL MdfA in 0.005% LMPG. B. DLS experiment of 6.7 mg/mL MdfA in 0.02% DDM. All measurements were taken at 20 °C. The results show the intensity of the light scattered by particles in solution as a percentage of the total mass in the sample.

To solve the tertiary structure of MdfA, trials were performed to obtain protein crystals suitable for X-ray crystallography. Protein was prepared for crystallization by Ni-NTA chromatography in 0.01% LMPG and 0.4% DDM, and was approximately 80% pure. MdfA in 0.005% LMPG was not used since mixing with crystal conditions causes the detergent concentration to fall below the MdfA solubilization point. Crystal trials with MdfA in 0.02% DDM were not performed due to time considerations.

High-throughput screening of 1536 conditions at the Hauptman-Woodward Institute at 23 °C did not yield any hits. We replicated conditions previously identified in our lab as potential crystal hits in a matrix screen; however, they did not yield crystals. On the other hand, it is possible that the phase separation observed under some conditions indicate regions of crystallization space to be investigated, since membrane protein crystals tend to appear around the phase separation boundary (Fig. 4.26A-C). Other crystal conditions remained under-saturated, and indicate that higher precipitant concentrations should be investigated (Fig. 4.26D). We performed in-house trials using the MemSys kit (Molecular Dimensions Ltd.), a kit that was developed based on reported crystal conditions for membrane protein. This kit covered 48 crystal conditions, and provided a couple of conditions that can be optimized in future studies (Fig. 4.26E-F).

In our opinion, the results here indicate that MdfA crystal trials should continue, but should be broadened in scope to include a variety of detergents, temperatures, and co-crystallization with known substrates.

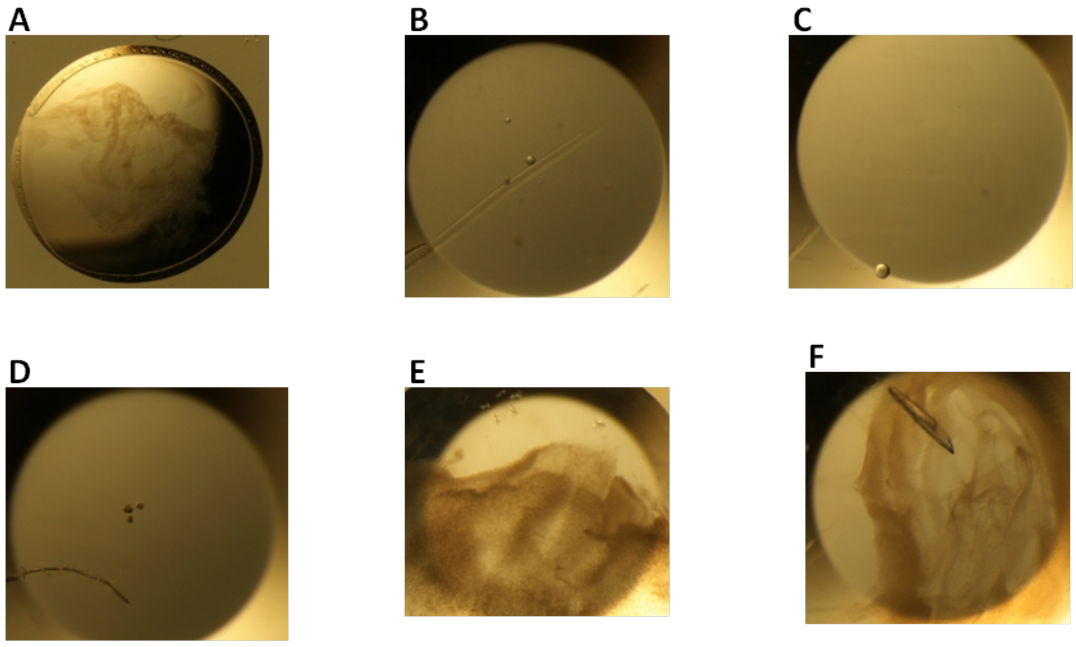

Figure 4.26. Selected in house crystal trials with MdfA in 0.01% (w/v) LMPG and MES buffer at 18 °C. Trials were performed using hanging drop method in 24-well plates. Phase separation is observed in conditions A-C. An undersaturated drop is shown in panel D. Protein precipitation and crystals are observed in conditions E and F. Sample conditions are as follows: A. 0.05 CsCl, 0.1 M MES-KOH, pH 6.5, and 30% Jeffamine M-600. B. 0.1 M Sodium citrate/citric acid, pH 5.5, 0.1 M NaCl, and 30% (v/v) PEG 400. C. 0.1 M Sodium Hepes-HCl, pH 7.5, and 30% (v/v) PEG 400. D. 0.1 M CAPSO-NaOH, pH 9.5, 0.1 M NaCl, 0.1 M Li_2SO_4, and 30% (v/v) PEG 400. E. 0.1 M Tris-HCl, pH 8.5, 0.1 M NaCl, 0.1 M $MgCl_2$, and 30% (v/v) PEG 400. F. 0.1 M Sodium-Hepes-HCl, pH 7.5, 0.1 M NaCl, 0.1 M $MgCl_2$, and 30% (v/v) PEG 400.

5. Discussion

The aim of this research project was to develop techniques for structural and functional characterization of putative multidrug transporters from *S. aureus*, using a model transporter, MdfA. While the particular details for the characterization of each protein will be different (i.e different detergent requirements for solubility, etc.), the overall approach to the study of the members of a family of MDT can be the same. To this end, we developed techniques for substrate profile analysis and transport kinetic measurements, and conducted preliminary crystallization trials. MdfA activity in whole cell membranes was confirmed. An assay that monitors proton transport across proteoliposomes by fluorescence was successfully developed. Chloramphenicol transport by MdfA was observed, but further optimization of the assay conditions is required. ^{13}C isotope labeling of Cml, an MdfA substrate, allowed for K_d estimation by NMR by monitoring linewidth broadening associated with specific interactions between Cml and MdfA. However, the data acquired was insufficient to accurately model substrate binding by MdfA. Further experiments, in which binding site saturation is achieved, are required. In addition, detergent screens and optimization using LMPG, DDM, OG, LDAO, and $C_{12}E_8$ for use in MdfA crystal trials have been performed and preliminary crystal trials have begun.

5.1 Development of activity assay for MFS multidrug transporters

An activity assay suitable for testing MFS multidrug transporters had been previously developed in our lab (O'Grady, 2010). This assay monitors substrate/proton counterflow using ACMA, a pH-sensitive fluorophore, following generation of a pH gradient using FCCP and valinomycin (Fig. 4.10). We optimized this assay and tested Cml transport by MdfA, but were not able to detect MdfA-specific effects. Given the complexity of characterizing a proteoliposome suspension, with no guarantee of results that would explain the observed effects, we adopted an alternative approach to test substrate transport.

For this assay system, two major questions have to be addressed. First, how will the proton motive force be generated? Second, what is the optimal reconstitution procedure? The above mentioned assay used valinomycin and FCCP to convert a potassium concentration gradient to a proton concentration gradient. In contrast, we selected the *E. coli* F_oF_1 ATPase, a powerful proton pump, to generate the energy required for drug transport. The proton gradient

generated was fine-tuned by optimizing the F_oF_1 ATPase:lipid (w/w) ratio and the amount of ATP used. This system provides several advantages over the valinomycin/FCCP method. First, the use of ATP to generate a proton-gradient allows a much greater degree of control of the rate and extent of ΔpH, enhancing both the sensitivity of the assay to substrate transport by MdfA, and the length of the assay itself. In addition, passive ion permeability is a major challenge with proteoliposomes. Stimulation of proton accumulation in proteoliposomes by valinomycin indicates that the liposomes are able to maintain Δψ and therefore have low non-specific ion permeability. We demonstrated proton counterflow coupled to Cml transport in membranes from cells overexpressing MdfA. This counterflow was not observed in membranes from cells with background expression level of MdfA. These results show that ΔpH generation by F_oF_1 ATPase, under these conditions, can be used to test the substrate profile of MdfA, and putative MFS MDT.

Two popular methods of protein-reconstitution into detergent-disrupted preformed liposomes are dialysis and detergent adsorption onto Bio-Beads (Rigaud and Levy, 2003). We tested both methods for co-reconstitution of MdfA and F_oF_1 ATPase. While Cml transport by MdfA using Bio-Beads for reconstitution was observed, we sought a known universal method for the reconstitution of MFS transporters. We chose dialysis, owing to its reproducibility and history of success with MFS transporters (Fig. 4.17) (Poolman and Konings, 1993). It is very likely that the reason why substrate transport was not observed in proteoliposomes reconstituted by dialysis is related to DHPC-mediated MdfA inactivation.

Since reconstitution by dialysis is relatively slow compared to other techniques, it is possible that MdfA is denatured during the time required for successful incorporation into the liposome. For these experiments, MdfA was in DHPC micelles. Since it is known that MdfA precipitates in DHPC solution (O'Grady, 2010), the protein samples were carefully handled and precipitation was prevented. However, it is possible that DHPC inactivates MdfA during purification. In previous studies, it has been shown that delipidation by detergents can be detrimental for membrane protein activity (Garavito and Ferguson-Miller, 2001). Added evidence for this possibility is provided by the fact that the Cml transport that was observed in co-reconstitution experiments using Bio-Beads used MdfA purified using LMPG. For protein reconstitution using the dialysis method, we preferred the use of DHPC due to its higher CMC (relative to LMPG), since residual detergent in liposome suspensions can drastically affect

transport assays. However, future studies should test various detergents (e.g. LMPG, DDM, and $C_{12}E_8$) to identify a detergent that preserves MdfA activity better than those tested. That detergent could then be successfully applied to putative multidrug transporters from the MFS.

However, the combined results of substrate transport observed in whole cell membranes and proteoliposomes reconstituted using Bio-Beads clearly indicate the need for optimization of the assay to enhance sensitivity to substrate transport. While MdfA confers resistance to a wide variety of cytotoxic compounds, the transport rates of these compounds vary. For example, MdfA can confer a 15-fold increase in resistance to Cml, but can only confer two-fold increase in resistance to kanamycin (Edgar and Bibi, 1997). As a result, this assay may not be sensitive enough to detect kanamycin transport. Since the goal of this project is to determine substrate profiles of putative MDT, the assay needs to be optimized to be sensitive to substrates with low transport rates.

5.2 Determination of substrate binding to MdfA by NMR

To determine kinetic parameters of substrate binding to MDR transporters, we tested the binding of a ^{13}C-labeled substrate to MdfA by NMR. NMR can be used to study protein-ligand interactions by detecting NMR signals of either the isotopically-labeled ligand or protein. Selection of which molecule to label is dependent on the purpose of the experiment as well as the limitations of NMR spectroscopy. For example, labeling of the transporter has the advantage of providing information both on the affinity for ligand, and which residues are involved in ligand binding. However, for larger proteins, including most membrane proteins, overlapping resonances and increased linewidths become major challenges to obtaining well-resolved spectra useful for kinetic studies (Breeze, 2000; Evans, 1995; Yanamala *et al*., 2010). Prior to this project, extensive NMR studies of MdfA were performed in our lab. These studies all showed extensive signal overlap due to fast relaxation of magnetization, which related to the large size of MdfA. Substrate binding was observed, but extraction of kinetic data was not possible (O'Grady, 2010). On the other hand, ligands are generally small molecules, which have much less signal overlap and have narrow linewidths. In other words, the signal from one or several nuclei per molecule is detected instead of the hundreds or more detected in proteins. A major disadvantage of the substrate detection method is that experiments are limited to

substrates that are available in isotopically labeled form. Substrates can be labeled with ^{1}H, ^{13}C, ^{15}N, and ^{19}F by a variety of methods, depending on the substrate source and the experimental requirements (Breeze, 2000; Lian and Middleton, 2001; Yanamala *et al*., 2010). Isotopic labeling, especially by non-biological isotopes such as ^{19}F, is usually performed by chemical synthesis. Given these considerations, we labeled Cml with a ^{13}C-isotope for kinetic studies.

Cml contains two hydroxyl groups that can be acetylated by reaction with an acyl halide (Derrick *et al.*, 1992). We were able to distinguish between mono- and di-acetylated Cml by thin layer chromatography and NMR, and used mono-acetylated Cml for all experiments. For MDT with large, flexible substrate-binding pockets, the addition of an acetyl group is not likely to cause large changes in binding kinetics. However, ^{13}C has 1.1% natural abundance; as a result, even with isotope-editing techniques such as HSQCs, care has to be taken to ensure that naturally occurring ^{13}C atoms, for example from detergent molecules, do not interfere with the reporter group signal. Less frequently occurring NMR-active isotopes, such as ^{15}N, or ^{19}F, which has 100% natural abundance, but does not occur naturally in biological systems, can be of benefit in this regard. In particular, ^{19}F has the added benefit of having high sensitivity to detection in NMR, and can be detected directly (Yanamala *et al*., 2010). It is also extremely sensitive to its chemical environment, providing evidence for substrate-protein interactions where ^{13}C and ^{15}N do not (Gerig, 2001; Yanamala *et al*., 2010). However, we chose ^{13}C labeling of Cml because it combines a sufficient level of detection with ease of chemical synthesis.

Linewidth broadening of the reporter signal was determined by measuring peak intensity changes. However, it was not possible to fit the data collected to a model of substrate binding: an improved signal-to-noise ratio is required, combined with data points in the saturation range of the substrate binding curve. As a result, we estimated K_d with the assumption that the decrease in peak intensity is proportional to the amount of free ligand in solution, and obtained a K_d on the order of 10 μM. These experiments will need to be repeated in the future.

5.3 Detergent selection for structural studies and development of conditions for crystallization trials

The purification protocol previously developed for MdfA was reproduced to a yield of 0.9 mg protein/L cell culture, and ~80% purity (O'Grady, 2010). This yield is low compared to that generally required for structural studies, even when compared to membrane proteins. For example, the final yield from GlpT expression and purification was 1.8 mg protein/L cell culture (Auer *et al*., 2001). However, scaling up of protein production to 6 L per purification provides a useable amount of protein (~6 mg) for crystal trials. Protein sample purity, on the other hand, does require improvement. For crystal trials, protein purity of 98% is recommended, but samples of lower purity can be used. We were unable to improve protein homogeneity by using imidazole gradient elution in Ni-NTA chromatography. Future studies could use size-exclusion chromatography to improve the likelihood of successful trials (Newby *et al.*, 2009).

Purification protocols had been previously developed for MdfA in 0.2% LMPG, 0.4% DHPC and 0.4% DDM (w/v) (O'Grady, 2010). MdfA was found to be monodisperse in all three detergents, a condition necessary for structural studies (Carpenter et al., 2008; Garavito, 1996; O'Grady, 2010). However, these detergent concentrations are well above their respective CMCs, and MdfA is not stable in DHPC micelles (O'Grady, 2010). Since the usual working range of detergents is 2-3 times the CMC, and detergent micelles lead to weak crystal contacts, it is important to optimize the detergent concentration used in structural studies (Garavito, 1996; Hunte and Michel, 2002; Iwata, 2003). In addition, it is important to test a variety of detergents for suitability in crystal trials, in order to improve the likelihood of obtaining a protein crystal (Iwata, 2003).

MdfA solubility in OG, LDAO and $C_{12}E_8$ was investigated, and the concentrations of LMPG and DDM optimized. MdfA was determined to be soluble in 0.005% LMPG, 0.02% DDM and 0.013% $C_{12}E_8$, but not in 1.75% OG and 0.07% LDAO. The aggregation state of MdfA in LMPG and DDM was investigated by dynamic light scattering, and MdfA was found to be monodisperse at concentrations suitable for structural studies. These results are not surprising, given that, though OG and LDAO have been successfully used in structural studies, they are relatively harsh detergents, especially prone to denaturing α-helical proteins (Privé, 2007). On the other hand, DDM and $C_{12}E_8$ are mild detergents that have been successfully

used to crystallize MFS transporters, including GlpT, LacY, and EmrD (Abramson *et al*., 2003; Huang *et al*., 2003; Privé, 2007; Yin *et al*., 2006). Finally, while LMPG is particularly known for its use in NMR studies, it should not be excluded from use in crystal trials, since, in general, conditions that produce good NMR spectra also favor protein crystallization (Patching, 2011; Privé, 2007; Wiener, 2004).

The initial crystal trials started here have been by no means exhaustive. First, screens have only been performed using LMPG and non-optimal concentrations of DDM. These now have to be performed with the optimal concentration of DDM and with $C_{12}E_8$. Second, the effects of temperature, buffer conditions, and detergent and protein concentration have not been systematically tested. Finally, it must be mentioned that though detergent phase separation in crystal often leads to protein precipitation and is generally avoided by membrane structural biologists, membrane protein crystals preferentially appear at the phase boundary, due to the attractive interactions between detergent micelles (Garavito, 1996; Hunte, 2003; Koszelak-Rosenblum *et al.*, 2009; Newby *et al.*, 2009). Phase separation is detergent-specific and affected by even small changes in additives, temperature, or precipitant (Garavito and Ferguson-Miller, 2001). As a result, we have opted to select conditions where phase separation is observed for further investigation (Fig 4.26A) (Koszelak-Rosenblum *et al*., 2009).

In addition, the conformational flexibility of MFS proteins must be taken into account. Mutants of MdfA that are less conformationally flexible should be identified and submitted to crystal trials. Co-crystallization with substrates such as EtBr and Cml, respectively, should also be attempted. Decreasing conformational flexibility and co-crystallization with substrate was essential for successful crystallization of LacY (Abramson *et al.*, 2003). The relatively tight binding of Cml measured in NMR studies favors this approach.

6. Conclusions and future directions

6.1 Conclusions

MdfA purification in LMPG, DDM, and $C_{12}E_8$ was optimized for use in crystal trials. Initial screens were performed using LMPG and DDM, but have not yet yielded protein crystals suitable for structural studies. The activity of MdfA in whole cell membranes was confirmed. An assay to test substrate transport of purified MdfA reconstituted in proteoliposomes was

developed, and validated in whole cell membranes. Substrate transport in MdfA and F_oF_1 ATPase co-reconstituted proteoliposomes was also observed. However, reproducible substrate transport was not observed. It was determined that NMR can be used to study the kinetics of substrate binding to MdfA by substrate isotope labeling, and isotope editing techniques. More data is required to accurately measure the K_d. However, these studies clearly show that NMR can be used to determine kinetic data for MFS multidrug transporters.

6.2 Future directions

Our aim was to develop techniques for structural and functional characterization of putative multidrug transporters from *S. aureus*, using a model transporter, MdfA. Co-reconstitution conditions should be more thoroughly investigated to enhance sensitivity of the assay for use in studies of putative transporters. MdfA purified in LMPG, DDM and $C_{12}E_8$, respectively, should be reconstituted into proteoliposomes with F_oF_1-ATPase, and its Cml transport activity investigated. Dialysis conditions, such as temperature and duration should be optimized. Finally, the effect of freeze/thaw cycles on MdfA reconstitution and activity can be investigated.

As mentioned, NMR experiments to confirm the K_d of AcCml binding to MdfA must be performed. Other MdfA substrates should be labeled, either with ^{13}C or other isotopes such as ^{15}N or, ideally, ^{19}F, and the kinetics of binding to MdfA investigated. Doing so will develop a bank of NMR experiments, and potential substrates, that can and should be used to test putative MDT.

The optimized LMPG and DDM concentrations should be used for crystal trials of MdfA. The aggregation state of MdfA in other detergents should be tested. Co-crystallization of MdfA and substrates such as EtBr and Cml should be performed. These studies should all be performed at both 4 and 18 °C. MdfA purity can be improved by size exclusion chromatography, and should be attempted if crystal trials do not yield suitable hits. MdfA mutants with reduced conformational flexibility should be generated and submitted to crystal screens. These mutants can be tested for Cml transport ability in whole membrane assays, and for substrate binding in NMR experiments.

7. References

Abramson, J., Kaback, H.R., and Iwata, S. (2004). Structural comparison of lactose permease and the glycerol-3-phosphate antiporter: members of the major facilitator superfamily. Curr. Opin. Struc. Biol. *14*, 413-419.

Abramson, J., Smirnova, I., Kasho, V., Verner, G., Kaback, H.R., and Iwata, S. (2003). Structure and Mechanism of the Lactose Permease of *Escherichia coli*. Science *301*, 610-615.

Adam, Y., Tayer, N., Rotem, D., Schreiber, G., and Schuldiner, S. (2007). The fast release of sticky protons: Kinetics of substrate binding and proton release in a multidrug transporter. Proc. Natl. Acad. Sci. USA *104*, 17989-17994.

Adler, J., and Bibi, E. (2002). Membrane Topology of the Multidrug Transporter MdfA: Complementary Gene Fusion Studies Reveal a Nonessential C-Terminal Domain. J. Bacteriol. *184*, 3313-3320.

Adler, J., and Bibi, E. (2004). Determinants of substrate recognition by the *Escherichia coli* multidrug transporter MdfA identified on both sides of the membrane. J. Biol. Chem. *279*, 8957-8965.

Adler, J., and Bibi, E. (2005). Promiscuity in the geometry of electrostatic interactions between the *Escherichia coli* multidrug resistance transporter MdfA and cationic substrates. J. Biol. Chem. *280*, 2721-2729.

Alekshun, M.N., and Levy, S.B. (2007). Molecular mechanisms of antibacterial multidrug resistance. Cell *128*, 1037-1050.

Almeida da Silva, P.E., Von Groll, A., Martin, A., and Palomino, J.C. (2011). Efflux as a mechanism for drug resistance in *Mycobacterium tuberculosis*. FEMS Immunol. Med. Micro. *63*, 1-9.

Angus, B.L., Carey, A.M., Caron, D.A., Kropinski, A.M., and Hancock, R.E. (1982). Outer membrane permeability in *Pseudomonas aeruginosa:* comparison of a wild-type with an antibiotic-supersusceptible mutant. Antimicrob. Agents Ch. *21*, 299-309.

Arnold, A.H. (1991). Metal-Affinity Separations: A New Dimension in Protein Processing. Bio-Technol. *9*.

Auer, M., Kim, M.J., Lemieux, M.J., Villa, A., Song, J.M., Li, X.D., and Wang, D.N. (2001). High-yield expression and functional analysis of *Escherichia coli* glycerol-3-phosphate transporter. Biochemistry-US *40*, 6628-6635.

Baker, J., Wright, S.H., and Tama, F. (2012). Simulations of substrate transport in the multidrug transporter EmrD. Proteins-Struc. Func. Bioinf. *80*, 1620-1632.

Baneyx, F. (1999). Recombinant protein expression in *Escherichia coli*. Curr. Opin. Biotechnol. *10*, 411-421.

Basting, D., Lehner, I., Lorch, M., and Glaubitz, C. (2006). Investigating transport proteins by solid state NMR. N-S Arch. Pharmakol. *372*, 451-464.

Breeze, A.L. (2000). Isotope-filtered NMR methods for the study of biomolecular structure and interactions. Prog. Nucl. Mag. Res. Sp. *36*, 323-372.

Butler, P.J.G., Ubarretxena-Belandia, I., Warne, T., and Tate, C.G. (2004). The *Escherichia coli* multidrug transporter EmrE is a dimer in the detergent-solubilised state. J. Mol. Bio. *340*, 797-808.

Carpenter, E.P., Beis, K., Cameron, A.D., and Iwata, S. (2008). Overcoming the challenges of membrane protein crystallography. Curr. Opin. Struc. Biol. *18*, 581-586.

Chao, Y., and Fu, D. (2004). Kinetic study of the antiport mechanism of an *Escherichia coli* zinc transporter, ZitB. J. Biol. Chem. *279*, 12043-12050.

Chen, Y.J., Pornillos, O., Lieu, S., Ma, C., Chen, A.P., and Chang, G. (2007). X-ray structure of EmrE supports dual topology model. Proc. Natl. Acad. Sci. USA *104*, 18999-19004.

Coates, A.R.M., Halls, Gerry, Hu, Yanmin (2011). Novel classes of antibiotics or more of the same? Brit. J. Pharmacol. *163*, 184-194.

Cook, M., Molto, E., and Anderson, C. (1989). Fluorochrome labeling in roman preiod skeletons from Dakhleh Oasis, Egypt Am. J. Phys. Anthropol. *80*, 137-143.

Dawson, R.J.P., and Locher, K.P. (2006). Structure of a bacterial multidrug ABC transporter. Nature *443*, 180-185.

Derrick, J.P., Lian, L.Y., Roberts, C.K., and Shaw, W.V. (1992). Analysis of the Binding of 1,3-Diacetylchloramphenicol to Chloramphenicol Acetyltransferase by Isotope-Edited ^{1}H NMR and Site-Directed Mutatgenesis. Biochemistry-US. *31*, 8191-8195.

Derrick, J.P., Lian, L.Y., Roberts, G.C.K., and Shaw, W.V. (1991). Identification of the C2-^{1}H Histidine NMR Resonances in Chloramphenicol Acetyltransferase by a ^{13}C-^{1}H Heteronuclear Multiple Quantum Coherence Method. FEBS Letters *280*, 125-128.

Doleans-Jordheim, A., Michalet, S., Bergeron, E., Boisset, S., Souard, F., Dumontet, C., Dijoux-Franca, M.G., and Freney, J. (2008). Efflux pumps: their role in *Staphylococcus aureus* antibiotic resistance. Annal. Biol. Clin. *66*, 499-508.

Doucleff, M.H.-S., Mary; Crane, Nicole J. (2011). Pocket Guide to Biomolecular NMR (London: Springer).

Dougherty, D.A. (1996). Cation-π interactions in chemistry and biology: A new view of benzene, Phe, Tyr, and Trp. Science *271*, 163-168.

Edgar, R., and Bibi, E. (1997). MdfA, an *Escherichia coli* Multidrug Resistance Protein with an Extraordinarily Broad Spectrum of Drug Recognition. J. Bacteriol. *179*, 2274-2280.

Edgar, R., and Bibi, E. (1999). A single membrane-embedded negative charge is critical for recognizing positively charged drugs by the *Escherichia coli* multidrug resistance protein MdfA. EMBO J. *18*, 822-832.

Engel, C.K., Chen, L., and Privé, G.G. (2002). Stability of the lactose permease in detergent solutions. Biochim. Biophys. Acta *1564*, 47-56.

Evans, J. (1995). Biomolecular NMR spectroscopy (USA: Oxford University Press).

Fernandez, C., and Wuthrich, K. (2003). NMR solution structure determination of membrane proteins reconstituted in detergent micelles. FEBS Letters *555*, 144-150.

Fluman, N., and Bibi, E. (2009). Bacterial multidrug transport through the lens of the major facilitator superfamily. Biochim. Biophys. Acta *1794*, 738-747.

Forrest, L.R., Kraemer, R., and Ziegler, C. (2011). The structural basis of secondary active transport mechanisms. BBA-Bioenergetics *1807*, 167-188.

Forrest, L.R., and Rudnick, G. (2009). The Rocking Bundle: A Mechanism for Ion-Coupled Solute Flux by Symmetrical Transporters. Physiology *24*, 377-386.

Foucaud, C., and Poolman, B. (1992). Lactose Transport-System Of *Streptococcus thermophilus* - Functional Reconstitution Of The Protein And Characterization Of The Kinetic Mechanism Of Transport. J. Biol. Chem. *267*, 22087-22094.

Garavito, R.M., and Ferguson-Miller, S. (2001). Detergents as tools in membrane biochemistry. J. Biol. Chem. *276*, 32403-32406.

Garavito, R.M., Picot, D., Loll, P.J. (1996). Strategies for Crystallizing Membrane Proteins. J. Bioenerg. Biomembr. *28*, 13-27.

Geertsma, E.R., Mahmood, N., Schuurman-Wolters, G.K., and Poolman, B. (2008). Membrane reconstitution of ABC transporters and assays of translocator function. Nature Protocols *3*, 256-266.

Gerig, J.T. (2001). Fluorine NMR. In Biophysics Textbook Online, D. Gorenstein, ed., pp. 1-35.

German, N., Wei, P., Kaatz, G.W., and Kerns, R.J. (2008). Synthesis and evaluation of fluoroquinolone derivatives as substrate-based inhibitors of bacterial efflux pumps. Eur. J. Med. Chem. *43*, 2453-2463.

Gootz, T.D. (2010). The Global Problem of Antibiotic Resistance. CRC CR. Rev. Immunol. *30*, 79-93.

Guzman, L.M., Belin, D., Carson, M. J., Beckwith, J. (1995). Tight regulation, modulation, and high-level expression by vectors containing the arabinose pBAD promoter. J. Bacteriol. *177*, 4121-4130.

Hancock, R.E.W. (1997). The bacterial outer membrane as a drug barrier. Trends Microbiol. *5*, 37-42.

Hayashi, S., Lin, E.C.C., and Koch, J.P. (1964). Active Transport Of L-Alpha-Glycerophosphate In *Escherichia coli*. J. Biol. Chem. *239*, 3098-3105.

Helling, R.B., Janes, B.K., Kimball, H., Tran, T., Bundesmann, M., Check, P., Phelan, D., and Miller, C. (2002). Toxic waste disposal in *Escherichia coli*. J. Bacteriol. *184*, 3699-3703.

Henkel, R.D., VandeBerg, J.L., and Walsh, R.A. (1988). A Microassay for ATPase. Anal. Biochem. *169*, 312-318.

Heuberger, E.H., and Poolman, B. (2000). A spectroscopic assay for the analysis of carbohydrate transport reactions. Eur. J. Biochem. *267*, 228-234.

Higgins, C.F. (2007). Multiple molecular mechanisms for multidrug resistance transporters. Nature *446*, 749-757.

Higgins, C.F., Linton, K. J. (2004). The ATP switch model for ABC transporters. Nat. Struct. Mol. Biol. *11*, 918-926.

Huang, Y., Lemieux, M.J., Song, J., Auer, M., and Wang, D.N. (2003). Structure and Mechanism of the Glycerol-3-Phosphate Transporter from *Escherichia coli.* Science *301*, 616-620.

Hunte, C., and Michel, H. (2002). Crystallization of membrane proteins mediated by antibody fragments. Curr. Opin. Struc. Biol. *12*, 503-508.

Hunte, C., Michel, H. (2003). Membrane Protein Crystallization. In Membrane Protein Purification and Crystallization: A Practical Approach, C. Hunte, Von Jagow, G., Schägger, H., ed. (San Diego: Academic Press).

Iwata, S. (2003). Crystallization Informatics of Membrane Proteins. In Methods and Results in Crystallization of Membrane Proteins, S. Iwata, ed. (La Jolla: International University Line), pp. 281-298.

Jardetzky, O. (1966). Simple Allosteric Model For Membrane Pumps. Nature *211*, 969-970.
Juge, N., Yoshida, Y., Yatsushiro, S., Omote, H., and Moriyama, Y. (2006). Vesicular glutamate transporter contains two independent transport machineries. J. Biol. Chem. *281*, 39499-39506.

Kaback, H.R., Sahin-Toth, M., and Weinglass, A.B. (2001). The kamikaze approach to membrane transport. Nat. Rev. Mol. Cell Bio. *2*, 610-620.

Knol, J., Veenhoff, L., Liang, W.J., Henderson, P.J.F., Leblanc, G., and Poolman, B. (1996). Unidirectional reconstitution into detergent-destabilized liposomes of the purified lactose transport system of *Streptococcus thermophilus* J. Biol. Chem. *271*, 15358-15366.

Korkhov, V.M., and Tate, C.G. (2009). An emerging consensus for the structure of EmrE. Acta Crystallographica Section D-Biological Crystallography *65*, 186-192.

Koszelak-Rosenblum, M., Krol, A., Mozumdar, N., Wunsch, K., Ferin, A., Cook, E., Veatch, C.K., Nagel, R., Luft, J.R., Detitta, G.T.*, et al.* (2009). Determination and application of empirically derived detergent phase boundaries to effectively crystallize membrane proteins. Protein Sci *18*, 1828-1839.

Kropinski, A.M.B., Kuzio, J., Angus B. L., Hancock, R. E. W. (1982). Chemical and Chromatographic Analysis of lipopolysaccharide from an antibiotic-supersusceptible mutant of *Pseudomonas aeruginosa*. Antimicrob. Agents Ch. *21*, 310-319.

Krulwich, T.A., Lewinson, O., Padan, E., and Bibi, E. (2005). Do physiological roles foster persistence of drug/multidrug-efflux transporters? A case study. Nature Reviews *3*, 566-572.
Kuroda, T., and Tsuchiya, T. (2009). Multidrug efflux transporters in the MATE family. BBA-Proteins Proteom. *1794*, 763-768.

Lacapere, J.J., Pebay-Peyroula, E., Neumann, J.M., and Etchebest, C. (2007). Determining membrane protein structures: still a challenge! Trends in Biochemical Sciences *32*, 259-270.

Lai, C.J., Weisblum, B. (1971). Altered Methylation of Ribosomal RNA in an Erythromycin-Resistant Strain of *Staphylococcus aureus*. Proc. Natl. Acad. Sci. USA *68*, 856-860.

Lakowicz, J.R. (2006). Principles of fluorescence spectroscopy, 3rd Ed. (New York: Springer).

Landau, E.M., and Rosenbusch, J.P. (1996). Lipidic cubic phases: a novel concept for the crystallization of membrane proteins. Proc. Natl. Acad. Sci. USA *93*, 14532-14535.

Lattman, E.E., and Loll, P.J. (2008). Protein Crystallography: A Concise Guide (Baltimore: Johns Hopkins University Press).

Laubinger, W., and Dimroth, P. (1988). Characterization of the ATP Synthase of *Propionigenium modestum* As A Primary Sodium-Pump. Biochemistry *27*, 7531-7537.

Law, C.J., Maloney, P.C., and Wang, D.N. (2008). Ins and Outs of Major Facilitator Superfamily Antiporters. Annu. Rev. of Microbiol. *62*, 289-305.

Law, C.J., Yang, Q., Soudant, C., Maloney, P.C., and Wang, D.N. (2007). Kinetic evidence is consistent with the rocker-switch mechanism of membrane transport by GlpT. Biochemistry *46*, 12190-12197.

Lemieux, M.J., Huang, Y., and Wang, D.N. (2004). The Structural basis of substrate translocation by the *Escherichia coli* glycerol-3-phosphate transporter: a member of the major facilitator superfamily. Curr. Opin. Struc. Biol. *14*, 405-412.

Lemieux, M.J., Song, J.M., Kim, M.J., Huang, Y.F., Villa, A., Auer, M., Li, X.D., and Wang, D.N. (2003). Three-dimensional crystallization of the *Escherichia coli* glycerol-3-phosphate transporter: A member of the major facilitator superfamily. Protein Sci.*12*, 2748-2756.

Levy, S.B., and Marshall, B. (2004). Antibacterial resistance worldwide: causes, challenges and responses. Nat. Med. *10*, S122-S129.

Lewinson, O., Adler, J., Poelarends, G.J., Mazurkiewicz, P., Driessen, A.J.M., and Bibi, E. (2003). The *Escherichia coli* multidrug transporter MdfA catalyzes both electrogenic and electroneutral transport reactions. Proc. Natl. Acad. Sci. USA *100*, 1667-1672.

Lewinson, O., Adler, J., Sigal, N., and Bibi, E. (2006). Promiscuity in multidrug recognition and transport: the bacterial MFS Mdr transporters. Mol. Microbiol. *61*, 277-284.

Lewinson, O., and Bibi, E. (2001). Evidence for Simultaneous Binding of Dissimilar Substrates by the *Escherichia coli* Multidrug Transporter MdfA. Biochemistry *40*, 12612-12618.

Lewinson, O., Padan, E., and Bibi, E. (2004). Alkalitolerance: a biological function for a multidrug transporter in pH homeostasis. Proc. Natl. Acad. Sci. USA *101*, 14073-14078.

Li, X.-Z., and Nikaido, H. (2004). Efflux-Mediated Drug Resistance in Bacteria. Drugs *64*, 159-204.

Li, X.Z., and Nikaido, H. (2009). Efflux-Mediated Drug Resistance in Bacteria An Update. Drugs *69*, 1555-1623.

Lian, L.Y., and Middleton, D.A. (2001). Labelling approaches for protein structural studies by solution-state and solid-state NMR. Prog. Nucl. Mag. Res. Sp. *39*, 171-190.

Locher, K.P. (2009). Structure and mechanism of ATP-binding cassette transporters. Philos. T. R. Soc. B. *364*, 239-245.

Loll, P.J. (2003). Membrane protein structural biology: the high throughput challenge. J. Struct. Biol. *142*, 144-153.

Lomovskaya, O., Zgurskaya, H.I., Totrov, M., and Watkins, W.J. (2007). Waltzing transporters and 'the dance macabre' between humans and bacteria. Nat. Rev. Drug Discov. *6*, 56-65.

Lowry, O.H., Rosebrough, N.J., Farr, A.L., and Randall, R.J. (1951). Protein Measurement with the Folin Phenol Reagent. J. Biol. Chem. *193*, 265-275.

Macdonald, R.C., Macdonald, R.I., Menco, B.P.M., Takeshita, K., Subbarao, N.K., and Hu, L.R. (1991). Small-Volume Extrusion Apparatus For Preparation Of Large, Unilamellar Vesicles. Biochim. Biophys. Acta *1061*, 297-303.

Markham, P.N., and Neyfakh, A.A. (1996). Inhibition of the multidrug transporter NorA prevents emergence of norfloxacin resistance in *Staphylococcus aureus*. Antimicrob. Agents Ch. *40*, 2673-2674.

Markham, P.N., and Neyfakh, A.A. (2001). Efflux-mediated drug resistance in Gram-positive bacteria. Curr. Opin. Microbiol. *4*, 509-514.

Mazurkiewicz, P., Driessen, A.J.M., and Konings, W.N. (2005). What do proton motive force driven multidrug resistance transporters have in common? Curr. Issues Mol. Biol. *7*, 7-21.

McMurry, L., Petrucci, R.E., and Levy, S.B. (1980). Active Efflux Of Tetracycline Encoded By 4 Genetically Different Tetracycline Resistance Determinants In *Escherichia coli*. Proc. Natl. Acad. Sci. USA-Biol. *77*, 3974-3977.

Meyer, B., and Peters, T. (2003). NMR Spectroscopy techniques for screening and identifying ligand binding to protein receptors. Angew. Chem.-Int. Edit. *42*, 864-890.

Murakami, S., Nakashima, R., Yamashita, E., Matsumoto, T., and Yamaguchi, A. (2006). Crystal structures of a multidrug transporter reveal a functionally rotating mechanism. Nature *443*, 173-179.

Nelson, D.L., Cox, Michael M. (2008). Lehninger Principles of Biochemistry, 5 Ed. (New York: W.H. Freeman and Company).

Nelson, J.H. (2003). Nuclear Magnetic Resonance Spectroscopy, Vol 1 (Upper Saddle River: Pearson Education, Inc).

Newby, Z.E.R., O'Connell, J.D., III, Gruswitz, F., Hays, F.A., Harries, W.E.C., Harwood, I.M., Ho, J.D., Lee, J.K., Savage, D.F., Mierke, L.J.W.*, et al.* (2009). A General Protocol for the Crystallization of Membrane Proteins for X-ray Structural Investigation. Nat. Protoc. *4*, 619-637.

Neyfakh, A.A. (1997). Natural functions of bacterial multidrug transporters. Trends Microbiol. *5*, 309-313.

Neyfakh, A.A. (2002). Mystery of multidrug transporters: the answer can be simple. Molecular Microbiology *44*, 1123-1130.

Nicholls, D.G. (1982). Bioenergetics: An Introduction to the Chemiosmotic Theory (New York, NY: Academic Press Inc.).

Nie, Y.L., Smirnova, I., Kasho, V., and Kaback, H.R. (2006). Energetics of ligand-induced conformational flexibility in the lactose permease of *Escherichia coli*. J. Biol. Chem. *281*, 35779-35784.

Nikaido, H. (1989). Outer Membrane Barrier as a Mechanism of Antimicrobial Resitance. Antimicrob. Agents Ch. *33*, 1831-1836.

Nikaido, H. (1994). Prevention of Drug Access to Bacterial Targets - Permeability Barriers and Active Efflux. Science *264*, 382-388.

Nikaido, H. (1998). Multiple antibiotic resistance and efflux. Curr. Opin. Microbiol. *1*, 516-523.

O'Grady, C.B. (2010). Multidrug transporter MdfA as a target for high-resolution structural studies. In Biochemistry (Saskatoon, University of Saskatchewan).

Okusu, H., Ma, D., and Nikaido, H. (1996). AcrAB efflux pump plays a major role in the antibiotic resistance phenotype of *Escherichia coli* multiple-antibiotic-resistance (Mar) mutants. J. Bacteriol. *178*, 306-308.

Ostermeier, C., Iwata, S., Ludwig, B., and Michel, H. (1995). F_V fragment mediated crystallization of the membrane protein bacterial cytochrome c oxidase. Nat. Struct. Biol. *2*, 842-846.

Ostermeier, C., and Michel, H. (1997). Crystallization of membrane proteins. Curr. Opin. Struc. Biol. *7*, 697-701.

Padan, E., Hunte, C., Reiländer, H. (2003). Production and Purification of Recombinant Membrane Proteins. In Membrane Protein Purification and Crystallization: A Practical Guide, C. Hunte, Von Jagow, G., Schägger, H., ed. (San Diego: Academic Press).

Padan, E., Kozachkov, L., Herz, K., and Rimon, A. (2009). NhaA crystal structure: functional-structural insights. J. Exp. Biol. *212*, 1593-1603.

Patching, S.G. (2011). NMR structures of polytopic integral membrane proteins. Mol. Membr. Biol. *28*, 370-397.

Paulsen, I.T., Brown, M.H., and Skurray, R.A. (1996). Proton-dependent multidrug efflux systems. Microbiol. Rev. *60*, 575-608.

Paulsen, I.T., Nguyen, L., Sliwinski, M.K., Rabus, R., and Saier, M.H. (2000). Microbial genome analyses: Comparative transport capabilities in eighteen prokaryotes. J. Mol. Biol. *301*, 75-100.

Picard, M., Verchere, A., and Broutin, I. (2012). Monitoring the active transport of efflux pumps after their reconstitution into proteoliposomes: Caveats and keys. Anal. Biochem. *420*, 194-196.

Pierson, H.E., Uhlemann, E.M.E., and Dmitriev, O.Y. (2011). Interaction with Monomeric Subunit c Drives Insertion of ATP Synthase Subunit *a* into the Membrane and Primes a-c Complex Formation. J. Biol. Chem. *286*, 38583-38591.

Poolman, B., Doeven, M.K., Geertsma, E.R., Biemans-Oldehinkel, E., Konings, W.N., and Rees, D.C. (2005). Functional analysis of detergent-solubilized and membrane-reconstituted ATP-binding cassette transporters. In Phase I Conjugation Enzymes and Transport Systems, H. Sies, and L. Packer, eds. (San Diego: Elsevier Academic Press Inc), pp. 429-459.

Poolman, B., and Konings, W.N. (1993). Secondary Solute Transport In Bacteria. Biochim. Biophys. Acta *1183*, 5-39.

Privé, G.G. (2007). Detergents for the stabilization and crystallization of membrane proteins. Methods *41*, 388-397.

Putman, M., van Veen, H.W., and Konings, W.N. (2000). Molecular Properties of Bacterial Multidrug Transporters. pp. 672-693.

Ramachandra, M., Ambudkar, S.V., Chen, D., Hrycyna, C.A., Dey, S., Gottesman, M.M., and Pastan, I. (1998). Human P-glycoprotein exhibits reduced affinity for substrates during a catalytic transition state. Biochemistry *37*, 5010-5019.

Raman, P., Cherezov, V., and Caffrey, M. (2006). The Membrane Protein Data Bank. Cell. Mol. Life Sci. *63*, 36-51.

Rhodes, G. (2000). Crystallography made Crystal Clear: A guide for users of Macromolecular Models, Vol 2 (San Diego: Academic Press).

Rice, L.B. (2010). Progress and challenges in implementing the research on ESKAPE pathogens. Infect. Control Hosp. Epidemiol. *31 Suppl 1*, S7-10.

Rigaud, J.L., and Levy, D. (2003). Reconstitution of Membrane Proteins into Liposomes. Methods Enzymol. *372*, 65-86.

Rigaud, J.L., Pitard, B., and Levy, D. (1995). Reconstitution of Membrane-Proteins Into Liposomes - Application to Energy-Transducing Membrane-Proteins. BBA-Bioener. *1231*, 223-246.

Rotem, D., and Schuldiner, S. (2004). EmrE, a multidrug transporter from *Escherichia coli*, transports monovalent and divalent substrates with the same stoichiometry. J. Biol. Chem. *279*, 48787-48793.

Roth, M., Lewitbentley, A., Michel, H., Deisenhofer, J., Huber, R., and Oesterhelt, D. (1989). Detergent Structure in Crystals of a Bacterial Photosynthetic Reaction Center. Nature *340*, 659-662.

Saidijam, M., Benedetti, G., Ren, Q., Xu, Z., Hoyle, C.J., Palmer, S.L., Ward, A., Bettaney, K.E., Szakonyi, G., Meuller, J.*, et al.* (2006). Microbial drug efflux proteins of the major facilitator superfamily. Curr. Drug Targets *7*, 793-811.

Saier, M.H. (2000). A functional-phylogenetic classification system for transmembrane solute transporters. Microbiol. Mol. Biol. R. *64*, 354-411.

Saier, M.H., and Paulsen, I.T. (2001). Phylogeny of multidrug transporters. Semin. Cell Dev. Biol. *12*, 205-213.

Sanders, C.R., and Sonnichsen, F. (2006). Solution NMR of membrane proteins: practice and challenges. Magn. Reson. Chem. *44*, S24-S40.

Schagger, H., and Vonjagow, G. (1987). Tricine Sodium Dodecyl-Sulfate Polyacrylamide-Gel Electrophoresis for the Separation of Proteins in the Range from 1-kDa to 100-kDa. Anal. Biochem. *166*, 368-379.

Sennhauser, G., Bukowska, M.A., Briand, C., and GrÅtter, M.G. (2009). Crystal Structure of the Multidrug Exporter MexB from *Pseudomonas aeruginosa*. J. Mol. Biol. *389*, 134-145.

Shi, K., Houston, D.R., and Berghuis, A.M. (2011). Crystal Structures of Antibiotic-Bound Complexes of Aminoglycoside 2"-Phosphotransferase IVa Highlight the Diversity in Substrate Binding Modes among Aminoglycoside Kinases. Biochemistry *50*, 6237-6244.

Shuker, S.B., Hajduk, P.J., Meadows, R.P., and Fesik, S.W. (1996). Discovering high-affinity ligands for proteins: SAR by NMR. Science *274*, 1531-1534.

Sigal, N., Vardy, E., Molshanski-Mor, S., Eitan, A., Pilpel, Y., Schuldiner, S., and Bibi, E. (2005). 3D Model of the *Escherichia coli* Multidrug Transporter MdfA Reveals an Essential Membrane-Embedded Positive Charge. Biochemistry *44*, 14870-14889.

Sköld, O. (2011). Antibiotics and antibiotic resistance (Hoboken, New Jersey: John Wiley & Sons, Inc.).

Smirnova, I.N., and Kaback, H.R. (2003). Mutation in the lactose permease of *Escherichia coli* that decreases conformational flexibility and increases protein stability. Biochemistry *42*, 3025-3031.

Soskine, M., Adam, Y., and Schuldiner, S. (2004). Direct evidence for substrate-induced proton release in detergent-solubilized EmrE, a multidrug transporter. J. Biol. Chem. *279*, 9951-9955.

Stalz, W.D., Greie, J.C., Deckers-Hebestreit, G., and Altendorf, K. (2003). Direct interaction of subunits a and b of the F_o complex of *Escherichia coli* ATP synthase by forming an ab(2) subcomplex. J. Biol. Chem. *278*, 27068-27071.

Stein, W.D. (1990). Channels, Carriers, and Pumps: An Introdcution to Membrane Transport (San Diego: Academic Press, Inc).

Tal, N., and Schuldiner, S. (2009). A coordinated network of transporters with overlapping specificities provides a robust survival strategy. Proc. Natl. Acad. Sci. USA *106*, 9051-9056.

Tsai, C.J., and Ziegler, C. (2010). Coupling electron cryomicroscopy and X-ray crystallography to understand secondary active transport. Curr. Opin. Struc. Biol. *20*, 448-455.

van Veen, H.W., Margolles, A., Muller, M., Higgins, C.F., and Konings, W.N. (2000). The homodimeric ATP-binding cassette transporter LmrA mediates multidrug transport by an alternating two-site (two-cylinder engine) mechanism. EMBO J. *19*, 2503-2514.

Venturi, M., Padan, E. (2003). Purification of NhaA Na^+/H^+ Antiporter of *Esherichia coli* for 3D or 2D Crystallization In Membrane Protein Purification and Crystallization: A Practical Guide, C. Hunte, Von Jagow, G., Schägger, H., ed. (San Diego: Academic Press).

Viveiros, M., Martins, M., Couto, I., Rodrigues, L., Spengler, G., Martins, A., Kristiansen, J.E., Molnar, J., and Amaral, L. (2008). New Methods for the Identification of Efflux Mediated MDR Bacteria, Genetic Assessment of Regulators and Efflux Pump Constituents, Characterization of Efflux Systems and Screening for Inhibitors of Efflux Pumps. Curr. Drug Targets *9*, 760-778.

Von Jagow, G., Link, T.A., Schägger, H. (2003). Purification Strategies for Membrane Proteins. In Membrane Protein Purification and Crystallization: A Practical Guide, C. Hunte, Von Jagow, G., Schägger, H., ed. (San Diego: Academic Press).

Ward, A., Hoyle, C., Palmer, S., O'Reilly, J., Griffith, J., Pos, M., Morrison, S., Poolman, B., Gwynne, M., and Henderson, P. (2001). Prokayote Multidrug Efflux Proteins of the Major Facilitator Superfamily: Amplified Expression, Purification and Characterisation. J. Mol. Microb. Biotech. *3*, 193-200.

Warschawski, D.E., Arnold, A.A., Beaugrand, M., Gravel, A., Chartrand, E., and Marcotte, I. (2011). Choosing membrane mimetics for NMR structural studies of transmembrane proteins. BBA-Biomembranes *1808*, 1957-1974.

Watanabe, T. (1963). Infective heredity of multiple drug resistance in bacteria Bacteriol. Rev. *27*, 87-115.

Weinglass, A.B., Soskine, M., Vazquez-Ibar, J.L., Whitelegge, J.P., Faull, K.F., Kabacko, H.R., and Schuldiner, S. (2005). Exploring the role of a unique carboxyl residue in EmrE by mass spectrometry. J. Biol. Chem. *280*, 7487-7492.

Wiener, M.C. (2004). A pedestrian guide to membrane protein crystallization. Methods (San Diego, Calif.) *34*, 364-372.

Xie, H. (2008). Activity assay of membrane transport proteins. Acta Bioch. Biophys. Sin. *40*, 269-277.

Xie, H., Patching, S.G., Gallagher, M.P., Litherland, G.J., Brough, A.R., Venter, H., Yao, S.Y.M., Ng, A.M.L., Young, J.D., Herbert, R.B*., et al.* (2004). Purification and properties of the *Escherichia coli* nucleoside transporter NupG, a paradigm for a major facilitator transporter sub-family. Mol. Membr. Biol. *21*, 323-336.

Yanamala, N., Dutta, A., Beck, B., van Fleet, B., Hay, K., Yazbak, A., Ishima, R., Doemling, A., and Klein-Seetharaman, J. (2010). NMR-Based Screening of Membrane Protein Ligands. Chem. Biol. Drug Des. *75*, 237-256.

Yerushalmi, H., and Schuldiner, S. (2000). A common binding site for substrates and protons in EmrE, an ion-coupled multidrug transporter. FEBS Letters *476*, 93-97.

Yin, Y., He, X., Szewczyk, P., Nguyen, T., and Chang, G. (2006). Structure of the multidrug transporter EmrD from *Escherichia coli* Science *317*, 741-744.

Zartler, E.R., Yan, J.L., Mo, H.P., Kline, A.D., and Shapiro, M.J. (2003). 1D NMR methods in ligand-receptor interactions. Curr. Top. Med. Chem. *3*, 25-37.

Zgurskaya, H.I., and Nikaido, H. (2000). Multidrug resistance mechanisms: drug efflux across two membranes. Mol. Microbiol. *37*, 219-225.